The PHILOSOPHICAL MAGAZINE

FIRST PUBLISHED IN 1798

1 Eighth Series No. 3 March 1956

A Journal of Theoretical Experimental and Applied Physics

PRICE 15s. 0d.
Annual Subscription £8 0s. 0d. payable in advance

Printed and Published by
TAYLOR & FRANCIS LTD.
RED LION COURT, FLEET STREET, LONDON, E.C.4

CONTENTS OF No. 3.

Page

XXI. The Magnetic Susceptibilities of Copper, Silver and Gold and Errors in the Gouy Method. By W. G. Henry and J. L. Rogers, Division of Applied Chemistry, National Research Council, Ottawa 223

XXII. The Magnetic Susceptibilities of some Diamagnetic Alloys: The Primary Solid Solutions of Zinc, Gallium, Germanium and Arsenic in Copper. By W. G. Henry and J. L. Rogers, Division of Applied Chemistry, National Research Council, Ottawa 237

XXIII. The Daily Variation of the Cosmic Ray Intensity Measured Near the 1954 Sunspot Minimum. By M. Possener and I. J. van Heerden, The Physical Laboratories, The University of Manchester ... 253

XXIV. The Inelastic Scattering of 2·5 mev Neutrons by Chromium, Manganese and Vanadium. By L. E. Beghian, D. Hicks and B. Milman, Clarendon Laboratory, Oxford 261

XXV. The Direct Observation of Dislocation Nets in Rock Salt Single Crystals. By S. Amelinckx, Laboratorium voor Kristalkunde Rijksuniversiteit te Gent, Ghent (Belgium) 269

XXVI. Isotopic Spin Selection Rules—VI: The 6·88 mev State of ^{10}B. By D. H. Wilkinson and A. B. Clegg, Cavendish Laboratory, Cambridge 291

XXVII. Correspondence :—

The Vibrations of a Perturbed Lattice. By R. J. Elliott, Physics Department, University of Reading 298

**All communications for the Philosophical Magazine should be addressed, post-paid, to the Editors, c/o Messrs. Taylor and Francis, Ltd., Red Lion Court, Fleet Street, London, England.

XXI. *The Magnetic Susceptibilities of Copper, Silver and Gold and Errors in the Gouy Method*

By W. G. Henry and J. L. Rogers*
Division of Applied Chemistry, National Research Council, Ottawa†

[Received October 18, 1955]

Abstract

A direct determination has been made of the absolute magnetic mass susceptibility of copper, silver and gold. The values at 23°C are: copper, $-0{\cdot}0859_9 \pm 0{\cdot}0002_7 \times 10^{-6}$; silver, $-0{\cdot}1812_8 \pm 0{\cdot}0005_4 \times 10^{-6}$; gold, $-0{\cdot}1421_6 \pm 0{\cdot}0004_8 \times 10^{-6}$, c.g.s. e.m.u. per gram. The probable errors of the relative values are 0·09%, 0·07% and 0·16% respectively.

The correction for ferromagnetic impurities is discussed. From an experimentally determined magnetization curve of the ferrromagnetic impurities in a silver specimen, it is shown that, although the error inherent in the long specimen method is greatly reduced by using a short specimen, an error may remain even when the smallest field acting on any part of the specimen is 6000 gauss.

The method of calibrating the field by means of a current-carrying loop and of making allowance for the variation of the field strength in the plane normal to the axis of the specimen are described in detail. A pole piece design which is particularly suitable for the short specimen method is given.

§ 1. Introduction

The apparatus described here was assembled primarily for measurements of the magnetic susceptibility at room temperature of diamagnetic copper, silver and gold based, primary solid solutions. The results for the alloy systems copper–zinc, copper–gallium, copper–germanium and copper–arsenic, are presented elsewhere in this journal (Henry and Rogers 1955).

The susceptibilities of copper, silver and gold have been measured by a number of workers. All attempts to obtain the magnetic susceptibilities of the Group IB metals, with an accuracy of more than 1%, have been made relative to water. In some cases the ratio of the forces on identical volumes of material have been used and in others a search coil has been calibrated from the force on a measured volume of water. In table 1 are collected the best room temperature measurements for these metals adjusted to the same value of water, $-0{\cdot}72183 \pm 0{\cdot}00048$ (Auer 1933 a).

* Present address: Bell Telephone Laboratories, Murray Hill, N.J.
† Communicated by the Authors.

Table 1. Magnetic Susceptibility of Copper, Silver and Gold

Copper $\chi_\infty \times 10^6$ c.g.s. e.m.u. per gram	Silver $\chi_\infty \times 10^6$ c.g.s. e.m.u. per gram	Gold $\chi_\infty \times 10^6$ c.g.s. e.m.u. per gram
$-0{\cdot}08527^{(a)}$	$-0{\cdot}1801^{(a)}$	$-0{\cdot}1454^{(a)}$
$-0{\cdot}0861^{(b)}$	$-0{\cdot}1772^{(e)}$	$-0{\cdot}1397^{(e)}$
$-0{\cdot}0810^{(c)}$	$-0{\cdot}1960^{(d)}$	$-0{\cdot}1555^{(d)}$
$-0{\cdot}0861^{(d)}$		

[(a)] Vogt (1932), [(b)] Ross (1934), [(c)] Gustafsonn (1936), [(d)] Shimizu (1937), [(e)] Auer, Riedl and Seemann (1934).

The temperatures at which these determinations were made, differed by as much as 4°c from 20°c. For copper this corresponds to a change of less than 0·1% (Ross 1934, Bitter, Kaufman, Starr and Pan 1941). Although there is not good agreement between investigators, it appears that the temperature coefficients of silver and gold are of the same order as that of copper. In table 1 the value for the susceptibility of copper determined by Ross (1934) is relative to gold as determined by Vogt (1932).

The lack of agreement between the authors indicates the need for further absolute measurements. The differences using the same standard are probably due to: the different techniques employed to take into account ferromagnetic impurities, the practical difficulties of using a liquid as a standard for a measurement on a solid and the relative purity of materials.

Auer (1933 b) used carefully calibrated search coils to determine the mean field acting on the specimen. In the present work, the absolute variation along the vertical axis of the horizontal component of the field was determined from the force on a carefully measured current-carrying loop. The variation of the horizontal component at right angles to the pole faces and the variation of the vertical component of the field parallel to the vertical axis were calculated and their functional form verified by direct measurement with a germanium probe.

One of the objects of this work was to establish a secondary standard to which the susceptibilities of alloys measured in this laboratory might be referred. The value of the susceptibility of copper given here serves as this secondary standard.

All susceptibilities quoted in this paper are in c.g.s.e.m.u. per gram.

§ 2. Apparatus

The method of measuring magnetic susceptibilities, illustrated in fig. 1 (*b*), is based on the Gouy method (Bates 1951). The cylindrical ($2{\cdot}0 \times 0{\cdot}75$ cm) specimen A is supported with its axis vertical, on the

flat table of the holder B between the poles of the electromagnet. The lower end of the specimen is in a field of strong magnetic induction B_{max} and the upper end in a weak field B_{min}. The holder is suspended from one arm of a balance and the vertical force on the specimen and holder is measured as an apparent change of mass. The accurate measurement of B_{max} and B_{min} permits the absolute value of the susceptibility to be determined.

Fig. 1

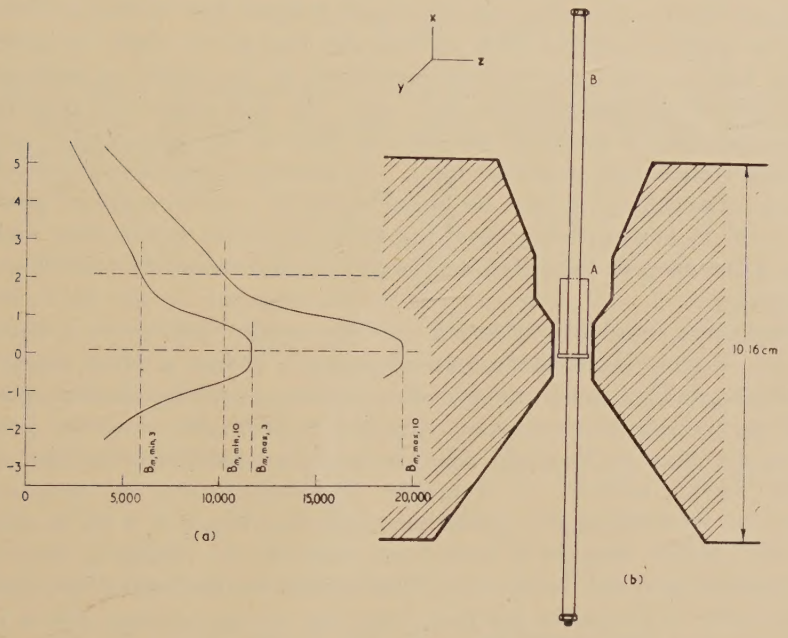

ord. cm. abs. field strength (gauss)

(*a*) The variation in the x direction of the field as measured by the loop.

(*b*) The location of the specimen A and the holder B in the field.

In the usual form of the Gouy method, the specimen is made sufficiently long to permit B^2_{min} to be neglected in comparison with B^2_{max}. But as this apparatus was designed primarily for measurements on alloys, it was desirable that a comparatively short specimen be used to reduce the difficulty of obtaining homogeneous specimens. In addition, as Knappwost (1941) has pointed out, a simpler and more reliable correction can be made for ferromagnetic impurities if the entire specimen is in a field of magnetic induction sufficiently strong to saturate these impurities. This is discussed in § 3. Accordingly, a specimen length of only 2 cm was chosen and the magnet was designed so that the weak field is of the order of one half of the strong field.

The electromagnet was constructed by Messrs. Tickford Ltd., Newport, England, from a design supplied by the Clarendon Laboratory, Oxford. It is equipped with 2 coils, each of 3600 turns of heavy gauge copper wire, and when these are connected in parallel a current of 10 amp may be drawn for limited periods. With the pole pieces used and a gap of 1 cm, a maximum magnetic induction of 19 600 gauss is obtained.

The pole pieces were cut from 4 in. diameter shafting of ' Netherton's Treble Best Iron ' (Mn 0·060 to 0·100%, C 0·020 to 0·035%). The five flat faces of each pole piece, fig. 1 (*b*), extend over the full width of the shaft and thus the induction is substantially independent of the y coordinate. The two pairs of vertical faces provide two regions in which the gradient of the field is small, in the neighbourhood of the upper as well as the lower end of the specimen (see fig. 1 (*a*)). By this means the positioning of the specimen is made far less critical than in the Knappwost method in which conical pole pieces are used. In practice a specimen is positioned with a cathetometer so that its upper end is in a predetermined position. The error in susceptibility resulting from imprecise positioning and the small differences in the machined lengths of the specimen is of the order of 0·05%.

The balance used for measuring the force on the specimen is a Christian Becker, Model AB-2, chainomatic balance. It has a rated sensitivity of 0·05 mg. The overdamping of the balance caused by the action of the field on a conducting specimen and the requirement that the position of the specimen in the field must be known, necessitate the use of the ' dead beat ' method of weighing. Reproducibility of weighing is improved by limiting the use of the chain to a range of 3 mg in steps of 0·1 mg. Major changes of weight are balanced by changing weights on the balance pan, and hundredths of milligrams are estimated by a parallax observation of the small residual deflection of the balance. It is found that changes of weight of the specimen may be measured with a reproducibility of about 0·02 mg.

The balance, specimen holder, specimen and pole pieces of the magnet, are enclosed in a draught-proof case. Provision has been made for lowering and arresting the balance beam, and for adjusting the chain from outside the case. A flexible plastic ' pocket ' allows the weights on the balance pan to be changed without opening the case.

The stabilized magnet current is measured potentiometrically and manual control of residual drifts allows the current to be controlled to $\pm 0{\cdot}01\%$ at 10 amp.

The apparatus used to melt some of the specimens is described elsewhere in this journal (Henry and Rogers 1955).

§ 3. Correction for Ferromagnetic Impurities

Vogt (1932), and Bitter and Kaufman (1939), have discussed methods of correcting for ferromagnetic impurities in a long specimen using the Gouy method. Knappwost (1941) pointed out the advantage of using a

short specimen in which the ferromagnetic impurities in the whole of the specimen are saturated for the field strengths used. He worked with powders and the accuracy of the experimental work was not high, $\pm 2{\cdot}5\%$. The work in this section comprises a more detailed study of the advantages of using a short specimen.

By consideration of the forces on a magnetic dipole, it may be shown that the component F_x of the force on a body in a vacuum in a region of inhomogeneous magnetic induction, generated by constant external sources is given by,

$$F_x = \int_v \mathbf{M} \,.\, \text{grad}\, B_x \, dv. \quad . \quad . \quad . \quad . \quad . \quad (3.1)$$

$\mathbf{M}$ is the intensity of magnetization in the body and B_x is the x component of the magnetic induction with the body absent. Because curl $\mathbf{B}=0$ where no currents flow

$$F_x = \int_v \mathbf{M} \,.\, \frac{\partial \mathbf{B}}{\partial x} dv. \quad . \quad . \quad . \quad . \quad . \quad . \quad . \quad (3.2)$$

$\mathbf{M}$ may be considered the sum of two parts $k\mathbf{B}$ and $c\mathbf{M}_{\text{Fe}}(\mathbf{B})$ where k is related to the volume susceptibility of the pure either dia or paramagnetic substance. cv is the volume of the ferromagnetic impurity particles and $\mathbf{M}_{\text{Fe}}(\mathbf{B})$ is the intensity of magnetization of these particles.

If the ferromagnetic impurity is considered saturated, $\mathbf{M}_{\text{Fe}}$ may be replaced by the constant $\mathbf{M}_s$. When the integration is carried out over the length x of the cylindrical specimen, but not over the cross section α,

$$F_x = -\int_\alpha \{\tfrac{1}{2}k(B^2_{\text{base}} - B^2_{\text{top}}) + c\mathbf{M}_s(\mathbf{B}_{\text{base}} - \mathbf{B}_{\text{top}})\}\, d\alpha \quad . \quad . \quad (3.3)$$

which on integration gives approximately,

$$F_x = -\tfrac{1}{2}k(B^2_{\max} - B^2_{\min}) - c\alpha\,|\,\mathbf{M}_s\,|(B_{\max} - B_{\min}) \quad . \quad . \quad (3.4)$$

where,

$$B^2_{\max} = \frac{1}{\alpha}\int_\alpha B^2_{\text{base}}\, d\alpha \quad \text{and} \quad B^2_{\min} = \frac{1}{\alpha}\int_\alpha B^2_{\text{top}}\, d\alpha. \quad . \quad (3.5)$$

The evaluation of $B_{\max}$ and $B_{\min}$ will be discussed in § 4. The small error in the approximation is entirely in the final term of eqn. (3.4) and may be neglected.

The volume susceptibility of a substance may be defined as the ratio of the magnetic moment per unit volume to the internal magnetic field, $\mathbf{H}_i$. The internal magnetic field is given by,

$$\mathbf{H}_i = \mathbf{H} + \mathbf{H}_d \quad . \quad . \quad . \quad . \quad . \quad . \quad . \quad . \quad (3.6)$$

where $\mathbf{H}$ is the external magnetic field and $\mathbf{H}_d$ is the demagnetizing field. Where dia and weakly paramagnetic media are involved, $|\,\mathbf{H}_d\,|$ is of the order of $|\,\mathbf{M}\,|$ which for a field of 10^4 oersteds is about 10^{-2} oersteds and hence may be neglected. Thus the internal and external magnetic fields are for practical purposes the same. Since the external medium

is a vacuum, the magnetic induction is equal to the external magnetic field and k is therefore, to this approximation, the volume susceptibility, κ_∞.

Since the measurements are made in air, it is necessary to apply an air correction ; eqn. (3.4) then becomes

$$F_x = -\tfrac{1}{2}(\kappa_\infty - \kappa_{\text{air}})(B^2_{\max} - B^2_{\min}) - c\alpha\,|\mathbf{M}_s|(B_{\max} - B_{\min}). \qquad (3.7)$$

The mass susceptibility, χ_∞, may be evaluated directly from the measurement of m the mass, l the length, α the cross sectional area and Δm the apparent change of mass of the specimen in the field. Let

$$\chi_\infty = \frac{\kappa_\infty l\alpha}{m}, \qquad (3.8)$$

then since

$$F_x = -g\Delta m \qquad (3.9)$$

therefore,

$$\frac{2lg\Delta m}{m(B^2_{\max} - B^2_{\min})} + \frac{\kappa_{\text{air}}\, l\alpha}{m} = \chi_\infty + \frac{2lc\alpha}{m} \cdot \frac{|\mathbf{M}_s|}{B_{\max} + B_{\min}}. \qquad (3.10)$$

The left-hand side of eqn. (3.10) is χ_B, the apparent susceptibility for some value of $B_{\max}$. A linear plot of χ_B, determined at a number of field strengths, against $(1/B_{\max} + B_{\min})$ enables χ_∞ to be determined.

It may be shown that an even distribution of holes in the specimen does not alter χ_∞, as determined by eqn. (3.10) except in a second order way through the small air correction term. The use of eqn. (3.10) in place of that suggested by Knappwost (1941), is preferable for two reasons. Firstly, the cross sectional area which can be measured with less precision than either l or m appears in the small air correction only. Secondly, no separate density measurement is required in order to obtain the mass susceptibility.

In practice, measurements were made at only χ_3 and χ_{10}, the values of χ_B obtained with magnet currents of 10 and 3 amp respectively. χ_3 and χ_{10} were each measured twice, the specimen was inverted and the procedure was repeated. The current of 3 amp was chosen as a compromise between the need to ensure that the ferromagnetic impurities were saturated throughout the specimen and the need to use two widely differing values of $(B_{\max} + B_{\min})$ in order to establish the slope of the straight line with precision. It is expected that a more accurate value of χ_∞ is obtained from the above method than from the extrapolation of unrepeated measurements of χ_B at eight different field strengths.

The validity of eqn. (3.10) was tested experimentally by finding the accuracy of the value of χ_∞ obtained for two silver specimens containing an appreciable concentration of ferromagnetic impurity. In these two specimens χ_{10} was found to be $-0{\cdot}1434 \times 10^{-6}$ and $-0{\cdot}1288 \times 10^{-6}$. The χ_∞ values obtained by extrapolation were $-0{\cdot}1810 \times 10^{-6}$ and $-0{\cdot}1801 \times 10^{-6}$ respectively. The mean value of χ_∞, obtained for five specimens of silver which contain comparatively negligible amounts of

ferromagnetic impurity is $-0{\cdot}1812_8\times10^{-6}$. Since the probable error for an individual silver specimen is 0·17% (see § 5), it is seen that the error caused by the ferromagnetic impurity is detectable in the presence of the error of measurement for the second specimen only.

The error results from considering $|\mathbf{M}_{Fe}|$ independent of the field. If eqn. (3.10) is derived directly from eqn. (3.2) without the assumption that $|\mathbf{M}_{Fe}|$ may be replaced by the constant $|\mathbf{M}_s|$, the following expression is obtained :

$$\chi_B=\chi_\infty+\frac{2lc\alpha}{m}\cdot\frac{1}{B_{max}+B_{min}}\left\{\frac{1}{B_{max}-B_{min}}\int_{B_{min}}^{B_{max}}\mathbf{M}_{Fe}\,.\,d\mathbf{B}\right\}. \quad (3.11)$$

The quantity in brackets will be termed M_{eff}. For the first of the above silver specimens with an appreciable quantity of ferromagnetic impurity, χ_B was measured at a number of field strengths and cM_{eff}, calculated from eqn. (3.11), was plotted against B_{max} (fig. 2, curve A). For the

Fig. 2

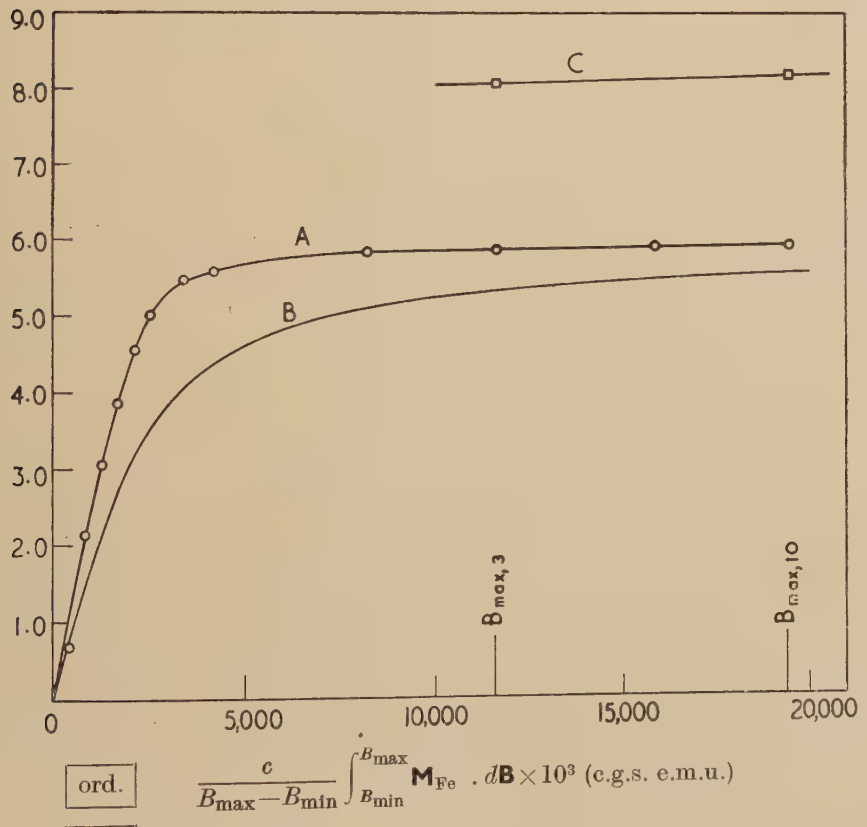

A, cM_{eff} for a short silver specimen; B, estimated cM_{eff} for a long silver specimen of the same material as A ; C, cM_{eff} for a short silver specimen.

second specimen cM_{eff} was calculated at two values of $B_{\max}$ (fig. 2, curve C). χ_∞ was assumed to be $-0{\cdot}1813\times10^{-6}$. It is seen (fig. 2) that for this type of impurity $|\mathbf{M}_{\text{Fe}}|$ is not entirely independent of the field strength in the range of fields employed.

If the bracketed term in eqn. (3.11) is approximated by

$$cM_{\text{eff}}=|\mathbf{M}_s|+\beta(B_{\max}+B_{\min}) \quad . \quad . \quad . \quad . \quad . \quad (3.12)$$

where β, the slope, depends on both the amount of ferromagnetic material and the field dependence of the magnetization, it follows from eqns. (3.11) and (3.12) that

$$\chi_{\text{extr}}-\chi_\infty=\frac{2l\alpha\beta}{m} \quad . \quad . \quad . \quad . \quad . \quad . \quad . \quad . \quad (3.13)$$

χ_{extr} is the extrapolated value for a specimen containing ferromagnetic impurities and χ_∞ is the extrapolated value for uncontaminated silver.

In the long specimen Gouy method $B_{\min}$ is approximately zero. In this case it is not to be expected that M_{eff} will reach a constant value. As illustration, the values of cM_{eff} that would be obtained with a long specimen of the same silver sample have been calculated from curve A of fig. 2 and are shown in curve B.

Vogt (1932), has shown that when a long specimen is used, χ_B is a quadratic function of $1/B_{\max}$, provided that the ferromagnetic impurity is saturated at the high field end of the specimen. He found however, no experimental verification when measuring gold–silver alloys in fields from 6500 to 22 000 gauss, and determined χ_∞ by linear extrapolation against $1/B_{\max}$. Auer, Riedl and Seemann (1934), used the same method. Many other investigators have assumed that the appearance of a linear plot justified the use of a linear extrapolation. To illustrate the error that may be caused by this procedure, a number of values of χ_B were computed from curve B of fig. 2 and plotted against $1/B_{\max}$. For values of $B_{\max}$ greater than 10 000 gauss, no point differed from the best straight line by more than $0{\cdot}25\%$, which is less than the experimental scatter normally obtained, but χ_∞ obtained from this straight line was $-0{\cdot}174\times10^{-6}$, which differs by nearly 4% from $-0{\cdot}1813\times10^{-6}$, the value of χ_∞ used to compute the points. This is to be compared with the error of the order of the probable error for an individual silver specimen, $0{\cdot}17\%$, obtained with the short specimen method. The disparity is directly related to the slope of curve B, fig. 2, which is considerably greater than that of curve A in the region 10 000 to 20 000 gauss.

It is concluded that, for the same absolute accuracy, the amount of ferromagnetic impurity may be much greater with the short specimen method than with the normal Gouy method. In the present work the concentration of ferromagnetic impurity in all specimens allowed eqn. (3.10) to be used without appreciable error.

Bitter and Kaufman (1939), have devised an ingenious procedure for obtaining a linear extrapolation with the long specimen method. However, their procedure requires a greater number of measurements than the short specimen method for the same accuracy.

§ 4. The Measurement of Field Strength

The magnetic induction was measured for magnet currents of 10 and 3 amp at the top and base of the specimen. The measurement was made by determining the force on a long U shaped current-carrying loop loaned by Mr. R. Bailey of the Applied Physics Division of the National Research Council. The loop was made from a strip of brass foil, 3 mm wide and 0·1 mm thick, wrapped on a carefully machined rectangular bakelite former, of length 20 cm and width 1 cm. The loop was freely suspended from an arm of the balance with its long sides vertical and the plane of the loop normal to the direction of the field. Long spirals of fine copper wire were used to connect the two upper ends of the loop to a source of current without unduly reducing the sensitivity of the balance. A change of weight of 0·03 mg could still be detected. The force F_x on the loop was measured as the apparent change of weight when current was allowed to flow. Then

$$F_x = i l_y B_z \qquad . \quad . \quad . \quad . \quad . \quad . \quad . \quad . \quad . \quad (4.1)$$

where, if the polarization of the air is neglected, B_z is the net magnetic induction present, before the loop was introduced. To a first approximation, l_y is the width of the loop. More accurately, the value used for l_y contained corrections for the non-parallelism of the sides of the loop and for the forces exerted on the current in the lead in wires by stray fields from the magnet and by the earth's field.

When a current of 0·35 amp was used losses of weight ranging from 200 mg for $B_{\min,\,3}$ to 660 mg for $B_{\max,\,10}$ were obtained. Repeated weighings reduced the weighing error to negligible size. Repeated demagnetizing and resetting of the magnet current showed that the fields could be reproduced with errors ranging from 0·05% for $B_{\min,\,3}$ to 0·006% for $B_{\max,\,10}$. These were also made negligible by repetition.

Other sources of error considered were buoyancy of the air on the standard weights used, possible unequal arms of the balance, imprecise positioning and orientation of the loop and measurement of loop current. However, the predominant error of approximately 0·1% arises from the determination of l_y.

The field strengths measured by this method are the mean values of B_z over the area $l_y w$ where w is the width of the strip. In order to determine $B_{\max}$ and $B_{\min}$ as defined in § 3, the variation of $\mathbf{B}$ with x and z must be considered. It is reasonable to assume that

$$B_x = \left(\frac{\partial B_x}{\partial z}\right)_{z=0} . z = \left(\frac{\partial B_z}{\partial x}\right)_{z=0} . z \qquad . \quad . \quad . \quad . \quad (4.2)$$

and

$$B_z = (B_z)_{z=0} + \tfrac{1}{2}\left(\frac{\partial^2 B_z}{\partial z^2}\right)_{z=0} . z^2 \qquad . \quad . \quad . \quad . \quad . \quad . \quad (4.3)$$

because from symmetry $(\partial B_z/\partial z)_{z=0}$ is zero. The two-dimensional nature of the field allows B_y and $\partial \mathbf{B}/\partial y$ to be neglected.

Upon carrying out the necessary integrations it follows that, to a good approximation,

$$B^2_{\max}=B^2_m+\frac{R^2}{4}\left\{B_m\frac{\partial^2 B_z}{\partial z^2}+\left(\frac{\partial B_z}{\partial x}\right)^2\right\}-\frac{w^2}{12}B_m\frac{\partial^2 B_z}{\partial z^2} \quad . \quad (4.4)$$

with a similar expression for $B^2_{\min}$. B_m is the field strength as measured by the loop ; R is the radius of the specimen.

At the top of the specimen, the experimentally determined decrease of B_z with z is accompanied by an increase in B_x and the resultant variation in $|\mathbf{B}|$ is small. If the measured value of the field strength is used for $B_{\min}$, the resultant error in χ_∞ is appreciably less than $0{\cdot}1\%$.

At the base of the specimen, because $\partial B_z/\partial x$ is small (see fig. 1 (a)), any measurable error will be caused by the variation of B_z with z. In the general case whether or not B_x, the component of the field parallel to the specimen, will cause a measurable error, depends on the shape of the pole piece and the resulting distribution. A reliable direct measurement of the variation of B_z with z was obtained by using a

Fig. 3

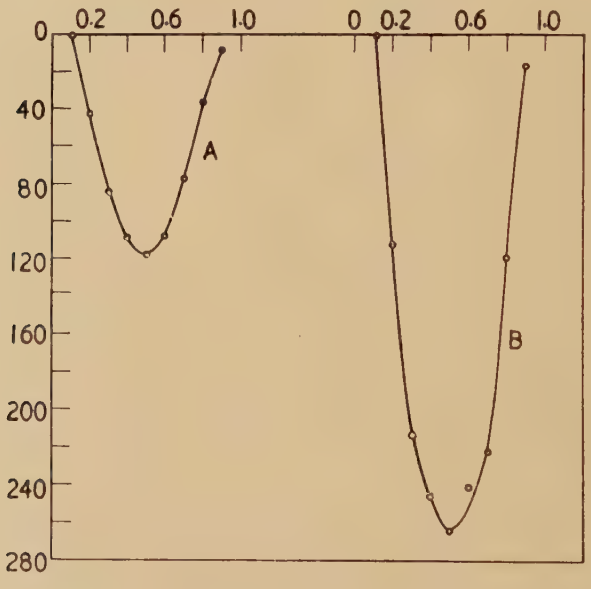

The variation of the horizontal component of the field, B_z.
A, at 3 amp ; B, at 10 amp.

British Thomson Houston Type G gaussmeter (see fig. 3). This measurement was greatly facilitated by the smallness of $\partial B_z/\partial x$. The effective $B^2_{\max}$ was then determined by eqn. (4.4). If $B^2_{\max}$ were taken as equivalent to the value measured by the loop, the measured value of the susceptibility would be $0{\cdot}30\%$ too large.

As a result of the calibration the overall estimated probable error in the absolute measurement of the magnetic susceptibility is 0·30%.

§ 5. Magnetic Susceptibilities of Copper, Silver and Gold

(*a*) *Copper*

Nine specimens of copper were measured. Of these, two were made by melting copper supplied by Johnson Matthey and Mallory Limited (J.M.). The analysis of this copper according to the manufacturer is: Ag 0·0005, Ni $<$0·0003, Pb $<$0·0004 weight %; Ga—trace. Fe—trace. The remainder of the specimens were made from copper supplied by the American Smelting and Refining Co. (A.S. and R.) of which the analysis according to the manufacturer is: Fe $<$0·00007, Sb $<$0·0001, Pb $<$0·0001, Sn $<$0·0001, Ni $<$0·0001, Bi $<$0·00001, Ag $<$0·00003, As $<$0·0002, Cr $<$ 0·00005, Si $<$0·00001, Te $<$0·0002, Se $<$0·0001, S $<$0·0001, O_2 $<$0·0001 weight %. Of the A.S. and R. specimens two were machined as received, one annealed at 550°c for one week and furnace cooled, one annealed and air cooled, two annealed and quenched, one melted in an alumina crucible, annealed and air cooled. The specimens were annealed in vacuum in pyrex containers. There was no clear indication that either the susceptibility was different for the two different sources of copper, or that the susceptibility was dependent upon the different heat treatments described above.

The possible errors due to the impurities oxygen and iron were investigated. One cubic centimeter of A.S. and R. copper, as received, yielded only 1 in 10^8 by weight of oxygen after one hour degassing at 800°c and none in the hour following. This amount would cause an error in the susceptibility of copper of 0·0012% if the oxygen were present in the molecular form. The manufacturers claim that the oxygen content is of the order of 0·0001% by weight. Phillips and Skinner (1941) found 0·0004% by weight, in analogous material. If 0·0004% by weight of oxygen were present in the copper as cuprous oxide (Laist 1954), the magnetic susceptibility of which is $-0{\cdot}18\times10^{-6}$ (Klemm and Schuth 1931), the resulting error in the susceptibility of the copper would be only 0·004%.

In order to determine the error due to the presence of paramagnetic iron it was first necessary to establish the effective mass susceptibility of iron in solution at low concentrations. Two copper–iron alloys were prepared containing on analysis 12 and 51 p.p.m. by weight. Both specimens were quenched from 1000°c and the effective susceptibility of the dissolved iron was found to be 92×10^{-6}. These results are in reasonable agreement with the values obtained by Bitter, Kaufman, Starr and Pan (1941). The iron impurity in the A.S. and R. copper was found by analysis to be 0·2 p.p.m. by weight. The error as a result of this amount of dissolved iron would be 0·02%. No correction was made for the small errors as a result of the oxygen and iron impurities.

The ferromagnetic iron content was in all cases very small and probably the differences between χ_{10} and χ_∞ (see table 2) for a specimen were due mainly to either random errors in measurement or errors in the field calibration. The mean value of χ_{10} differs from the mean value of χ_∞ by only 0·16%.

Chemical analysis showed that the iron content of the A.S. and R. copper was less than that of the J.M. copper and thus the A.S. and R. copper was taken as the standard. The probable error in the arithmetic mean of the seven specimens is 0·09% and the probable error in an individual measurement 0·20%. These errors include all errors other than the error in the calibration of the field. When this latter error is taken into account the resultant error in the absolute value of the susceptibility of copper is 0·31%. The mean measured susceptibility of the A.S. and R. copper is found to be $-0{\cdot}0859_9\times10^{-6}\pm0{\cdot}0002_7$.

The volume susceptibility of air used in this work was $0{\cdot}0284\times10^{-6}$ c.g.s. e.m.u. per cm^3.

Table 2. Magnetic Susceptibility of Copper, Silver and Gold

	No. of Specimens	$\chi_{10}\times10^6$ c.g.s. e.m.u. per gram	$\chi_\infty\times10^6$ c.g.s. e.m.u. per gram	
Copper	7	$-0{\cdot}0858_3$	$-0{\cdot}0859_9$*	$\pm0{\cdot}0002_7$
Silver	5	$-0{\cdot}1784_8$	$-0{\cdot}1812_8$	$\pm0{\cdot}0005_4$
Gold	4	$-0{\cdot}1397_6$	$-0{\cdot}1421_6$	$\pm0{\cdot}0004_8$

* The precision of these results relative to one another is considerably higher than indicated by the probable errors shown.

(b) Silver

Five specimens were measured. Three were made from one lot of J.M. silver, the analysis of which according to the manufacturer is: Fe 0·0005–0·0010, Na 0·0005–0·0010, Si 0·0005, Pb 0·0005, Mn 0·0002, Cu 0·0003, Sn 0·0002, Cd 0·0002, Mg 0·0001, Al 0·0001 weight %, Ca faintly visible. The iron analysis was ascertained chemically to be $1{\cdot}2\pm0{\cdot}2$ p.p.m. by weight. One was made from a special lot of J.M. silver, the analysis of which according to the manufacturer is: Ca not detectable, Fe faintly visible, Si faintly visible, Cu very faintly visible, Mg faintly visible, Na very faintly visible. One was made from silver electrolized twice from 0·8 normal silver nitrate by Dr. G. Harrow of the Applied Chemistry Division, National Research Council, the analysis of which is: Fe 0·0002, Si 0·0005, Pb 0·0005, Cu 0·0001, Mg 0·0001, Cd 0·0002, Mn 0·0002. Of these five, one specimen was made from the J.M. silver as received; two were melted in purified argon in alumina crucibles and two more in quartz crucibles. The specimens which were melted were annealed in vacuum in pyrex containers for one week at

500°C and water quenched. There was no indication either that the susceptibility was different for the different sources of silver, or that the susceptibility was dependent upon the crucible material. The as received specimen was degassed (Steacie and Johnson 1926, Auer, Riedl and Seemann 1934). The susceptibility of the as received specimen before degassing was $-0{\cdot}1802\times10^{-6}$ and after degassing $-0{\cdot}1812_1\times10^{-6}$, a change of 0·51%. Although this is only three times the probable error in an individual measurement, it is about six times the probable error of one of a number of repeated measurements on the same sample.

The degassing was carried out as follows: the gas was allowed to accumulate in a small volume about the specimen for 10 minutes at 800°C and then released into a large known volume and the pressure measured. The specimen was again isolated and the large volume evacuated. The degassing was continued until the rate of gas evolution had dropped to 0·2% of its highest value.

The amount of gas liberated from the as received specimen was 0·27cm³. One of the melted specimens after heating at 850°C for 24 hours in 3 atmospheres of oxygen and quenching into ice water yielded 0·38 cm³ on degassing. The evolution of gas was accompanied by a change in the susceptibility of the silver of 0·71%. On assuming that all the gas measured was oxygen, the mean mass susceptibility of oxygen dissolved in silver is found to be $22\pm2\times10^{-6}$.

The susceptibilities of the specimens melted in argon and vacuum annealed did not alter, by more than 0·1%, when degassed at 800°C.

The ferromagnetic content was on the average considerably larger than in the case of copper specimens. The mean value of χ_{10} differed from χ_∞ by 1·5% (table 2).

The probable error in the arithmetic mean of the five specimens is 0·07%, and the probable error in an individual measurement is 0·17%. When the error in the calibration of the field is taken into account the resultant error in the absolute value of the susceptibility of silver is 0·30%. The mean measured susceptibility of silver is found to be $-0{\cdot}1812_8\times10^{-6}\pm0{\cdot}0005_4$.

(*c*) *Gold*

Four specimens of gold were measured. The Royal Mint kindly supplied sufficient of their gold proof plate, fineness 999·9 1/2, for one specimen. On analysis, this specimen was found to contain 1·0 p.p.m. by weight of iron while cobalt and nickel were absent. Three specimens were made from mint grade gold which on analysis was found to contain 1·2 p.p.m. by weight of iron; cobalt and nickel were absent. Three of the specimens were melted in alumina crucibles and one in a quartz crucible. All specimens were annealed for one week at 550°C in vacuum in pyrex containers. There was no clear indication that either the susceptibility was different for the two different lots of gold or that the susceptibility depended on the crucible used.

The ferromagnetic iron contamination was of the same order as that for silver. The mean value of χ_{10} differed from χ_α by 1·6% (table 2).

Shih (1931) found the mass susceptibility for iron dissolved in gold at room temperature to be approximately 130×10^{-6}. When it is assumed that there is 1·0 p.p.m. by weight of iron in solution in the gold a correction must be applied of 0·09%. The measured value of the susceptibility of gold has been corrected by this amount.

The probable error in the arithmetic mean of the four specimens is 0·16%, and the probable error in an individual measurement is 0·32%. When the error in the calibration of the field is taken into account, the resultant error in the absolute value of the susceptibility of gold is 0·34%. The mean measured susceptibility of gold is found to be $-0{\cdot}1421_6\pm0{\cdot}0004_8$.

Acknowledgments

The authors wish to thank Mr. A. Blair and Mr. K. Hyndman for preparing the specimens and Mrs. M. Vamos and Mr. P. Tymchak for carrying out the chemical analyses.

References

Auer, H., 1933 a, *Ann. Phys. Lpz.*, **18,** 593 ; 1933 b, *Ibid.*, **18,** 613.
Auer, H., Riedl, E., and Seemann, H. J., 1934, *Z. Phys.*, **92,** 291.
Bates, L. F., 1951, *Modern Magnetism* (Cambridge: The University Press), p. 115.
Bitter, F., and Kaufman, A. R., 1939, *Phys. Rev.*, **56,** 1044.
Bitter, F., Kaufman, A. R., Starr, C., and Pan, S. T., 1941. *Phys. Rev.*, **60,** 134.
Gustafson, G., 1936, *Ann. Phys. Lpz.*, **25,** 545.
Henry, W. G., and Rogers, J. L., 1956, *Phil. Mag.*, **1,** paper 1616.
Klemm, W., and Schuth, W., 1931, *Z. anorg. Chem.*, **203,** 104.
Knappwost, A., 1941, *Z. phys. Chem.* A, **188,** 246.
Laist, J. W., 1954, *Comprehensive Inorganic Chemistry*, 2 (Toronto: D. Van Nostrand Company Inc.), p. 60.
Phillips, A., and Skinner, E. N., 1941, *Trans. Amer. Inst. Min. (Metall.) Engrs.*, **143,** 301.
Ross, W. H., 1934, *Phys. Rev.*, **46,** 46.
Shih, J. W., 1931, *Phys. Rev.*, **38,** 2051.
Shimizu, Y., 1937, *Sci. Rep. Tohoku Univ.*, **25,** 921.
Steacie, E. W. R., and Johnson, F. M. G., 1926, *Proc. Roy. Soc.* A, **112,** 542.
Vogt, E., 1932, *Ann. Phys. Lpz.*, **14,** 1.

XXII. *The Magnetic Susceptibilities of some Diamagnetic Alloys: The Primary Solid Solutions of Zinc, Gallium, Germanium and Arsenic in Copper*

By W. G. Henry and J. L. Rogers*
Division of Applied Chemistry, National Research Council, Ottawa†

[Received October 18, 1955]

Abstract

The results of the measurements, by a modified Gouy method, of the rates of change of the diamagnetic susceptibility with concentration in the solid solution region of the four systems are presented. A method of alloy preparation is given which, although conducive to some lateral and vertical segregation, produces a sound melt.

The magnetic properties of the systems are discussed theoretically. An interpretation follows for which it is assumed that all the electrons outside the $3d^{10}$ shell occupy states in the band and that all but one contribute their normal atomic diamagnetism. Instead of a parabolic band with a positive slope, it is found necessary to use a band which has approximately the same negative slope as that calculated by Jones (1937) for pure copper. The constancy of the density of states curve at the top of the band for a one-dimensional alloy is demonstrated by a first order perturbation treatment. The atomic magnetic susceptibilities as calculated from the self-consistent fields without exchange are given for: Zn^{2+}, $Zn(4s)^1$, Ga^{3+}, $Ga(4s)^2$, Ge^{4+}, $Ge(4s)^2(4p)^1$, As^{5+}, $As(4s)^2(4p)^2$, Al^{3+}, $Al(3s)^2$, Si^{4+}, C^0 and with exchange for Si^{4+} and C^0. The results of a preliminary examination of twenty-nine copper, silver and gold based solid solutions are mentioned. They show the absence of the paramagnetism that would be expected from the existence of the singly occupied states predicted by Mott (1952) and Friedel (1952).

§ 1. Introduction

Vogt and Harms (1942–1943) found that the diamagnetic susceptibility in the primary solid solution region of the copper–aluminium alloy system increases approximately linearly with composition. They pointed out the inconsistency between this result and that expected from theoretical considerations. For the Hume-Rothery rules apparently require

---

* Present address: Bell Telephone Laboratories, Murray Hill, N.J.
† Communicated by the Authors.

that aluminium is present as a triply charged ion and that the number of electrons per atom in the conduction band increases with concentration. According to the free electron theory of metals, the net paramagnetic contribution of the free electrons varies directly with the square root of the band width and, since the diamagnetic contribution of Al^{3+} is small, the magnetic susceptibility should increase in the paramagnetic direction with aluminium concentration. The same difficulty is found in attempting to explain the results of Endo (1925) for the copper–zinc and copper–tin systems.

Friedel (1952) discussed the copper–aluminium and copper–zinc systems and obtained numerical agreement with experiment, by attributing the increased diamagnetism to the two 3s electrons of Al^{+} and the one 4s electron of Zn^{+}. This idea is retained in the present work. He neglected any possible change in the net paramagnetic contribution from the band, despite his pointing out that states are subtracted from the band. There is, however, a substantial error in his calculation of the susceptibility of Al^{+} and Zn^{+} which renders the agreement with experiment artificial. Friedel (1954) again treated the copper–aluminium system and included a contribution from a parabolic band. However, when several numerical errors are corrected the agreement with experiment no longer exists.

There has been no systematic investigation of the magnetic properties of the monovalent base, polyvalent solute alloy systems to determine the relative properties of solutes. One of the systems, copper–zinc, discussed in this paper was investigated in a general way by Endo (1925).

The present work was commenced in order to obtain information on the variation of the density of states with concentration and the relation to the apparent valency of the solute in the primary solid solution region in copper alloys with non-transition elements. The experimental work gives strong support to the band shape beyond the peak as calculated by Jones (1937) for face-centred cubic copper. It also seems clear for the solutes investigated, that, although all but one of their electrons are retained in the neighbourhood, they occupy a number of states in the perturbed band equal to the number of electrons outside the closed $3d^{10}$ shell. This gives strong support to the assumption made by Jones (1937) in order to explain the observed Hume-Rothery rules concerning the limits of solid solubility in the alloy systems considered here.

Friedel (1952) and Mott (1952) have suggested that in the case of an excess charge unity, as for example zinc in copper, a bound level may exist which is occupied by one electron. An experimental survey of the primary solid solution region of twenty-nine systems with copper, silver and gold as solvents did not show the presence, in any case, of the strong paramagnetism which would be expected to be associated with a singly occupied level. Three systems of this group were previously reported to show a strong paramagnetism, copper–magnesium, copper–antimony (Davies and Keeping 1929) and silver–lead (Spencer and John 1927).

§ 2. Preparation of Alloys

The approximate purity, iron content in atomic parts per million and source of supply of the metals used in the preparation of the alloys are :

(i) Copper, greater than 99·999%, 0·2 p.p.m., supplied by the American Smelting and Refining Co.

(ii) Zinc, 99·999%, 1·0 p.p.m., supplied by the New Jersey Zinc Co.

(iii) Gallium, 99·99%, 15 p.p.m., supplied by the Eagle-Picher Co.

(iv) Germanium, 99·99%, 10 p.p.m., supplied by the Eagle-Picher Co.

(v) Arsenic, 99·99%, 10 p.p.m., supplied by Johnson Matthey and Co., Ltd.

The iron analysis only has been made in this laboratory.

The most undesirable impurity is iron. One atomic part per million of dissolved iron causes an error in the absolute value of the susceptibility of approximately 0·1%. In view of the purity of the major constituent the error from this source is of the order of the experimental error and no correction has been applied.

The weighed constituents, sufficient to give a 20 g melt, were acid cleaned, dried and then melted in vitrified alumina crucibles (9×50 mm) by a two kilowatt Lepel induction unit. A few copper–zinc alloys were melted in quartz crucibles. The melting apparatus is shown in fig. 1.

It was found necessary to shake the crucible up and down to dislodge gas bubbles trapped between the melt and the crucible wall. In order to prevent the formation of a pipe, the melt was allowed to solidify with the top of the specimen just inside the bottom of the heating coil so that the specimen solidified from the base upwards. The melts were made and allowed to cool in an oxygen-free atmosphere of argon (Meyer and Ronge 1939). For the gallium alloys an attempt was made to remove traces of nitrogen by holding the argon in contact with calcium vapour. Gallium alloys prepared *in vacuo* gave concordant results.

The method of preparation is conducive to some lateral and vertical segregation. Lateral segregation introduces no measurable error in the susceptibility. Since most of the force arises, with the present susceptibility apparatus, in the middle of the specimen, the error as a result of a linear vertical segregation is minimized. The specimens examined microscopically were free from internal holes.

Alloys not near an $\alpha/\alpha+\beta$ boundary were annealed for one week at 550°C in pyrex in an argon atmosphere and air cooled. A specimen $7{\cdot}5\times 20$ mm was machined from the annealed melt. The specimen was acid cleaned before measuring to remove iron contamination as a result of machining.

The analysis of the copper–zinc, gallium and germanium alloys was carried out by measuring the difference between the lattice parameter of pure copper and that of the alloy and by making a comparison with the results of Owen and Roberts (1939). The lattice parameters were determined on a 19 cm Debye–Scherrer Unicam camera with copper radiation,

Fig. 1

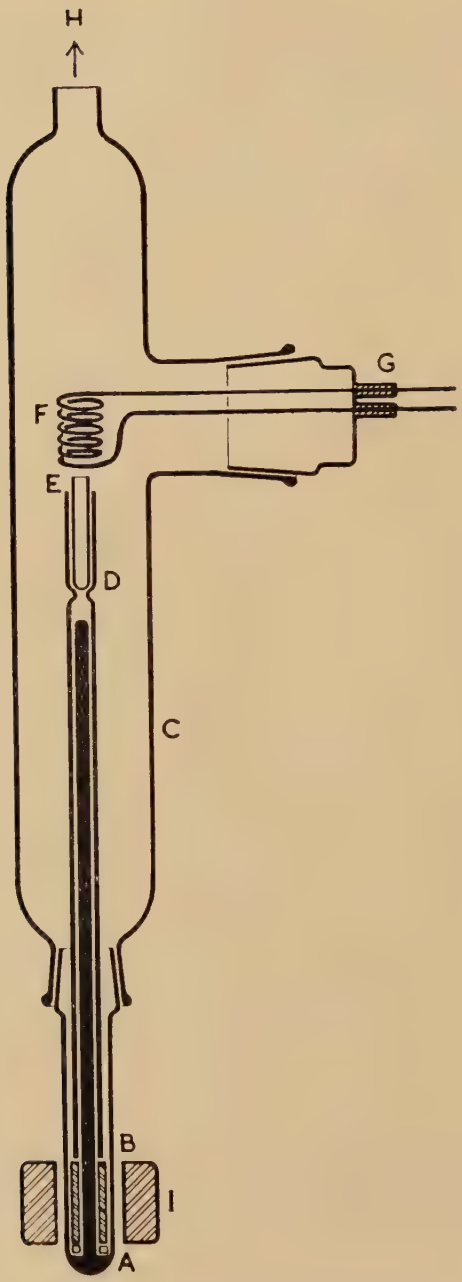

Schematic representation of melting apparatus.

A, rubber shock absorber ; B, iron sleeve ; C, pyrex tube ; D, quartz crucible holder ; E, vitrified alumina crucible ; F, induction coil ; G, de Khotinsky seal ; H, to vacuum system ; I, magnet.

$K\alpha_1 = 1{\cdot}537\,395$ kx. Θ_k was determined by direct measurement. The extrapolation method of Nelson and Riley (1945) was used. The lattice parameter of copper was found to be 3·60765 kx units at 22°C.

For each alloy, filings were taken from the melt as near as possible to the top and bottom surfaces of the machined specimen and the mean of the two compositions was taken. The copper–arsenic alloys were analysed chemically.

§ 3. Magnetic Susceptibility Measurement

The apparatus, method of measurement, errors in susceptibility and method for correcting for ferromagnetic iron have been discussed in an earlier paper (Henry and Rogers 1955). The specimens were inverted after the first measurement and measured again. The susceptibility of the specimen was calculated for each position and then averaged. The measurements were made at room temperature 23±2°C. The atomic susceptibility of an alloy specimen, $\chi_A{}^a$, at infinite field is equal to the product of the mass susceptibility at infinite field, χ_∞, and the mean atomic weight.

The results of the measurements for the four systems are shown in table 1 and fig. 2. The error recorded in the analysis is the probable error in the mean value of the composition of the two ends of the specimen.

Copper–zinc System

The maximum solubility of zinc in copper is 38·5 at. % at 450°C (Raynor 1944). The air-cooled alloy 13 contained no β phase. Alloy 1 was analysed chemically.

The equation, calculated by the method of averages, which fits the points of the atomic susceptibility, composition curve with the precision expected from the probable errors of the susceptibility and composition measurements is

$$-10^6 \times \chi_A{}^a = 5{\cdot}483 + 7{\cdot}21x + 17{\cdot}3x^2 \quad . \quad . \quad . \quad . \quad . \quad (3.1)$$

where x is the mole fraction of zinc in the alloy. This is the equation of the curve shown in fig. 2.

Copper–gallium System

Owen and Rowlands (1940) found the solubility of gallium in copper to be 19·7 at.% at 620°C and 18·8 at.% at 300°C. Their results are approximately lower by 1 at.% than earlier investigations.

The machined specimen from alloy 7 was quenched in iced water in a thin-walled quartz container after 26 hours at 620°C. A section taken from the middle of the specimen contained no β phase. The lattice parameter determinations were made on the quenched specimen.

Copper–germanium System

Owen and Rowlands (1940) found the solubility of germanium in copper to be 11·1 at.% at 750°C and 8·7 at.% at 200°C. Their results, which are

lower, agree within 1 at.% at 750°C and within 1·8 at.% at 200°C with earlier investigations.

The machined specimen from alloy 7 was quenched in iced water from a rapid quench furnace (Owen 1944) after 76 hours at 600°C. No β phase was found in the specimen.

The composition of alloy 1 was calculated from the weights of the constituents. One end only was available for lattice parameter determinations on the specimens from alloys 2 and 6. The compositions as calculated from the weights of the constituents were 1·74 and 5·60.

Copper–arsenic System

Owen and Rowlands (1940) found the solubility of arsenic in copper to be 6·7$_5$ at.% at 603°C and 6·0 at.% at 215°C. Their results are approximately 0·4 at.% higher at 600°C and within 0·1 at.% at 200°C in relation to earlier investigations.

Fig. 2

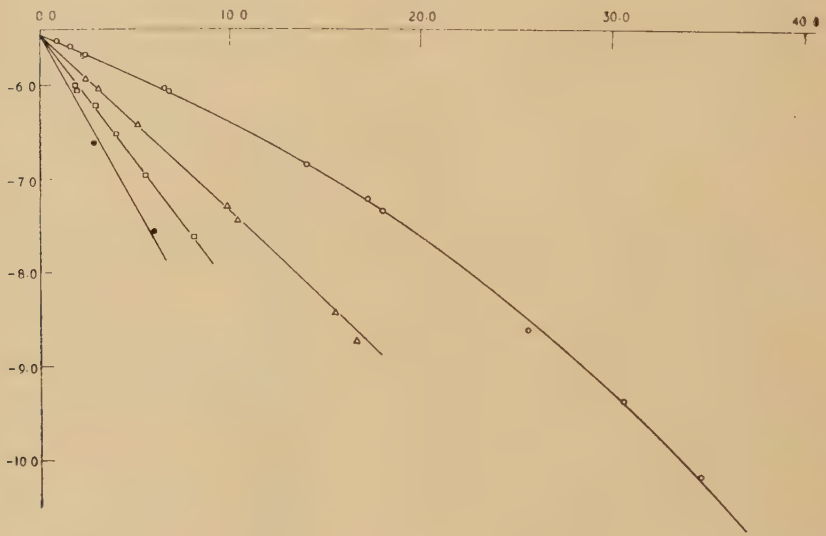

ord. atomic magnetic susceptibility c.g.s. e.m.u. $\times 10^6$.

abs. concentration (atomic %).

Magnetic susceptibility measurements.

O, copper–zinc system; △, copper–gallium system; □, copper–germanium system; ●, copper–arsenic system.

Alloys 1 and 2 were quenched in iced water after 5 days at 600°C. On examination of the machined specimen from alloy 2 no β phase was found.

§ 4. Theoretical Considerations

In this section the ground work will be laid for the discussion of the experimental results of § 3.

Table 1. Magnetic Susceptibility of Solid Solutions

Alloy	Mean lattice parameter difference (Å)	Mean composition (atomic %)	Mean $\chi_{10} \times 10^6$ (c.g.s. e.m.u. per gram)	Mean $\chi_\infty \times 10^6$ (c.g.s. e.m.u. per gram)	Mean $\chi_A{}^a \times 10^6$ (c.g.s. e.m.u. per gram atom)
		Copper–zinc system			
Copper					$-5{\cdot}46_7$
1		$0{\cdot}024 \pm 0{\cdot}002$	$-0{\cdot}0858$	$-0{\cdot}0863$	$-5{\cdot}48$
2	$0{\cdot}0016_5$	$0{\cdot}86 \pm 0{\cdot}02$	$-0{\cdot}0865$	$-0{\cdot}0865$	$-5{\cdot}50$
3	$0{\cdot}0030_0$	$1{\cdot}56 \pm 0{\cdot}07$	$-0{\cdot}0875$	$-0{\cdot}0875$	$-5{\cdot}56$
4	$0{\cdot}0045_0$	$2{\cdot}32 \pm 0{\cdot}09$	$-0{\cdot}0889$	$-0{\cdot}0889$	$-5{\cdot}65$
5	$0{\cdot}0046_5$	$2{\cdot}40 \pm 0{\cdot}03$	$-0{\cdot}0886$	$-0{\cdot}0888$	$-5{\cdot}65$
6	$0{\cdot}0132_5$	$6{\cdot}58 \pm 0{\cdot}08$	$-0{\cdot}0935$	$-0{\cdot}0945$	$-6{\cdot}02$
7	$0{\cdot}0135_9$	$6{\cdot}74 \pm 0{\cdot}12$	$-0{\cdot}0942$	$-0{\cdot}0949$	$-6{\cdot}04$
8	$0{\cdot}0293_1$	$14{\cdot}00 \pm 0{\cdot}08$	$-0{\cdot}1059$	$-0{\cdot}1069$	$-6{\cdot}82$
9	$0{\cdot}0366_2$	$17{\cdot}26 \pm 0{\cdot}01$	$-0{\cdot}1119$	$-0{\cdot}1125$	$-7{\cdot}18$
10	$0{\cdot}0384_4$	$18{\cdot}06 \pm 0{\cdot}03$	$-0{\cdot}1138$	$-0{\cdot}1144$	$-7{\cdot}31$
11	$0{\cdot}0566_8$	$25{\cdot}82 \pm 0{\cdot}20$	$-0{\cdot}1317$	$-0{\cdot}1333$	$-8{\cdot}53$
12	$0{\cdot}0689_5$	$30{\cdot}80 \pm 0{\cdot}03$	$-0{\cdot}1444$	$-0{\cdot}1446$	$-9{\cdot}27$
13	$0{\cdot}0793_2$	$34{\cdot}84 \pm 0{\cdot}17$	$-0{\cdot}1554$	$-0{\cdot}1565$	$-10{\cdot}05$
		Copper–gallium system			
1	$0{\cdot}0063_2$	$2{\cdot}36 \pm 0{\cdot}11$	$-0{\cdot}0922$	$-0{\cdot}0928$	$-5{\cdot}91$
2	$0{\cdot}0083_2$	$3{\cdot}04 \pm 0{\cdot}05$	$-0{\cdot}0939$	$-0{\cdot}0944$	$-6{\cdot}02$
3	$0{\cdot}0144_2$	$5{\cdot}12 \pm 0{\cdot}13$	$-0{\cdot}0996$	$-0{\cdot}1002$	$-6{\cdot}40$
4	$0{\cdot}0282_9$	$9{\cdot}89 \pm 0{\cdot}18$	$-0{\cdot}1134$	$-0{\cdot}1136$	$-7{\cdot}29$
5	$0{\cdot}0296_6$	$10{\cdot}36 \pm 0{\cdot}03$	$-0{\cdot}1152$	$-0{\cdot}1156$	$-7{\cdot}42$
6	$0{\cdot}0448_0$	$15{\cdot}64 \pm 0{\cdot}23$	$-0{\cdot}1292$	$-0{\cdot}1301$	$-8{\cdot}39$
7	$0{\cdot}0478_8$	$16{\cdot}72 \pm 0{\cdot}16$	$-0{\cdot}1334$	$-0{\cdot}1344$	$-8{\cdot}68$
		Copper–germanium system			
1		0·0150	$-0{\cdot}0858$	$-0{\cdot}0861$	$-5{\cdot}47$
2	$0{\cdot}0061_3$	1·84	$-0{\cdot}0933$	$-0{\cdot}0938$	$-5{\cdot}98$
3	$0{\cdot}0063_6$	$1{\cdot}91 \pm 0{\cdot}01$	$-0{\cdot}0941$	$-0{\cdot}0947$	$-6{\cdot}03$
4	$0{\cdot}0095_4$	$2{\cdot}91 \pm 0{\cdot}05$	$-0{\cdot}0967$	$-0{\cdot}0971$	$-6{\cdot}20$
5	$0{\cdot}0130_6$	$4{\cdot}00 \pm 0{\cdot}17$	$-0{\cdot}1005$	$-0{\cdot}1017$	$-6{\cdot}50$
6	$0{\cdot}0180_7$	5·52	$-0{\cdot}1072$	$-0{\cdot}1083$	$-6{\cdot}94$
7	$0{\cdot}0263_0$	$7{\cdot}94 \pm 0{\cdot}04$	$-0{\cdot}1179$	$-0{\cdot}1182$	$-7{\cdot}60$
		Copper–arsenic system			
1	—	$2{\cdot}86 \pm 0{\cdot}20$	$-0{\cdot}1025$	$-0{\cdot}1031$	$-6{\cdot}59$
2		$6{\cdot}00 \pm 0{\cdot}00$	$-0{\cdot}1168$	$-0{\cdot}1171$	$-7{\cdot}52$

Isenberg (1950) and Mott and Jones (1936) have investigated the form of the potential about a solute atom by means of the method of Thomas and Fermi, with and without exchange respectively. They found that the potential was given by

$$\Phi = \frac{Z\mathbf{e}}{r} \exp(-qr) \quad . \quad . \quad . \quad . \quad . \quad . \quad . \quad . \quad (4.1)$$

where $Z+1$ is the number of electrons outside a closed shell. Thus if the solvent is copper, Z is one for zinc and two for gallium. q is a constant depending on the solvent and **e** the electronic charge.

The amount of charge accumulated about a solute atom in a volume equal to the atomic volume of the solvent is

$$\int_0^{r_0} \rho(r)\, 4\pi r^2\, dr = Z\mathbf{e}\,[1-\exp(-qr)]. \quad . \quad . \quad . \quad . \quad . \quad (4.2)$$

r_0 for copper is 1·41 Å. Mott and Jones (1936) give a value for $1/q$ of 0·55 Å and Isenberg (1950) of approximately 0·43 Å. The amount of charge accumulated within a volume equal to the atomic volume of copper is therefore 0·96 $Z\mathbf{e}$ and 0·92 $Z\mathbf{e}$ with and without exchange respectively. It is apparent that according to this model the presence of the other sources of potential do not disturb appreciably the spatial distribution of the Z electrons.

Jones (1937) has discussed the relationship between E, the energy and **k**, the wave vector, in the first Brillouin zone for face-centred cubic copper. The zone is divided into eight prisms and within each prism the following function is set up

$$E = \frac{h^2}{2m}\left[k_x^2 + k_y^2 + (k_0 - k_z)^2 - 2k_0\left\{(k_0-k_z)^2 + \frac{k_0^2}{(\alpha-1)^2}\right\}\right] \quad . \quad (4.3)$$

where k_z is perpendicular to the plane of the energy discontinuity located at k_z equal to k_0. α is related to the magnitude of the energy discontinuity. It is then shown that the limits of solid solubility of zinc, gallium, germanium and arsenic in copper are reasonably consistent with the assumption that the E, **k** relationship of eqn. (4.3) holds and that $Z+1$ electrons occupy states in the band. Friedel (1952) has discussed how accumulated electrons may subtract states from the band.

The E. **k** relationship of eqn. (4.3) may be used (Jones 1937) to calculate the density of states as a function of E (fig. 3). The abscissa electrons (states) per atom has been determined by graphical integration of the curve given by Jones (1937).

In the rigid band approximation used by Jones (1937), it is implicitly assumed that the bottom of the band remains fixed and that the density of states as a function of the number of electrons per atom is not altered by the introduction of the solute atoms. Friedel (1954) has discussed this point on the basis of the assumption that the local density of states in the pure and perturbed solids are related by

$$\rho(E, \mathbf{r}) = \rho_0(E - V_p, \mathbf{r}) \quad . \quad . \quad . \quad . \quad . \quad . \quad . \quad (4.4)$$

where ρ_0 is the density in the unperturbed solid, V_p is the perturbing potential and $\mathbf{r}$ gives the position of the particle. This assumption is only strictly true when V_p is averaged over the whole volume of the metal. This is equivalent only to a change of the zero of potential energy and hence it follows directly that the band preserves its form and is shifted by an amount

$$\mathfrak{E}_0 = \frac{1}{V}\int V_p \, d\tau \qquad \ldots\ldots\ldots \quad (4.5)$$

where V is the volume of the metal and the integration is over the volume.

Fig. 3

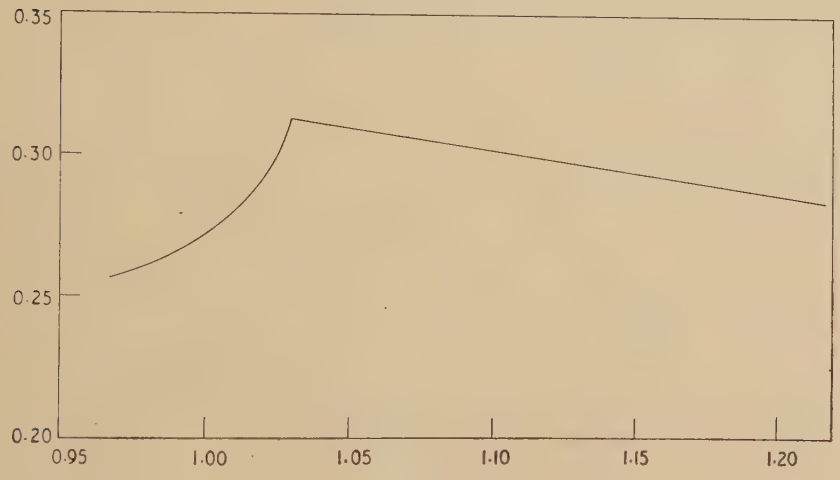

A portion of the density of states curve for face-centred cubic copper (Jones 1937).

It is possible however, without using the relationship (4.4), to demonstrate for a simple model that the top of the band preserves its form and is lowered by an amount $\mathfrak{E}_0$.

The unperturbed wave functions in the free electron model in one dimension are

$$\psi_n = \frac{1}{\sqrt{l}} \sin \frac{n\pi x}{l} \qquad \ldots\ldots\ldots \quad (4.6)$$

where l is the length of the box. Introduce a perturbing potential, V_p, into the box such that V_p is equal to a constant over the distance δ where δ is the length of the unit cell (fig. 4).

First order perturbation theory leads to the result that

$$E_n = \frac{h^2 k_n^{\,2}}{2m} + V_p \left\{ \frac{\delta}{l} + \frac{1}{n\pi} \sin\left(n\pi - \frac{n\pi\delta}{l} \right) \right\} \qquad \ldots\ldots \quad (4.7)$$

where $E_0 = h^2 k_n^{\,2}/2m$ and $k_n = n/2l$. Near the top of the band, the mean energy of a pair of adjacent levels E_{2n} and E_{2n+1}, neglecting terms in $(\delta/l)^2$, is given by

$$\frac{1}{2}\left\{ \frac{h^2 k_{2n}^{\,2}}{2m} + \frac{h^2 k^2_{2n+1}}{2m} \right\} + \frac{V_p \delta}{l} \qquad \ldots\ldots\ldots \quad (4.8)$$

Thus if the levels are considered in pairs, then the mean energy of the two levels in the perturbed system is reduced by approximately $V_p\delta/l$ which is equal to V_p averaged over the volume. The relative distribution of energy levels at the top of the band is not altered appreciably and hence the density of states is approximately the same as in the unperturbed state. The top of the band therefore retains its form and is displaced on the absolute scale by an amount equal to $\mathfrak{E}_0$. Therefore in this approximation Jones' (1937) assumption is correct for the top of the band.

It will be assumed in what follows that the density of states at the top of the band as calculated from eqn. (4.3) holds for the alloys under consideration. It is also assumed that changes in α may be neglected.

Fig. 4

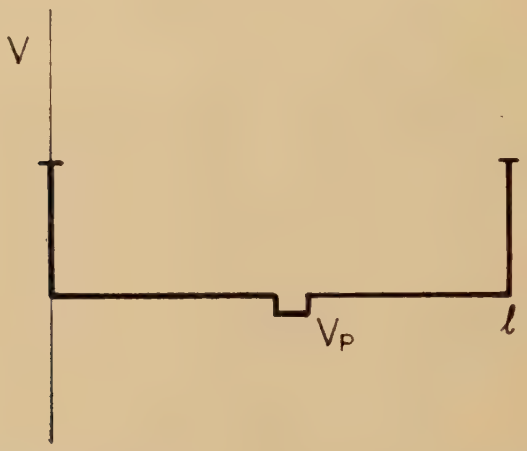

The perturbed potential in a one-dimensional metal of length l.

For the purpose of calculating the magnetic susceptibility of the system, it is convenient to differentiate between two classes of electrons. The model discussed at the beginning of the section suggests that the electrons localized about a lattice site should be grouped together, while the electron outside the $3d^{10}$ shell of copper and one of the outermost electrons of the solute atoms should form another. It will be assumed that the potential function for the former is independent of the positions of electrons and nuclei at other lattice sites and is that of the free neutral atom. That is the Fermi electrons are allowed to screen. The potential function for the latter electrons is dependent on the position of all the other electrons and nuclei.

The atomic susceptibility of the localized electrons is given by the sum of the susceptibilities of the ions

$$\chi_A = \frac{\mathbf{e}^2}{8mc^2} \sum_n \int |\phi_n|^2 (x^2+y^2)\, d\tau \qquad \ldots\ldots (4.9)$$

where the summation is over all solute and solvent lattice sites in a gram

atom of alloy. ϕ_n are the respective atomic wave functions of the singly ionized atoms. The integration is over the volume about a lattice site. The formula for the ionic susceptibility is due to Stoner (1929).

For the essentially free electrons in a pure metal it may be shown (Wilson 1936) that the diamagnetic contribution consists of several terms: $\chi_{A,\,1}$, $\chi_{A,\,2}$ and $\chi_{A,\,3}$.

The first is given by,

$$\chi_{A,\,1}=-\frac{1}{12\pi^2}\gamma^2\int\int\left\{\frac{\partial^2 E}{\partial k_x^{\,2}}\frac{\partial^2 E}{\partial k_y^{\,2}}-\frac{\partial^2 E}{\partial k_x \partial k_y}\right\}\frac{2V}{|\mathrm{grad}\,E|}dS \quad . \quad (4.10)$$

which is proportional to the density of states at the top of the band. $\gamma=\mathbf{e}/2hc$ and V is the volume of a gram atom of alloy. If $E(\mathbf{k})$, which retains cubic symmetry, as given by eqn. (4.3), is substituted into (4.10)

$$\chi_{A,\,1}=-\frac{2}{3}\beta^2\int\int\frac{2V}{|\mathrm{grad}\,E|}dS \quad . \quad . \quad . \quad . \quad . \quad (4.11)$$

where $\beta=\mathbf{e}h/4\pi mc$ and the integral is equal to the density of states per atom per erg at the Fermi surface.

$\chi_{A,\,2}$ and $\chi_{A,\,3}$ may be neglected for free electrons since they are proportional to

$$\frac{\Omega}{V}\times\text{the atomic susceptibility of one bound electron} \quad . \quad . \quad (4.12)$$

where Ω is the atomic volume.

The paramagnetic susceptibility of electrons in a band is given by (Frenkel 1928)

$$\chi_A=2\beta^2\int\int\frac{2V}{|\mathrm{grad}\,E|}dS. \quad . \quad . \quad . \quad . \quad . \quad . \quad (4.13)$$

It is to be noted that $|\chi_{A,\,1}|$, as given by (4.11), is equal to one third the paramagnetic contribution, which is the same result as for free electrons.

§ 5. Discussion of Results

In this section an interpretation of the experimental results of § 3 is given which depends on the assumptions discussed in § 4. The interpretation applies to the initial slopes of the susceptibility, composition curves. All magnetic susceptibilities in this section are in atomic c.g.s. e.m.u.

Let the susceptibility of the alloy, $\chi_A{}^a$ be represented by

$$\chi_A{}^a=(1-x)\,\chi_A^{i,1}+x\,(\chi_A{}^{i,\,2}+\chi_A{}^e)+\chi_A{}^F(x) \quad . \quad . \quad . \quad . \quad (5.1)$$

where x is the mole fraction of the solute; $\chi_A{}^{i,\,1}$ is the susceptibility of the Cu^+ ion; $\chi_A{}^{i,\,2}$ is the susceptibility of the solute ion, $1s^22s^22p^63s^23p^63d^{10}$; $\chi_A{}^e$ is the susceptibility of the localized electrons. $\chi_A{}^F(x)$ is the net paramagnetic contribution of the band. If the variation of $\chi_A{}^a$ is linear with x then

$$\frac{\chi_A{}^a-\chi_A{}^{\mathrm{Cu}}}{x}=(\chi_A{}^{i,\,2}+\chi_A{}^e)-\chi_A{}^{i,\,1}+\frac{d\chi_A{}^F(x)}{dx} \quad . \quad . \quad . \quad . \quad (5.2)$$

where $\chi_A{}^{\mathrm{Cu}}$ is the susceptibility of pure copper.

The first term on the right-hand side of eqn. (5.2) may be evaluated by using eqn. (4.9). The formula used for mechanical quadrature was Simpson's Rule. The self-consistent fields with exchange for copper (Hartree and Hartree 1936 b) and without exchange for zinc, gallium, arsenic (Hartree, Hartree and Manning 1941 a), germanium (Hartree, Hartree and Manning 1941 b) and aluminium (Biermann and Harting 1942) were used for the spatial charge distribution.

Hartree and Hartree (1936 b) showed that the susceptibility of the singly charged copper ion calculated from the field with exchange ($-14{\cdot}67\times10^{-6}$) agreed better with the experimental value (-14×10^{-6}) than that calculated from the field without exchange ($-18{\cdot}54\times10^{-6}$). This conclusion is also borne out by the work of Klemm (1940) and Stoner (1929) who calculated the susceptibility of argon with and without exchange respectively to be $-20{\cdot}6\times10^{-6}$ and $-24{\cdot}8\times10^{-6}$. The most probable experimental value for argon (Klemm 1940) is $-19{\cdot}4\times10^{-6}$.

Table 2. Calculated Values of $\chi_A{}^{i,\,2}$ and $\chi_A{}^{e}$

Ion or group	$\chi_A\times10^6$ without exchange (c.g.s. e.m.u.)	$\chi_A\times10^6$ with exchange (c.g.s. e.m.u.)
Zn^{2+}	−14·39	—
$Zn(4s)^1$	− 8·9	—
Ga^{3+}	−11·4	—
$Ga(4s)^2$	−12·2	—
Ge^{4+}	− 9·56	—
$Ge(4s)^2(4p)^1$	−20·9	—
As^{5+}	− 8·25	—
$As(4s)^2(4p)^2$	−24·45	—
Al^{3+}	− 3·14	—
$Al(3s)^2$	−12·20	—
Cu^{+}	−18·54	−14·67
Si^{4+}	− 2·45	− 2·28
Cl^{-}	−41·3	−30·4
C^0	−13·09	−10·8
A	−24·8	−20·6

The calculated values for the copper ion and argon from the fields with exchange have been verified by the authors. An exchange correction was applied where necessary in the present work by multiplying by a factor 0·800. The factor was arrived at by making a comparison of values determined from fields with and without exchange. The five cases where this is possible are: Si^4 , Cl^-, Cu^+, A and C^0 for which the ratios are: 0·937, 0·736, 0·790, 0·831 and 0·823. The calculated values of $\chi_A{}^{i,\,2}$ and $\chi_A{}^{e}$ are summarized in table 2.

The following self-consistent fields were used to obtain the values contained in table 2: Si^{3+}, without exchange (MacDougall 1932); Si^{4+},

with exchange (Hartree, Hartree and Manning 1941 c); C^0, without exchange (Torrance 1934); C^0, with exchange (Jucys 1939). The values of χ_A for Cl^- were calculated by Hartree and Hartree (1936 a).

The third term was evaluated as follows. Beyond the peak, the density of states curve for pure copper is approximately a linear function of x (see fig. 3). It follows that $\chi_A{}^F(x)$ for an alloy in which there is no volume change, varies linearly with x. It is assumed that $\chi_A{}^F(x)$ reduces to the value required to obtain numerical agreement with the observed value for copper and thus

$$\chi_A{}^F(x)=\chi_A{}^F(0)-5{\cdot}2Zx\times10^{-6} \quad . \quad . \quad . \quad . \quad . \quad (5.3)$$

where $\chi_A{}^F(0)$ is equal to the observed susceptibility of copper less $\chi_A{}^{i,1}$.

For free electrons and a parabolic band, it may be shown that

$$\frac{\chi_A{}^F(x)}{\chi_A{}^F(0)}=\frac{d(x)^2}{d(0)^2} \quad . \quad . \quad . \quad . \quad . \quad . \quad . \quad . \quad . \quad (5.4)$$

where $d(x)$ and $d(0)$ are the lattice parameters of the alloy and copper respectively. It may be shown that (5.4) is a good approximation for the band shape calculated by Jones (1937) and therefore

$$\frac{d\chi_A{}^F(x)}{dx}\simeq2\zeta\chi_A{}^F(0)=5{\cdot}2Z\times10^{-6} \quad . \quad . \quad . \quad . \quad . \quad . \quad (5.5)$$

where ζ is the proportional change in lattice parameter for unit concentration (Owen 1947).

The calculated and observed values of the slope are shown in table 3. The observed (Vogt and Harms 1942–1943) and calculated results for the copper–aluminium system are included to demonstrate the applicability of the method. No explanation is offered for the marked variation of slope with concentration in the copper–zinc system.

If the experimentally determined susceptibilities are plotted against electron to atom ratio a superposition occurs. If the explanation suggested in this paper is substantially correct, then there appears to be, in this case, no special significance attached to the superposition.

Table 3. Calculated and Observed Slopes

(1)	(2)	(3)	(4)	(5)	(6)	
					calc.	obs.
Copper–zinc	−11·5	− 7·1	14·7	1·0– 5·2	− 8·1	− 7·2
Copper–gallium	− 9·2	− 9·8	14·7	1·4–10·4	−13·3	−19·3
Copper–germanium	− 7·7	−16·7	14·7	1·7–15·6	−23·6	−27·4
Copper–arsenic	− 6·6	−19·5	14·7	2·4–20·8	−29·8	−38±2
Copper–aluminium	− 2·5	− 9·8	14·7	1·3–10·4	− 6·7	− 6·8

(1) Alloy system, (2) $\chi_A{}^{i,2}\times10^6$ (c.g.s. e.m.u. per gram atom of solute), (3) $\chi_A{}^e\times10^6$ (c.g.s. e.m.u. per gram atom of solute), (4) $-\chi_A{}^{i,1}\times10^6$ (c.g.s. e.m.u. per gram atom of solvent), (5) $(d\chi_A{}^F(x)/dx)\times10^6$ (c.g.s. e.m.u. per gram atom of alloy), (6) $(\chi_A-\chi_A{}^{Cu}/x)\times10^6$ (c.g.s. e.m.u. per gram atom of alloy).

Friedel (1952) took as his expression for the slope, eqn. (5.2) with $d\chi_A{}^F(x)/dx$ equal to zero. It will be seen from table 3 that, in the case of

the copper–aluminium system, the susceptibility of the ion core plus the $(3s)^2$ electrons is approximately cancelled by $\chi_A^{i,1}$ and that a major contribution to the slope comes from $d\chi_A^F(x)/dx$. Friedel calculated the susceptibility of the singly charged aluminium ion by a method due to Slater (1930). The present authors have repeated the calculation and find the susceptibility to be $-10{\cdot}6\times10^{-6}$, in reasonable agreement with the result calculated from eqn. (4.9), as against the value $-23{\cdot}5\times10^{-6}$ calculated by Friedel. The error gave him agreement with experiment.

Friedel (1954) included a term taking into account the paramagnetism of the conduction electrons. The slope, in our notation, is given by

$$\frac{\chi_A^a-\chi_A^{Cu}}{x}=(\chi_A^{i,2}+\chi_A^e)-\chi_A^{i,1}+\frac{ZX\chi_A^F(0)}{3p} \quad . \quad . \quad (5.6)$$

where p is one for copper. The third term with X equal unity is $d\chi_A^F(x)/dx$ for the case of a parabolic band with no volume change, and the assumption that the constant of proportionality between the density of states and the net paramagnetism of the free electrons, is determined by $\chi_A^F(0)$ for copper. The factor X is introduced in a further approximation of his treatment of primary solid solutions based on the approximation discussed in § 4. The value of 0·7 is given for copper for X.

Friedel (1954) makes the following errors in the calculation of the slope; (1) places Z equal to one instead of two for aluminium, (2) discards the diamagnetism of the conduction electrons, see § 4, (3) uses the incorrectly computed value for the susceptibility of the aluminium ion, (4) quotes $-5{\cdot}9$ as the slope for the copper–aluminium system, whereas the observed value, contained in his first paper (Friedel 1952), is $-6{\cdot}8$. When the necessary corrections are made to the calculations the slope has the wrong sign. The reason for this lies in the fact that a parabolic band has been assumed for which $d\chi_A^F(x)/dx$ is positive.

It is interesting to calculate the mean radius for the localized electrons which would be necessary to give a sufficiently large negative contribution to the slope to give agreement with experiment for a case of a parabolic band. It is assumed that the spatial distribution of the electrons $1s^22s^22p^63s^23p^63d^{10}$ is as before. For an electron in an orbit of radius r

$$\chi_A=\frac{N\mathbf{e}^2}{6m}\overline{r^2}. \quad . \quad . \quad . \quad . \quad . \quad . \quad . \quad . \quad (5.7)$$

If the corrected value for the third term in eqn. (5.6) is used, then the necessary mean radii are 2·40 Å and 2·22 Å for zinc and gallium respectively. These are comparable to the closest distances of approach and hence the model is unlikely.

The peak of the calculated density of states curve for copper (fig. 3) occurs at an electron to atom ratio of 1·03 which corresponds to 3 at.% zinc. No discontinuity in the susceptibility, composition curve (fig. 2) indicating a peak is observed. It is to be concluded therefore that in copper the band is filled up to or beyond the peak.

§ 6. Remarks on Bound States

Mott (1952) and Friedel (1952) have suggested that a bound state will exist when

$$I_2{}^1 < I_1 + W_1 + \tfrac{2}{5} E_F \quad . \quad . \quad . \quad . \quad . \quad . \quad . \quad (6.1)$$

where $I_2{}^1$ is the second ionization potential of the solute; I_1, W_1 and I_2 are the first ionization potential, the heat of sublimation and the Fermi energy of the solvent. The right-hand side of (6.1) is an approximation to the energy of the bottom of the band.

The case of the singly occupied state is particularly interesting. Equation (6.1) indicates that the lone localized electron of zinc dissolved in copper should be in a bound state. An unpaired electron associated with each zinc solute would result in a large positive slope. In order to explain the experimentally observed negative slope, they suggest that there is a sufficient screening by the Fermi electrons to raise the level into the band. The work of Davies and Keeping (1929) on the copper–magnesium and copper–antimony systems and of Spencer and John (1927) on the silver–lead system are cited as examples where singly occupied states exist.

In order to test this hypothesis, one or two points in the primary solid solution region of the following systems were measured: (1) with copper as solvent, magnesium, aluminium, zinc, gallium, germanium, arsenic, cadmium, indium, tin and antimony; (2) with silver as solvent, aluminium, zinc, gallium, germanium, cadmium, indium, tin, antimony, mercury, lead and bismuth; (3) with gold as solvent, magnesium, aluminium, zinc, gallium, germanium, cadmium, indium and tin. An indication of a singly occupied state as envisaged by Mott (1952) and Friedel (1952) was not found in any case. The primary solid solution region of the silver–lead system has been recently investigated by Vogt (1954) who also found no indication of a large paramagnetism. The systems enumerated here will be treated in more detail in a later paper.

The work on the four primary solid solutions discussed leads to the following conclusions. The spin of the localized ' 4s like ' electron of the zinc solute is quenched at all concentrations. Both the spin and the orbital motion of the localized ' 4p like ' electron of the germanium solute is quenched at all concentrations. The number of electrons localized about a solute site is approximately equal to Z where $Z+1$ is the valency, in the Hume-Rothery sense, of the solute. The density of states for the alloys at low concentrations decreases with increasing electron to atom ratio with approximately the same slope as that calculated for pure copper (Jones 1937). The number of states occupied in the perturbed band per solute atom is equal to $Z+1$.

Acknowledgments

The authors wish to thank Mr. A. Blair and Mr. K. Hyndman for preparing the specimens, Mr. D. S. Russell for chemical analysis and Miss R. Pothier for carrying out various computations.

References

Biermann, L., and Harting, H., 1942, *Z. Astrophys.*, **22,** 81.
Davies, W. G., and Keeping, E. S., 1929, *Phil. Mag.*, **7,** 145.
Endo, H., 1925, *Sci. Rep. Tohoku Univ.*, **14,** 479.
Frenkel, J., 1928, *Z. Phys.*, **49,** 31.
Friedel, J., 1952, *Phil. Mag.*, **43,** 153 ; 1954, *Advances in Physics*, **3,** 446.
Hartree, D. R., and Hartree, W., 1936 a, *Proc. Roy. Soc.* A, **156,** 45 ; 1936 b, *Ibid.*, **157,** 490.
Hartree, W., Hartree, D. R., and Manning, M. F., 1941 a, *Phys. Rev.*, **59,** 299 ; 1941 b, *Ibid.*, **59,** 306 ; 1941 c, *Ibid.*, **60,** 857.
Henry, W. G., and Rogers, J. L., 1956, *Phil. Mag.*, **1,** 223.
Isenberg, I., 1950, *Phys. Rev.*, **79,** 736.
Jones, H., 1937, *Proc. Phys. Soc.*, **49,** 250.
Jucys, A., 1939, *Proc. Roy. Soc.* A, **173,** 59.
Klemm, W., 1940, *Z. anorg. Chem.*, **244,** 377.
MacDougall, J., 1932, *Proc. Roy. Soc.* A, **138,** 550.
Meyer, F. R., and Ronge, G., 1939, *Angew. Chem.*, **52,** 637.
Mott, N. F., 1952, *Progress in Metal Physics* (New York : Interscience Publishers Inc.), **3,** 102.
Mott, N. F., and Jones, H., 1936, *The Theory of the Properties of Metals and Alloys* (Oxford : The Clarendon Press), p. 86.
Nelson, J. B., and Riley, D. P., 1945, *Proc. Phys. Soc.*, **57,** 160.
Owen, E. A., 1944, *J. Sci. Instrum.*, **21,** 65 ; 1947, *J. Inst. Met.*, **73,** 471.
Owen, E. A., and Roberts, E. W., 1939, *Phil. Mag.*, **27,** 294.
Owen, E. A., and Rowlands, V. W., 1940, *J. Inst. Met.*, **66,** 361.
Raynor, G. V., 1944, *Annotated Equilibrium Diagrams*, No. 3 (London : The Institute of Metals).
Slater, J. C., 1930, *Phys. Rev.*, **36,** 57.
Spencer, J. F., and John, M. E., 1927, *Proc. Roy. Soc.* A, **116,** 61.
Stoner, E. C., 1929, *Proc. Leeds phil. lit. Soc.*, **1,** Pt. 10, 484.
Torrance, C. C., 1934, *Phys. Rev.*, **46,** 388.
Vogt, E., 1954, *App. sci. Res.* B, Hague, **4,** 34.
Vogt, E., and Harms, B., 1942–1943, *Ann. Phys., Lpz.*, **42,** 501.
Wilson, A. H., 1936, *The Theory of Metals* (Cambridge : University Press), p. 118.

XXIII. *The Daily Variation of the Cosmic Ray Intensity Measured Near the 1954 Sunspot Minimum*

By M. Possener* and I. J. van Heerden†
The Physical Laboratories, The University of Manchester‡

[Received October 14, 1955]

Summary

The solar daily variation of the ionizing component of cosmic radiation has been measured at sea-level by means of unshielded counter telescopes pointing in the north and south directions at a zenith angle of 45° during the years 1948, 1951, 1952, 1953 and 1954. The amplitude of the daily variation has decreased steadily over these years. For several months during 1953 and 1954, the variation showed an anomolous change in phase, the time of maximum intensity occurring during the night. During these months, the amplitude of the daily variation of the nucleonic component of cosmic radiation was found to decrease to a value not significantly different from zero.

§ 1. Introduction

It has been shown that the solar daily variation of the ionizing component of cosmic radiation at sea-level does not remain constant in amplitude or in phase from year to year but shows changes which appear to be related to the sunspot cycle (Thambyahpillai and Elliot 1953, Sarabhai and Kane 1953). It has also been shown that the solar variation depends on the orientation of the direction of maximum sensitivity of the measuring instrument (Malmfors 1949, Elliot and Dolbear 1950). For counter telescopes inclined to the north and south, these authors have found that although the amplitude is about the same for both directions, the time of maximum is later for the south-pointing telescope than for the north. Brunberg and Dattner (1954) have estimated from this that the mean momentum of the primary cosmic radiation giving rise to the daily variation is about 2×10^{10} ev/c.

This paper gives details of the solar daily variation near the sunspot minimum of 1954 measured with counter telescopes and also with a neutron monitor. This latter type of apparatus has only been in operation for a short time so no information on the long-term changes in amplitude or in phase of the solar daily variation of the nucleonic component is available.

---

* Now at Imperial College, London.

† Now on leave from the National Physical Laboratory, Pretoria, South Africa.

‡ Communicated by Professor P. M. S. Mackett, F.R.S.

§ 2. Description of Apparatus

(*a*) *Counter Telescopes*

The ionizing component of cosmic radiation at sea-level has been continuously recorded in Manchester ($\lambda_{\text{geomag}}=57°$N.) since 1951 using the apparatus described by Elliot and Dolbear. Briefly summarized, this consisted of two independent arrays of unshielded Geiger–Muller counters, each array comprising three trays with ten counters in each tray (active area 2 400 cm^2) ; one array pointed towards the south at an angle of 45° to the vertical and the other towards the north. Adjacent trays were separated by 6·5 cm so that the solid angle within which particles could be accepted was large ; in the north–south plane each array had maximum sensitivity (defined as the product of the effective area and the intensity of radiation in that direction) at a zenith angle of 25°. The sensitivity dropped to half its maximum value at an angle of 27° on either side. In the plane inclined at 25° to the vertical in the east–west direction, the half-width was about 40°. The counting rate was ~50 000 three-fold coincidences per hour from each array.

(*b*) *Neutron Monitor*

The nucleonic component of the cosmic radiation at sea-level was recorded in Manchester by means of a neutron monitor. This consisted of a block of lead surrounded by paraffin wax which slowed down to thermal energies the neutrons emitted from stars produced in the lead by fast nucleons. The thermal neutrons were then detected by three proportional counters containing enriched boron trifluoride, which were connected in parallel and placed inside the lead. The output pulses from the counters were fed through a high gain amplifier to a discriminator and scaling unit. The output of the scaling unit was used to drive a mechanical counter which was photographed every hour. The counting rate was about 2 500 neutrons per hour.

§ 3. Experimental Results

(*a*) *Results obtained from Counter Telescopes*

In order to eliminate any systematic difference which may have existed between the two arrays, the apparatus was rotated through 180° about a vertical axis at fortnightly intervals. One year's data for each array were harmonically analysed, each array having spent the same number of days pointing north and south. The first and second harmonic coefficients of the daily variation agreed within the statistical error, thus verifying the absence of any systematic difference.

Figure 1 shows the solar daily variations for the north and south directions averaged over periods of approximately one year each. The bi-hourly totals for each year have been corrected for variations in atmospheric pressure. The standard deviations shown were estimated from the total number of particles counted in each bi-hourly period (about 3×10^7 for each direction). The curves drawn through the experimental points are the sums of the first and second harmonics of

best fit. Similar curves obtained for 1948 by Elliot and Dolbear are shown for comparison. The experiment was discontinued during 1954 so that 1953 was the last complete year's results available.

Fig. 1

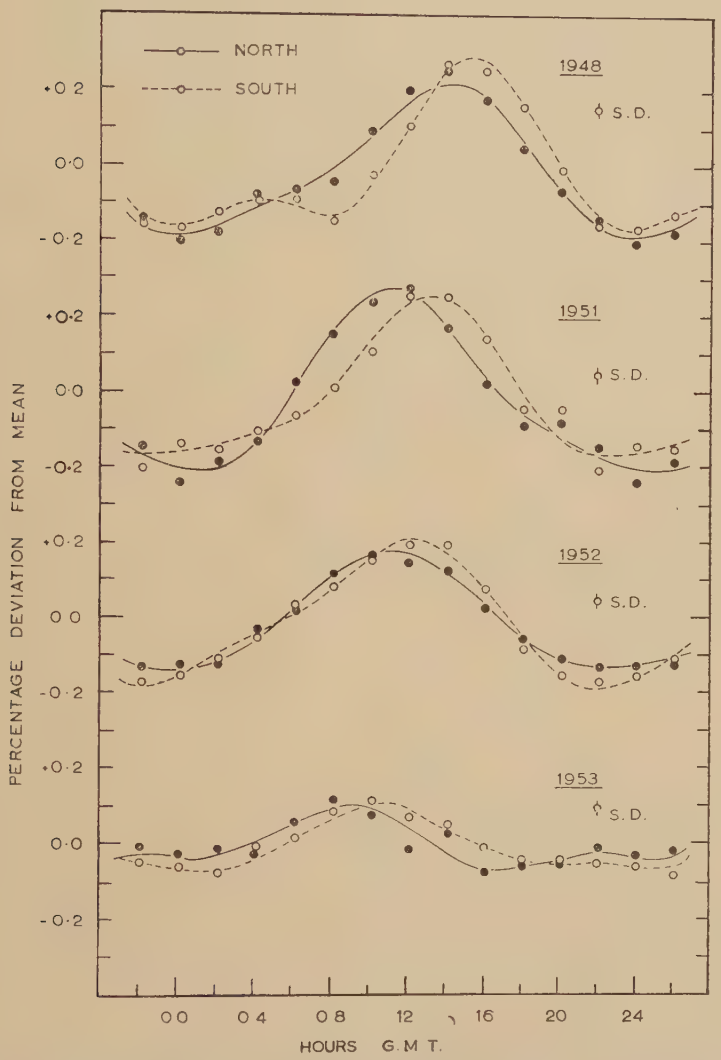

Yearly means of the solar daily variation in the ionizing component of cosmic ray intensity measured in the north and south directions.

Discussion

Several points are noticeable from fig. 1.

1. The mean time of maximum of the daily variation for the two directions gradually became earlier from 1948 to 1952 as was shown by Thambyahpillai and Elliot in their curve illustrating the world-wide

secular change in phase of the daily variation. The time of maximum for 1953 is earlier still and fits in well with the downward trend of their curve.

2. The amplitude of the daily variation decreased from 1948 to 1953 in agreement with the results of Sarabhai and Kane for the sunspot minimum of 1944.

3. The differences in phase between the two directions decreased from 1948 to 1953. Although the phase difference in 1953 appears to be greater than that in 1952, the error in the phase difference for 1952 is large ($\sim$1·2 hours) due to the small amplitude. This trend towards smaller phase difference would seem to indicate, on the argument of Brunberg and Dattner, that the momentum of the primary particles giving rise to the daily variation has decreased from 1948 to 1953.

(*b*) *Abnormal Time of Maximum of the Daily Variation*

Since the amplitude of the mean daily variation in 1953 was a factor of two smaller than that in 1952, the variation for each month in 1953 was investigated to see whether large changes occurred from month to month. It was found that the times of maximum of the monthly mean daily variations were near midnight for July, August and September, whereas they were near 10 hours for the rest of the year. Figure 2 shows on harmonic dials the first harmonics of the daily variation in the two directions during specified groups of months; all the data have been corrected for variations in atmospheric pressure. The circles indicate the standard error in the amplitude calculated from the total number of counts in each period.

Fig. 2

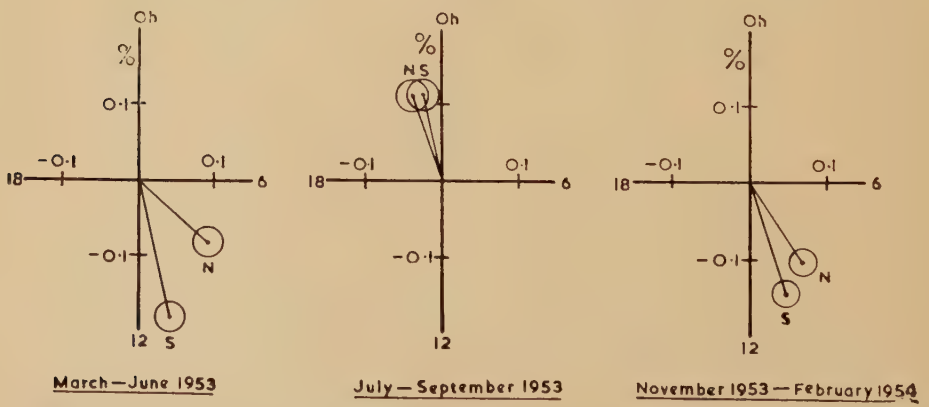

Harmonic dials showing the first harmonic of the daily variation in the ionizing component measured in the two directions during the periods shown.

It can clearly be seen that

1. For the months March to June inclusive, the mean time of maximum was about 10 hours local time.

2. For July to September, the mean time of maximum was about 23 hours.

3. For the months November 1953 to February 1954, the mean time of maximum returned to 10 hours.

Both the north- and south-pointing telescopes showed this abnormal time of maximum and the phase difference between the two directions became non-significant for the second and third groups of months.

Thus, for a period of about four months in 1953, the time of maximum of the solar daily variation was almost twelve hours different from its mean value for the rest of the year. This was obviously one of the reasons why the mean amplitude during 1953 was much smaller than the mean during 1952. However, the mean amplitude during the other eight months in 1953 was still found to be smaller than the mean amplitude over the same period in 1952 although only by two standard deviations.

Data until June 1954 were available and were similarly investigated to see if this unusual effect was repeated. It can be seen from fig. 3 that the time of maximum of about 10 hours G.M.T. was retained during March to May 1954 and then in June 1954, the time of maximum for both directions moved to about 04 hours.

Fig. 3

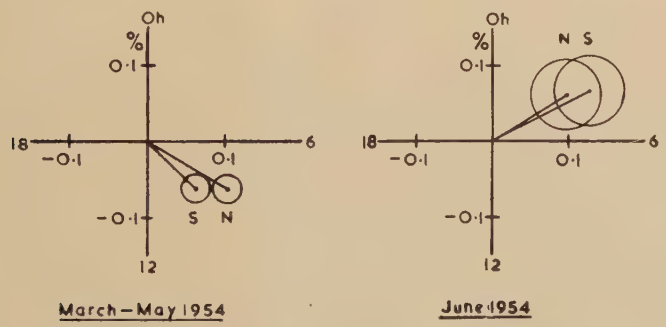

Harmonic dials showing the first harmonic of the daily variation in the ionizing component measured in the two directions during the periods shown.

From the beginning of August 1954, the two counter telescopes were set up in London ($\lambda_{\text{geomag}} = 54°\text{N}$) so as to measure the cosmic ray intensity in the vertical direction. In order to see whether data obtained in Manchester with the apparatus inclined at 45° could be directly compared with data obtained in London from the same apparatus pointing vertically, data obtained by Rothwell and Elliot (private communication) were examined. They used a similar apparatus in London pointing vertically whilst the inclined apparatus in Manchester was still operating. The daily variation from the vertical apparatus showed no significant difference from the mean of the daily variations in the north and south directions, thus showing that results obtained from the vertical apparatus could be directly compared with those from the inclined apparatus.

Figure 4 shows the daily variation of cosmic radiation recorded in London by the apparatus directed towards the vertical. The data were corrected for variations in atmospheric pressure. During the months August to November 1954, the time of maximum occurred at about 03 hours as it did in June. During the months December 1954 to February 1955, the time of maximum returned to about 10 hours. Steinmaurer and Gheri (1955) have reported that during July to September 1954, the daily variation of cosmic radiation recorded by a shielded ionization chamber on the Hafelekar (2 300 metres above sea-level at geomagnetic latitude 47°N) also showed a time of maximum at 2 a.m.

Fig. 4

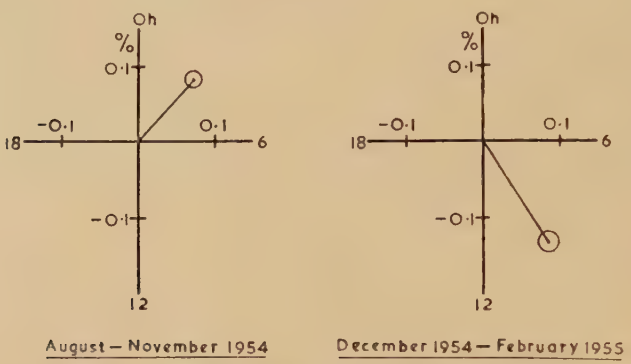

Harmonic dials showing the first harmonic of the daily variation in the ionizing component measured in the vertical direction during the periods shown.

During the first half of 1955, the time of maximum remained at 10 hours but in August and September it moved to 06 hours. This change in phase appears to be much less pronounced than that which occurred during the previous two years and seems to indicate that the effect is gradually decreasing with the beginning of a new cycle of solar activity.

(*c*) *Results obtained from the Neutron Monitor*

The daily variation in the nucleonic component recorded by the neutron monitor was investigated to see whether any changes in amplitude or in phase had occurred at the same time as those in the ionizing component. Until June 1954 the monitor was operating in Manchester, whilst from September 1954 it was operating in London. This change in geomagnetic latitude of 3° was considered too small to make any significant difference to the response of the neutron monitor ; the two sets of data obtained in Manchester and in London were therefore directly compared.

Significant results were obtained by combining data for the same periods in both 1953 and 1954, having corrected the data for variations in atmospheric pressure. Thus, on the harmonic dial of fig. 5, point 1 represents the first harmonic of the mean daily variation the in nucleonic component

for the months in 1953 and 1954 which preceded the two periods of unusual time of maximum in the ionising component, i.e. it represents the mean daily variation over the months March to June 1953 and March to May 1954. Point 2 represents the first harmonic of the mean daily variation during the two periods of unusual time of maximum, namely, (1) July to October 1953 and (2) June, September, October and November 1954. Point 3 covers the months after the two periods of unusual behaviour, namely, November 1953 to February 1954 and December 1954 to March 1955.

It can be seen from fig. 5 that although the time of maximum of the first harmonic remained remarkably constant over the three periods, the amplitude during the period of unusual behaviour had decreased to a value not significantly different from zero.

Fig. 5

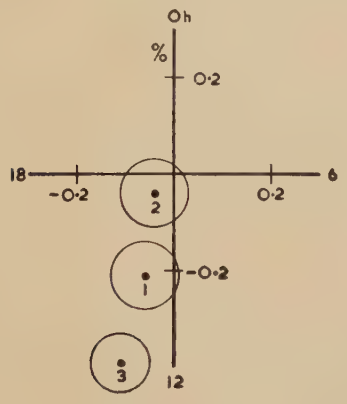

Harmonic dial showing the first harmonic of the mean solar daily variation in the nucleonic component.

(*d*) *Sunspot Minimum of* 1944

Since this unusual behaviour in the daily variation occurred near the sunspot minimum of 1954, it was of interest to see if there was any evidence for a similar effect during the last sunspot minimum in 1944. The ionization chamber data for Cheltenham, U.S.A., Christchurch, New Zealand, and for Huancayo, Peru (Lange and Forbush 1948) were analysed and the mean daily variation for groups of three months was determined for the years 1943, 1944, 1945 (1945 data for Christchurch were missing). Although there were indications at both Cheltenham and Christchurch that the time of maximum of the mean daily variation during August to October 1944 occurred an hour or so earlier than for the remaining groups of months, no change in the time of maximum as large as that reported above for the ionizing component was detected. There seems, therefore, to be a significant difference between the behaviour of the daily variation at the two sunspot minima.

§ 4. Conclusion

Measurements of the daily variation of the cosmic ray intensity at sea-level during the past few years have revealed the presence of changes in amplitude and phase of the variation. In particular, during 1953 and 1954, which were years of minimum sunspot activity, the variation has shown remarkable changes over the course of the year. During July, August and September 1953, the time of maximum intensity of the ionizing component occurred at about 23 hours, whereas for the rest of the year it was near 10 hours. Again, during the period June to November 1954, the time of maximum was at 03 hours compared with 10 hours for the remainder of the year. During these months of anomalous behaviour, the amplitude of the daily variation for the nucleonic component decreased to a value which was not statistically different from zero. These remarkable changes in the daily variation seemed to have been a peculiarity of the 1954 sunspot minimum since, as far as can be seen, there were no comparable changes during the 1944 minimum.

Acknowledgments

We are indebted to Dr. H. Elliot for his constant advice and supervision and to Professor P. M. S. Blackett for providing the facilities for this work. One of us (M.P.) wishes to thank the Department of Scientific and Industrial Research for a maintenance grant ; the other (I.J.v.H.) wishes to thank the British Council for a scholarship.

References

Brunberg, E. A., and Dattner, A., 1954, *Tellus*, **6**, 1.
Elliot, H., and Dolbear, D. W. N., 1950, *Proc. Phys. Soc.* A., **63**, 137.
Lange, I., and Forbush, S. E., 1948, *Carnegie Institution of Washington Publication* 175.
Malmfors, K. G., 1949, *Tellus*, **1**, 2.
Sarabhai, V., and Kane, R. P., 1953, *Phys. Rev.*, **90**, 204.
Steinmaurer, R., and Gheri, H., 1955, *Naturwiss.*, **42**, 10, 204.
Thambyahpillai, T., and Elliot, H., 1953, *Nature, Lond.*, **171**, 918.

XXIV. *The Inelastic Scattering of* 2·5 MEV *Neutrons by Chromium, Manganese and Vanadium*

By L. E. BEGHIAN, D. HICKS and B. MILMAN
Clarendon Laboratory, Oxford *

[Received October 3, 1955]

ABSTRACT

Experiments have been carried out on the inelastic scattering of 2·5 MEV neutrons by chromium, manganese and vanadium. Both gamma-rays and inelastically scattered neutrons were observed. The following levels were identified :

Chromium 1·44±0·03 MEV, Manganese 0·126±0·005 MEV, 0·98±0·05 MEV, 1·34±0·05 MEV, 1·65±0·05 MEV, 2·40±0·05 MEV ; Vanadium 0·32±0·02 MEV, 0·92±0·04 MEV, 1·62±0·04 MEV, 1·83±0·04 MEV.

The decay scheme of the levels excited in ^{55}Mn was investigated by the method of gamma–gamma coincidences, and it was shown that the higher energy states decay by cascade via the 0·126 MEV level.

§ 1. INTRODUCTION

WE have investigated the inelastic scattering of 2·5 MEV neutrons by chromium, manganese and vanadium, by the methods of scintillation spectrometry described in a previous publication (Eliot *et al.* 1954).

Since this early work the resolution obtained in the experiments with neutron groups has been improved, both by reducing the amount of extraneous material in the vicinity of the detector, and by using a photomultiplier possessing twice the photocathode sensitivity (Dumont 6292). In addition the technique of γ–γ coincidence has been adapted to elucidate the decay scheme of the levels of ^{55}Mn excited by the inelastic scattering process.

§ 2. CHROMIUM

The improvement in resolution is apparent on comparing the ratio plot for chromium, fig. 1, with fig. 6 of the previous publication (Eliot *et al.* 1954). The plot shows the presence of a single neutron group corresponding to the excitation of a level at 1·45±0·05 MEV with a cross section of 0·6±0·2 barns. The gamma-ray spectrum (fig. 2) consists of a single line of 1·44±0·03 MEV which must therefore correspond to a ground state transition from the level excited by the neutrons. The

*Communicated by the Authors.

good agreement between the values assigned to the energy of the level by gamma-ray and neutron measurements is a further indication of the validity of Birks's pulse height formula for organic scintillators (Birks 1951).

Fig. 1

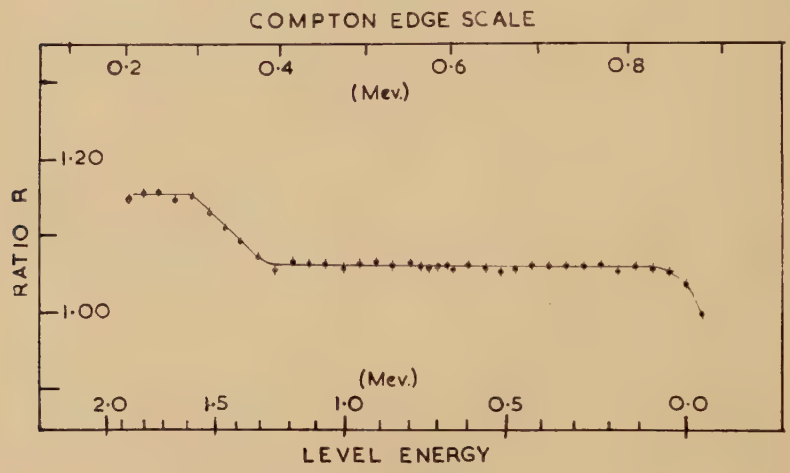

Chromium. Ratio plot.

Fig. 2

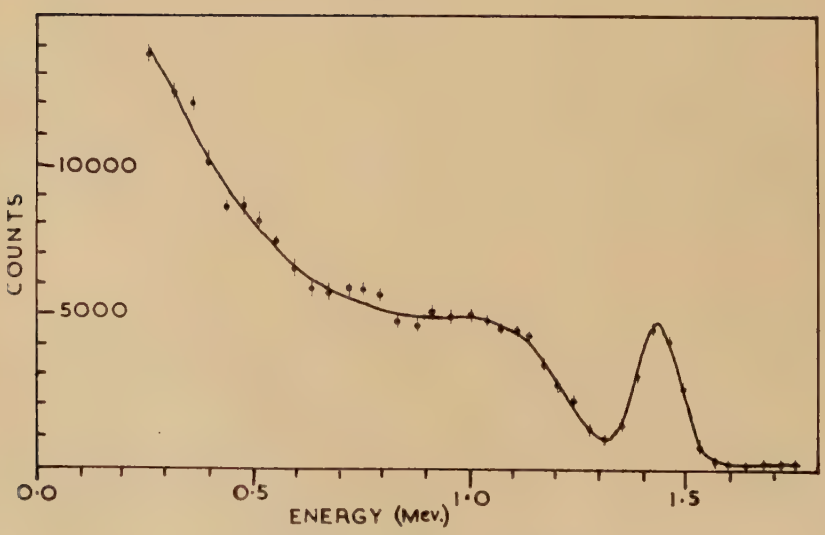

Chromium. Gamma-ray spectrum.

§ 3. MANGANESE

(*a*) *Gamma-Ray Spectrum*

The scatterer consisted of 105 g of finely powdered manganese packed in a cylindrical can of thin (0·3 mm) aluminium 3 cm in diameter and 1 cm deep.

Fig. 3

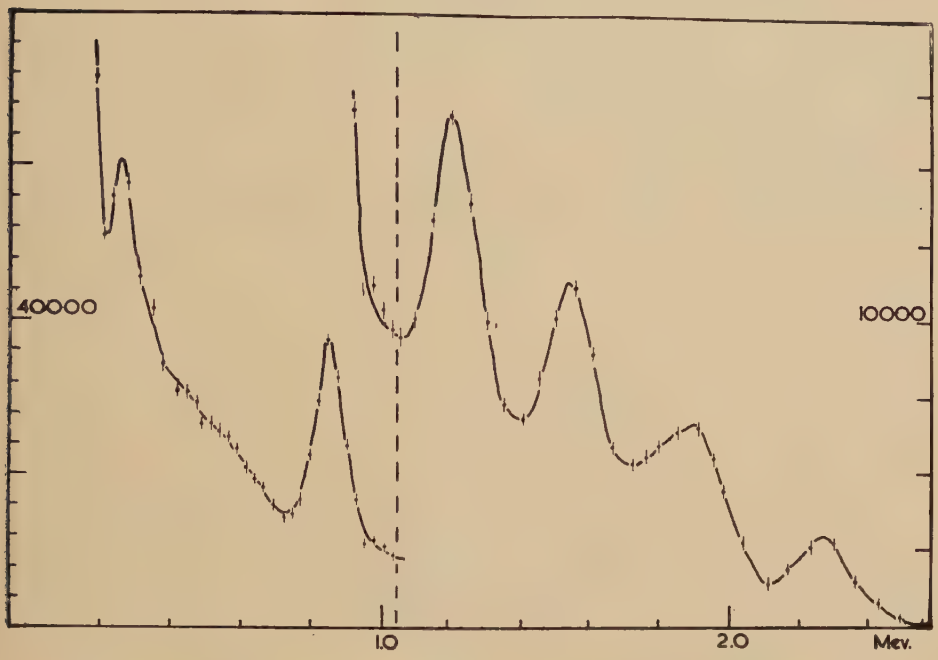

Manganese. Gamma-ray spectrum from 1 in. cube NaI(Tl) crystal.

The gamma-ray spectrum is shown in figs. 3 and 4. Gamma-rays of 0·126±0·005 MEV, 0·32±0·02 MEV, 0·86±0·03 MEV, 1·21±0·03 MEV, 1·53±0·03 MEV, and 2·27±0·04 MEV are present. As previously, a 1 in. cube NaI (Tl) crystal was used to investigate the region above 0·2 MEV (fig. 3).

In order to reduce the background in the low energy region (fig. 4) a thin NaI (Tl) crystal (2·5 cm in diameter, 1 mm thick) was used. Such a crystal, whilst possessing a high detection efficiency (30%) for the 0·126 MEV gamma-rays, absorbs less than 2% of the neutrons and the higher energy gamma radiations.

(*b*) *The Neutron Spectrum*

The ratio plot (Eliot *et al.* 1954) is shown in fig. 5 and is consistent with the excitation of levels at 0·94±0·05 MEV (0·4 barns) 1·37±0·05 MEV (0·3 barns), 1·65±0·05 MEV (0·1 barns).

This data, taken in conjunction with the gamma-ray spectrum suggests that the levels decay by cascade through a 0·126 MEV state.

Excited states of ^{55}Mn have been shown to exist at 0·13 MEV and 0·98 MEV (Temmer *et al.* 1954, Hausman *et al.* 1952). Moreover it has

Fig. 4

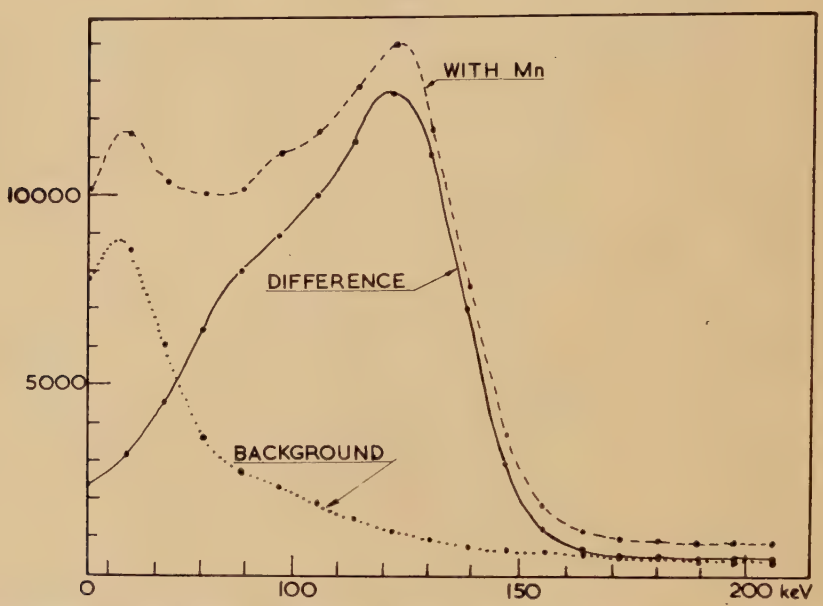

Manganese. Gamma-ray spectrum from 2·5 cm diameter by 1 mm thick NaI (Tl) crystal.

Fig. 5

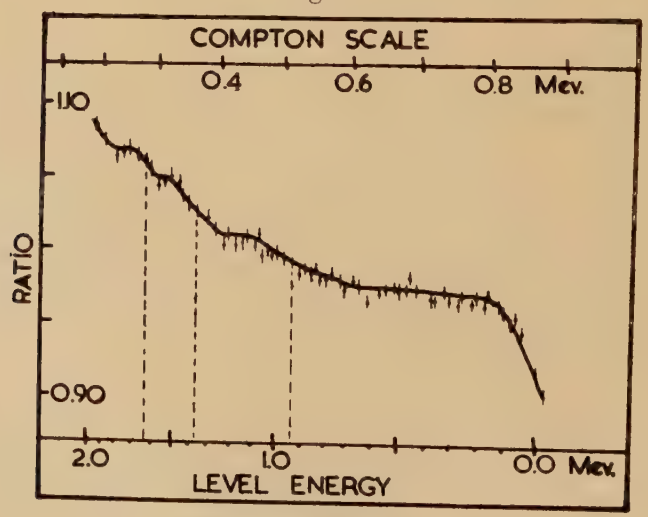

Manganese. Ratio plot.

already been established by excitation methods that the 0·98 MEV level decays to the ground state by cascade via the 0·126 MEV level (Freeman 1955).

In order to obtain a direct confirmation of the decay scheme suggested above, the following γ–γ coincidence experiment was carried out.

(*c*) γ–γ *Coincidences*

The apparatus used is shown schematically in fig. 6. It consisted of two sodium iodide scintillation spectrometers operated in coincidence with a resolving time of 10^{-7} sec. The mode of operation was as follows. Pulses from A were allowed to pass to the kicksorter for analysis only when in coincidence with selected pulses from B. The pulses selected correspond to an energy interval of 105–145 kev (' the window '). It is clear that with this arrangement the kicksorter recorded the spectrum of those gamma-rays in coincidence with the 126 kev radiation.

Fig. 6

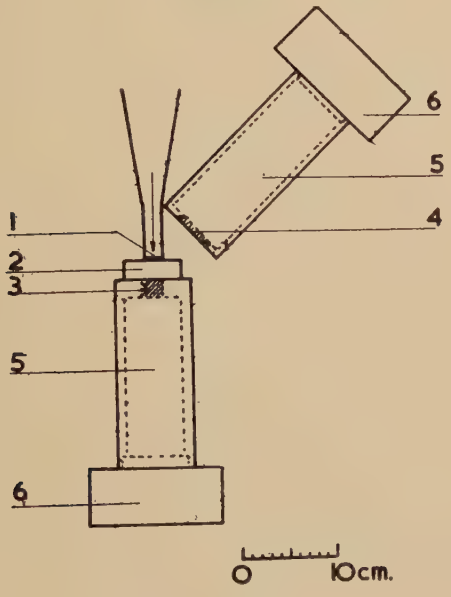

Manganese. Experimental arrangement for γ–γ coincidences.—(1) Neutron source. (2) Scatterer. (3) Crystal A. 1 in. cube of NaI (Tl). (4) Crystal B. 2·5 cm diameter by 1 mm thick cylinder of NaI (Tl). (5) Photomultiplier. (6) Pre-amplifier.

Pulses due to the following types of event were also recorded.

(i) Random coincidences. These were estimated in the usual way by introducing a delay (0·3 μsec) in channel B.

(ii) True coincidences. Inelastic scattering in the scatterer itself or in the crystals gave rise to coincident radiations of other types, either

(γ, γ) or (n, γ). Since neutrons or gamma-rays of higher energy than 126 kev produce pulses in the window some of these events were recorded.

In order to minimize both these effects crystal B was chosen to be 1 mm thick 2·5 cm in diameter for the reasons already discussed in § 3 (*a*).

Fig. 7

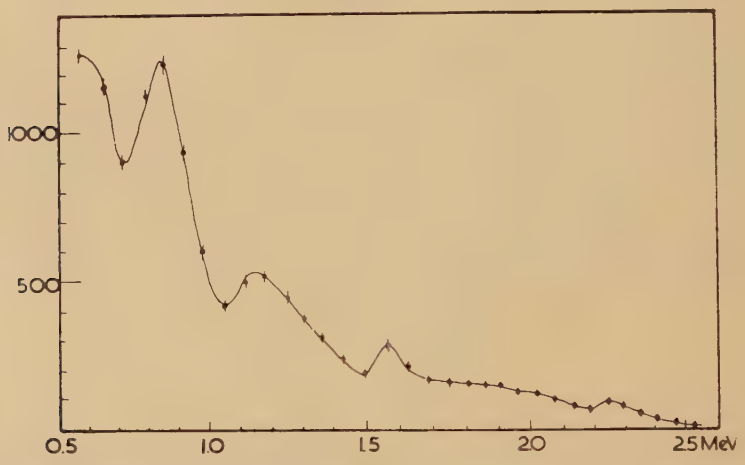

Manganese. Spectrum of gamma-rays in coincidence with the 0·126 Mev gamma-ray.

Fig. 8

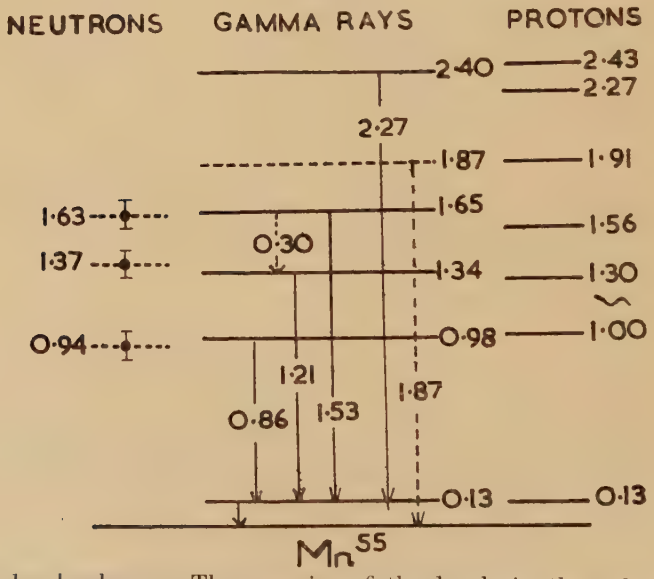

Manganese level scheme. The energies of the levels in the column headed protons are taken from the results of Hausmann *et al.*

The following test was made in order to determine the magnitude of effect (ii). A lead absorber (0·61 g/cm^2) was inserted between the scatterer and crystal B. This transmitted only 10% of the 126 kev radiation

while the effect on the higher energy gamma-rays and the neutrons was inappreciable (transmission 95%). With the absorber in position the coincidence rate fell to 15% of the previous value. Thus the number of counts due to events of type (ii) was not greater than 5% of the total counts recorded.

Figure 7 is the result of the measurements after subtracting the random background. This shows that the γ-rays of 0·86, 1·21, 1·53 and 2·27 MEV are in coincidence with the 126 kev radiation and confirms the conclusion reached in § 3 (*b*) that the 0·94, 1·37 and 1·63 MEV levels decay by cascade. In addition the gamma-ray of 2·27 MEV is also in coincidence, which indicated that a 2·40 MEV level is excited by the neutrons. Figure 7 shows the peak at 1·87 MEV to be relatively less intense than in the single crystal measurements (fig. 3). This suggests that the 1·87 MEV peak of fig. 3 is only partially due to Compton electrons from the 2·27 MEV gamma-ray. However, there may also be present radiation of about 1·87 MEV which is not in coincidence with the 126 kev line.

A level scheme summarizing the data available for manganese from both inelastic scattering of neutrons and protons is given in fig. 8. The weak 0·30 MEV radiation cannot be assigned a definite position in the scheme, but from energy considerations may correspond to the transition from 1·65–1·33 MEV.

§ 4. VANADIUM

The scatterer consisted of 65 g of powdered vanadium enclosed in an aluminium can 5 cm in diameter and 1 cm deep.

Fig. 9

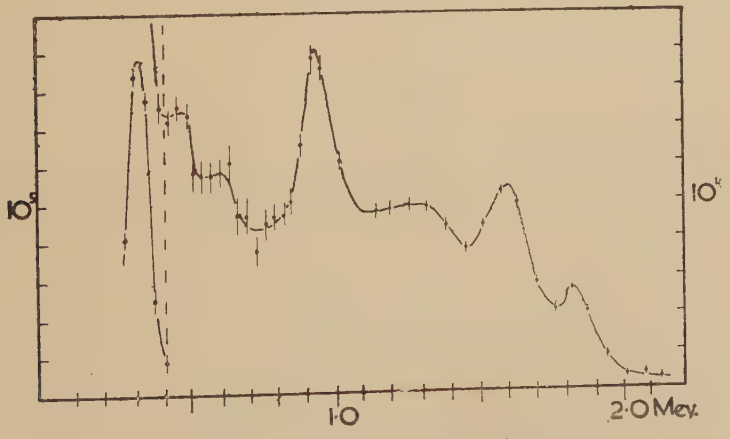

Vanadium. Gamma-ray spectrum.

The gamma-ray spectrum is shown in fig. 9. Gamma-rays of $0{\cdot}32\pm0{\cdot}02$, $0{\cdot}92\pm0{\cdot}04$, $1{\cdot}62\pm0{\cdot}04$ MEV and $1{\cdot}83\pm0{\cdot}04$ MEV are present. The existence of levels in ^{51}V at 0·321, 0·925, 1·609 MEV and 1·813 MEV have been established by inelastic proton scattering experiments (Nussbaum 1954).

As can be seen from fig. 10 the observed gamma-rays fit unambiguously into this level scheme and it is not necessary to make neutron measurements in this case.

Fig. 10

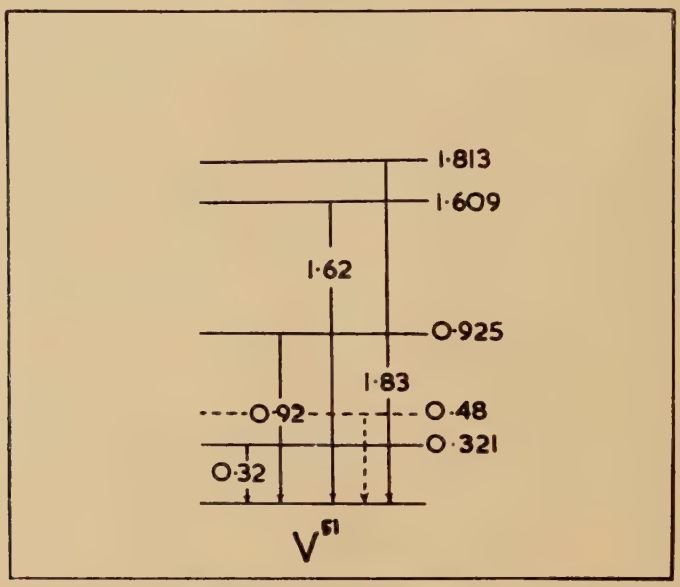

Vanadium. Level scheme.

The presence of a level at 0·48 MEV has been reported from inelastic proton scattering measurements (Hausman *et al.* 1952). Our results are consistent with the presence of a weak gamma-ray of 0·48 MEV which may possibly be associated with this level.

ACKNOWLEDGMENTS

We would like to thank Professor H. Halban for helpful discussion, Mrs. E. A. Wolf (*née* Eliot) for her assistance with the chromium measurements, and Professor Lord Cherwell for extending to us the facilities of this Laboratory.

REFERENCES

BIRKS, J. B., 1951, *Proc. Phys. Soc.* A, **64**, 874.

ELIOT, E. A., HICKS, D., BEGHIAN, L. E., and HALBAN, H., 1954, *Phys. Rev.*, **94**, 144.

FREEMAN, J. M., 1955, *Phil. Mag.*, **46**, 12.

HAUSMAN, H. J., ALLEN, A. J., ARTHUR, J. S., BENDER, R. S., and DOLE, C. J., 1952, *Phys. Rev.*, **88**, 1296.

NUSSBAUM, R. H., 1954, *Thesis*, University of Amsterdam.

TEMMER, G. M., and HEYDENBURG, N. P., 1954, *Phys. Rev.*, **96**, 426.

XXV. *The Direct Observation of Dislocation Nets in Rock Salt Single Crystals*

By S. Amelinckx
Laboratorium voor Kristalkunde Rijksuniversiteit te Gent, Ghent (Belgium)*

[Received September 21, 1955]

Summary

A method for decorating dislocation lines in rocksalt single crystals is described. The method consists in colouring the crystals additively by means of sodium metal. It is found that specks are formed along the dislocation lines, which are, as a consequence, visible in ultra microscopic observation. It is thought that the specks are colloidal sodium particles, and an explanation is given for the decorating mechanism. The method is used for the study of the geometry of dislocations in deformed and annealed single crystals (i.e., polygonized).

Hexagonal, square and lozenge shaped networks, as well as sets of parallel lines are found. Deviations from the ideal pattern are discussed from a theoretical point of view and compared with observations.

It is found that the density of decorating particles is a function of the orientation of the dislocation line with respect to its Burgers vector. Evidence is found that screw dislocations are not decorated ; it is further concluded that the nodes of a network are decorated preferentially.

The emergence points of the dislocation lines correspond to the centres of the etchpits produced by the methyl alcohol etch.

§ 1. Introduction

The most straightforward way for the study of the geometry of dislocations would be to make the dislocation lines directly visible by some decoration process. This has in fact already been achieved by Hedges and Mitchell (1953) in the case of silver bromide, by the segregation of photolytic silver along the dislocation lines as a consequence of the print-out effect. This method is however restricted to silver bromide, or in any case to the silver halides and the resolving power is not so good as would be desirable for the observation of fine detail of the patterns. In this paper we describe some results which have been obtained in the case of sodiumchloride ; the method of decoration can however be applied to a much larger variety of crystals. The resolving power is further better than in the case of AgBr. Preliminary results have already been published earlier (Amelinckx, Van der Vorst, Gevers and Dekeyser 1955).

The geometry of dislocation nets in crystals of the NaCl type has been studied from the theoretical point of view by Frank (1955) and in this

* Communicated by Professor W. Dekeyser.

paper experimental evidence will be presented which confirms many of the predictions of Frank.

§ 2. Experimental Procedure

2.1. *Preparation of Specimens*

Specimens were additively coloured using the method of Rexer (1932) in a slightly modified way. The method essentially consists in introducing a certain quantity of the alkali metal (in our case sodium) into a cavity made in the crystal. On subsequent heating to near the melting point a coloured zone of roughly spherical shape, centred on the cavity, is formed. The colour is not homogeneous in the whole of the specimen. Figure 1 represents schematically a cut through the specimen.

Fig. 1

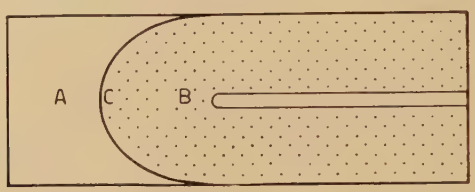

Schematic view of the diffusion zone in a coloured crystal.

Region A is perfectly clear like the original crystal. Region B has apparently an homogeneous colour in deformed specimens, but is almost as clear as region A in undeformed ones. The absorption spectrum of region B will be discussed further.

Between A and B there is a narrow (1/2 mm or less) transition area where concentric rings are visible, similar in appearance to Liesegang rings. The colour varies very often (going from A to B) from yellow over white and blue to pink. In some cases the transition area is not discernible. The surface C separating the regions A and B expands with increased heating time. Where this surface reaches the surface of the specimen, green, olive coloured stains are formed.

When undeformed specimens (i.e. containing only a small number of dislocations) were used, the colour of region B was fainter and only the transition area was appreciably coloured, as well as the region where the surface C was in contact with the surface of the specimen.

When on the contrary heavily deformed and annealed specimens were used, the colour of region B was deeper. Prolonged heating does *not* at first result in an appreciable increase in colour density of the region B ; the first result is an expansion of it. Very long heating with a large stock of sodium results however in the formation of a cloudy region, densely filled with colloidal particles. In all cases the dimensions of the

colloidal particles depend on the cooling rate. The best resolution is obtained when the colloidal particles are just large enough to give an observable diffraction disk.

2.2. *Observation Method*

We observed the coloured crystals in ultra-microscopic illumination, using unfiltered light from a small mercury arc incident perpendicularly to the optical axis of the microscope.

The contrast is maximum for a certain azimuth ; this position is easily found by rotating the object table, and photographs were made in this position.

To avoid the scattering of light by cleavage steps and other surface irregularities the specimen was enclosed in a liquid of the same index of refraction as NaCl, and covered with a thin cover glass.

As cleavage lamellae were used the plane normal to the optical axis of the microscope is (001). The small working distance of the objectives did not allow to incline the specimen so as to bring the whole network into focus ; moreover the networks are in general not plane so that it is not possible at all to have them in focus over a large area. We therefore took successive pictures of the same network at different depths in the crystal.

The mean inclination of the plane of the net with respect to the cube plane was deduced from the width of the part of the image which is in focus. To allow an objective determination of this angle, the following experimental procedure was used. A piece of exposed and developed film was put, the emulsion side upward, on a Fedorow table and observed with the same ultramicroscopic illumination. The emulsion particles scatter light in a way comparable to the colloidal sodium particles but we are now sure that they are situated in one plane. The Fedorow table was then given known inclinations with respect to the focal plane of the objective, and in each position a photograph was made. The width W of the part which is in focus is now directly related to the inclination angle ϕ : $tg\phi = d/W$, where d is the focal depth, which can now be calculated from the observed values of w. It is however not even necessary to compute a value for d, as we can directly compare the width of the ' in focus ' part of an observed network with one of the standard photographs, which are calibrated in inclination angles.

2.3. *The Decoration of Dislocation Lines*

In region A the crystals were in general optically empty. Often however needle shaped inclusions were found in this region immediately in front of the surface C. These inclusions were oriented preferentially in several well defined crystallographic orientations with respect to the matrix. These directions are ⟨100⟩ and ⟨110⟩. They are very probably due to the segregation of impurities e.g. chlorides of bivalent metals. This conclusion is justified by the similarity in aspect and

orientation with respect to the matrix of these needles with the ones formed in crystals where bivalent impurities were added deliberately ($BaCl_2$ and $CaCl_2$).

In region B one observes at small magnification an optically empty background which is cut by the traces of surfaces which become visible as a consequence of the light scattered by them. The density of light scattering centres and the size of the latter are probably too small to reveal individual specks or lines of specks. Only when seen in a direction 'head on' to the surfaces, do they scatter enough light to make them visible.

Region C, i.e. in the neighbourhood of the separating surface, is the most interesting area. The individual light scattering centres (we call them specks) can here be observed at moderate magnification ($25\times$ objective) and it becomes now evident that they are arranged along lines and that the lines are situated on surfaces. The best 'decoration' of lines is found in the neighbourhood of the separating surface C, i.e. in a region which is only a fraction of a mm thick. It is most convenient for observation to prepare the specimens so that the cleavage face is tangent to the surface C.

We can conveniently classify the observed configurations of specks under the following headings.

(i) Along inner surfaces and forming :

(a) Parallel lines (see e.g. photograph 10, Plate 16),

(b) polygonal nets (see e.g. photograph 1, Plate 12),

(c) patterns intermediate between (a) and (b).

(ii) Along a three dimensional network of lines.

We believe that the observed line patterns correspond to dislocation lines. This opinion is based upon the following arguments :

(i) The configurations of lines are exactly like those to be expected from theory for dislocation lines (Frank 1955).

(ii) The lines along which the inner surfaces cut the cleavage face can be revealed by means of etch pits (methyl alcohol etch) (Amelinckx 1954). It is further found that these lines separate crystal grains which differ in orientation. This is deduced from the examination of the cleavage face by means of the Françon method of observation in polarized light (Françon 1952).

(iii) The number of lines increases with deformation.

(iv) The pattern of lines (and surfaces) of bent and annealed (polygonized) specimens corresponds exactly to the dislocation pattern that is to be expected from the theory of polygonization (Cottrell 1953).

§ 3. The Decoration Process

3.1. *Nature of the Decorating Particles*

It is not a simple matter to make sure what phenomenon is responsible for the decoration of the dislocation lines. We see several possibilities.

(i) The specks are colloidal sodium metal formed by the coagulation of the colour centres, which are generated during additive coloration.

(ii) The specks are segregates formed during the thermal treatment and they consist of impurities already present in the crystal.

(iii) The decoration is due to a combined effect of impurities and coagulated colour centres.

In an attempt to discriminate between the different possibilities we have made the following tests :

(i) We treated specimens of the same crystal material in exactly the same way as the other specimens but without the enclosure of sodium metal. No specks were observed ; this proves at least that sodium (or another alkali metal) is essential.

(ii) The absorption spectrum of the coloured part of the specimen was measured by means of a Beckman spectrophotometer. For a crystal exhibiting a well decorated network of dislocations the absorption maximum was found at 5725 Å. This corresponds to a colloidal band according to Sovastianowa (1930).

According to the same author, particles producing this absorption band should scatter yellow light at right angles. The scattering particles look in fact yellow. The absorption maximum should shift to shorter wavelength on growth of the particle size ; this is in fact observed.

(iii) Crystals were prepared containing small quantities of impurities (chlorides of bivalent metals). The segregates look needle-shaped (they may however be platelets) and similar in aspect to those sometimes observed in region A of the specimen. They have the same orientations with respect to the matrix. The precipitates are also localized along grain boundaries, but isolated dislocation lines could not be resolved as the needles are too coarse to give an image of a line. This confirms that there is an interaction between impurities and dislocations as foreseen by Cottrell. The light scattered by them is however not coloured.

(iv) From (i) it is evident that the concentration of impurities originally present is not sufficient to produce the observed specks ; the formation of needle-shaped inclusions in front of the diffusion surface C suggests however that this region might be enriched in impurities in such a way that the concentration becomes sufficient to produce precipitates. To test this possibility small slabs of material were taken in the regions A and B just before and behind the surface C ; these were analysed spectrochemically for trace elements. As expected a marked decrease in impurity concentration was found for the region behind the diffusion surface. This effect is the subject of more detailed study.

(v) The number of colloidal particles formed after prolonged heating with a large stock of sodium is so great that their formation from impurities would imply an unreasonably high amount of impurity atoms.

3.2. *Mechanism of Speck Formation*

As hitherto no unambiguous conclusion concerning the identity of the decorating particles could be reached it is not possible to make any well founded hypothesis concerning the mechanism of speck formation. We will however give a survey of the different possibilities which can be considered.

(i) If the particles should be impurities, the simplest explanation would be Cottrell interaction between impurity atoms and dislocations. In the region where the crystal is supersaturated in impurities this would give rise to precipitation of very small crystals of the impurity substance. The role of the sodium would then be restricted to its function in the enriching process.

(ii) We think the most probable hypothesis is that the particles are colloidal sodium. The discontinuous decoration suggests that certain points of the dislocation line are more active in generating sodium specks.

As pointed out by Seitz (1951) in connection with the segregation of photolytic silver in silver bromide, jogs in dislocation lines in crystal structures of the type here considered have an effective charge. Seeger (1955) has reconsidered the problem and he comes to the conclusion that only neutral jogs result from the intersection of dislocation lines ; charged jogs can however be generated from these by decomposition as a consequence of thermal agitation at higher temperature.

At the temperature whereby the sodium chloride crystals are coloured additively, charged jogs will certainly be present as a consequence of the dissociation of intersection jogs.

The formation of the specks at the dislocation line could then be explained as follows.

The segregation of metallic sodium at the dislocation line necessitates the arrival of chlorine vacancies and of electrons ; both can be provided at the same time by F-centres. The same result can also be obtained if a more complex colour centre, the M-centre, arrives at the dislocation line. The arrival of e.g. an F-centre at a jog would move the jog one spacing (two ions) sideways and would moreover convert one sodium ion into one sodium atom. The process can then start over again and finally the dislocations would climb leaving a trail of sodium atoms. The result of the arrival of a number of F-centres would be the formation of a row or a plane of sodium atoms. These would have a certain mobility along the dislocation line ; this would allow them as a consequence to agglomerate and form the first nucleus for a sodium speck. Nothing would change in the result if electrons and chlorine vacancies were supposed to arrive separately at the dislocation line. We must now consider the driving force for this mechanism. When the crystal is treated for coloration its temperature is about 750°. At that temperature a high concentration of F-centres is in equilibrium with the sodium. When subsequently the crystal cools it becomes supersaturated in F-centres

(and in vacancies). Both will as a consequence have a tendency to disappear either at the surface or at a dislocation.

According to Pratt (1955) there is an elastic interaction between an edge dislocation and a vacancy such that vacancies will be attracted to the expanded region of the lattice. As they have further an effective positive charge, they will be attracted to negatively charged jogs. Electrons will further be attracted by the positively charged jogs so that both components are attracted when separate. Whether the F-centre itself is attracted to the edge dislocation by elastic interaction is, according to Pratt (1955) not so sure.

The role of the sodium stock is clearly to provide electrons and vacancies to the crystal ; the process consists in a transport of electrons and anion vacancies from the sodium stock to the dislocations.

In both hypothesis (i) and (ii) the orientation of the dislocation line with respect to its Burgers vector is of importance. This point will be illustrated in a striking way by our observations (see § 4.5).

It is found that a very long annealing time before coloration diminishes the decoration ability of the dislocation lines in an appreciable way. This can be understood when taking into account that on annealing the number of jogs in the dislocation lines decreases.

When crystals exhibiting a decorated network are deformed and subsequently brought to the temperature of coloration, specks are formed, after cooling, along the newly formed dislocation pattern.

§ 4. The Geometry of Dislocations

4.1. *Introduction*

We will now analyse the observed line patterns assuming that they are dislocation lines. We will however first extend some of the theoretical predictions made by Frank (1955) in order to cover observed patterns as well as to find new patterns exhibiting observable anomalies.

4.2. *Dislocation Nets : Theoretical Predictions*

According to Frank (*loc. cit.*) two typical basic dislocation patterns are to be expected for crystals with the NaCl structure, one consisting of regular hexagons and the other consisting of squares. The first pattern is characteristic for a boundary having a rotation axis [111] and a contact plane (111), and the second for a boundary having [100] as a rotation axis and (100) as a contact plane. According to Frank, the squares should probably degenerate into hexagons as well, by splitting of the fourfold node into two threefold nodes.

An example of a very regular hexagonal network is visible on photograph 1 (Plate 12), whilst photograph 3 (Plate 13) represents a network consisting mainly of squares. In general however the observed nets will be less regular.

From the other observed examples it will be clear that the perfectly regular net is rather exceptional. In reality many nets contain singular dislocations, which complicate the interpretation. It is as a consequence justified to derive a few of the anomalies, which are expected to give an observable deviation from the hexagonal patterns. We will use here Thompson's notation (1955) for the Burgers vectors in a face-centred cubic lattice and we will apply Frank's way of summarizing the results of the analysis of a pattern by means of a lettering diagram which represents at the same time the shape of the net.

Frank has given already two examples of complexities which lead to observable effects : one produces a ' hole ', the other a ' star '. Frank's method is formal and consists in changing the lettering of the regular pattern and then deducing the effect of this change on the pattern. We will on the contrary start with a given set of straight dislocation lines shown on fig. 2, as might be present in the crystal after deformation, and then derive how the pattern will appear after having evolved towards its equilibrium shape, i.e., as we observe it after annealing.

Fig. 2

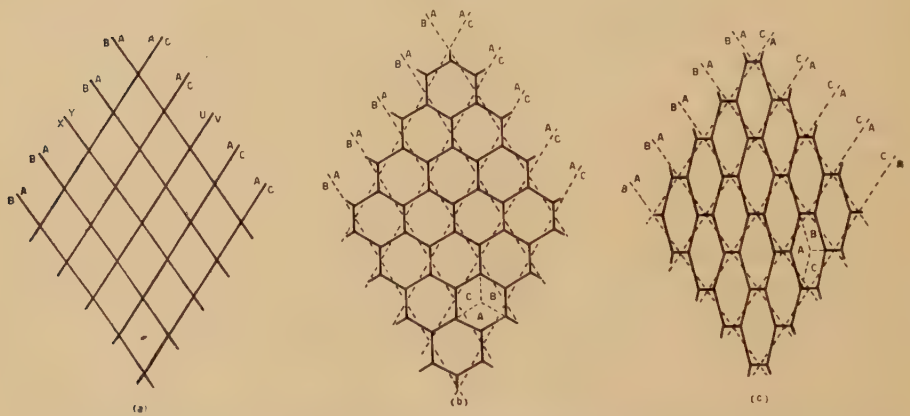

Formation of hexagonal patterns from two intersecting sets of dislocation lines.

4.2.1. *Hexagonal Patterns*

We will first illustrate our way of considering the problem with the simple example of two sets of similar dislocations. Applying the rules derived by Frank concerning the combination of dislocation lines to fig. 2 (*a*) where XY=BA and UV=AC it is clear that this pattern will evolve towards an hexagonal pattern of the shape shown on fig. 2 (*b*). The lettering of all the meshes is the same and it is therefore indicated only once. This pattern is equivalent to the stable pattern deduced by Frank (his fig. 7). Changing the sign of one of the Burgers vectors (making UV=CA) leads on the contrary to a pattern of the shape of

fig. 2 (*c*). The ultimate equilibrium shape will probably be the same for both, but as we do not observe in general this equilibrium shape, it is not meaningless to distinguish both possibilities.

From this way of reasoning it is evident that although the hexagonal pattern of fig. 2 (*b*) (or (*c*)) contains three kinds of dislocations, it can be formed (and it will in practice) from two sets only.

We will now start with the configuration of lines of fig. 2 (*a*) and derive the patterns corresponding to changes of the Burgers vector of one of the lines, e.g. the line marked XY, which we have called a foreign or singular dislocation.

It is clear that only lines which are kept in equilibrium between the parallel lines of the set have to be considered. We will as a consequence only consider four possibilities : XY=BD, BC, CA, DA.

(i) XY=BD ; (UV=AC) (fig. 3 (*a*)). One of the lines AB is replaced by BD, which has a vector which is perpendicular to AC. A row of four-fold nodes, and as a consequence two rows of pentagons are formed. This will be easily recognized on an observed pattern.

Fig. 3

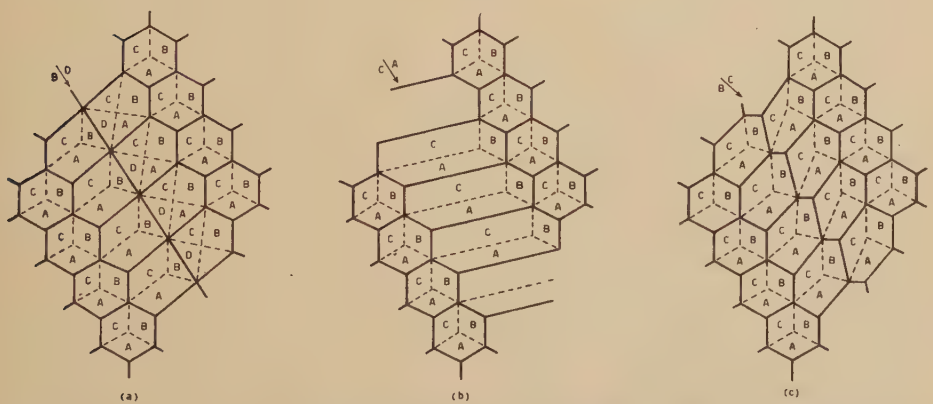

Complexities which arise when *one* singular dislocation line is introduced into an hexagonal network.

(ii) XY=CA (UV=AC) (fig. 3 (*b*)). A row of larger and elongated hexagons is formed. As the lettering is the same in all hexagons, they will evolve towards an equal development. It is as a consequence doubtful whether this effect will be observable.

(iii) XY=BC (UV=AC) (fig. 3 (*c*)). Two rows of deformed and differently oriented hexagons are formed. The same remark as under (ii) applies.

(iv) XY=DA (UV=AC). This case has been considered by Frank (*loc. cit.*). The pattern remains regular. Observation is as a consequence *a priori* impossible.

We can now add a foreign dislocation to each of the two sets of parallel lines. This will lead to patterns which have a greater chance to be observable.

We can take as XY : BC, BD, CA and DA, and as UV : AD, AB, BC and DC, so that *a priori* 16 combinations can be considered ; some of them will not be really different as they only differ by a symmetry operation or by the lettering. One of them, i.e. XY=DA and UV=AD has been discussed by Frank (*loc. cit.*) and leads to the formation of a ' hole '. We will now discuss a few more typical examples :

(i) XY=BD ; UV=DC (fig. 4 (*a*)). Two intersecting rows of fourfold nodes will be formed. At the point of intersection there is a small portion of new dislocation line.

(ii) XY=BD ; UV=AB (fig. 4 (*b*)). A row of larger hexagons is formed, in one direction and in the other direction there will be a row of fourfold nodes and the associated pentagons.

(iii) XY=BD ; UV=BC (fig. 4 (*c*)). There is again a characteristic row of fourfold nodes.

(iv) XY=BC ; UV=AD (fig. 5 (*a*)). This pattern is characterized by the occurrence of four pentagonal meshes associated with the fourfold node at the point of intersection of the two singular dislocation lines.

(v) XY=CA ; UV=AB (fig. 5 (*c*)). The pattern now contains two rows of larger, elongated hexagonal meshes. At the crossing point two still larger hexagonal meshes are present. There will however be a tendency to equalize the dimensions of all the hexagons, so that it is doubtful whether the effect will be visible.

(vi) XY=BC ; UV=BC (fig. 5 (*b*)). The pattern contains a larger, elongated hexagon at the centre. There will again be a tendency to equalize the dimension of all meshes.

These six examples will be sufficient to show what kind of complications one can expect and in which way they can be analysed. It is clear from them that in a number of cases the resulting pattern is topologically equivalent with the simple regular hexagonal net (e.g. (v) and (vi)). These patterns will ultimately evolve towards this shape. Some of the patterns however differ intrinsically from the simple hexagonal net and the presence of singular dislocations can then be derived ; this is always the case when fourfold nodes are formed. The splitting of a fourfold node into two threefold nodes would again produce nets consisting exclusively of hexagons. From our observations it is however doubtful whether this splitting will occur so that we can conclude that some of the described anomalies will be observable.

4.2.2. *Square Patterns*

The same procedure which was used to derive the complexities which occur when singular dislocations are taken up into hexagonal patterns, can also be applied to square patterns.

The dislocation which is added to the sequence AB will be called XY and the singular dislocation which is added to the sequence DC will be called UV. As XY we can take AC, AD, CB and DB, and for UV we can use AC, BC, DA and DB ; sixteen combinations in total.

Fig. 4

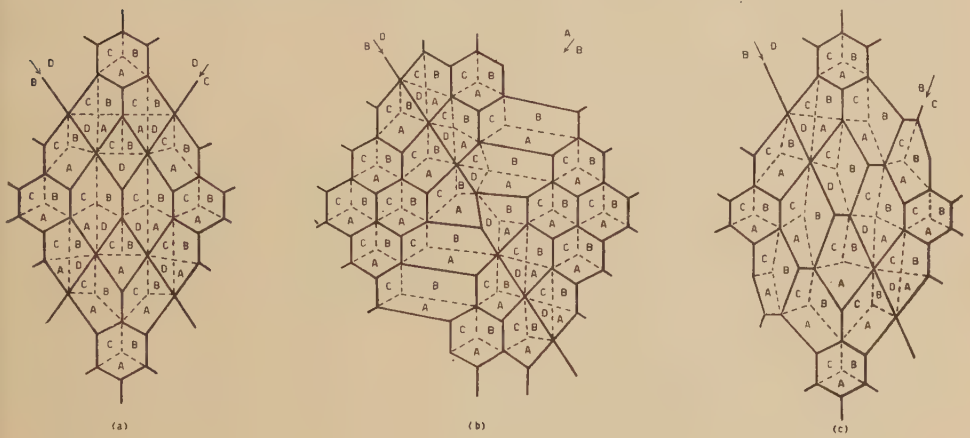

Fig. 5

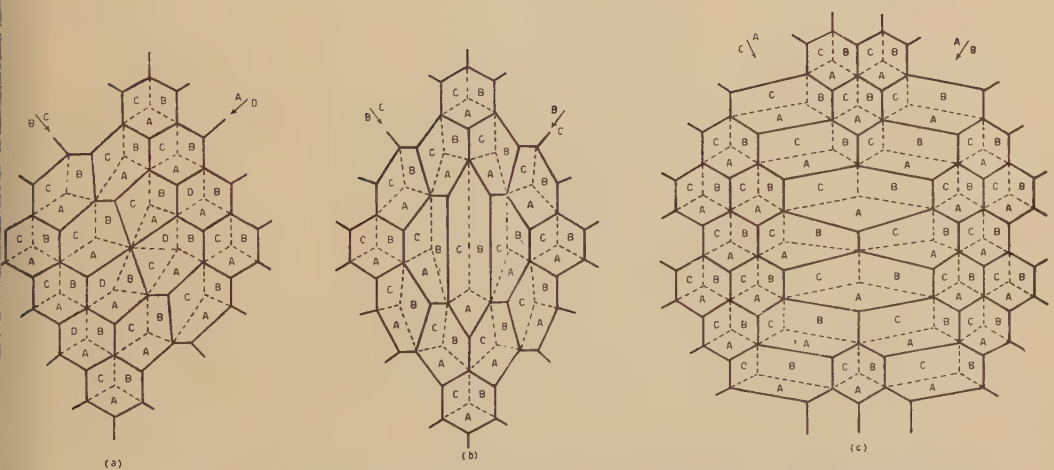

Complexities which arise when *two* intersecting singular dislocation lines are introduced into an hexagonal network.

Let us first consider the simplest case XY=CA, UV=DC. A characteristic zig-zag line will result as shown on fig. 6. When the original dislocation crossed one or more dislocations of the sequence DC, a pattern of the kind shown on fig. 7 may result.

We now consider the effect of adding simultaneously foreign dislocations to the sets AB and DC. The 16 possible combinations can conveniently be ordered into three groups :

(i) XY and UV are mutually perpendicular (4 combinations).

(ii) XY and UV have the same lettering (4 combinations).

(iii) XY and UV form an angle of 60° (4 combinations) or 120° (4 combinations).

Fig. 6

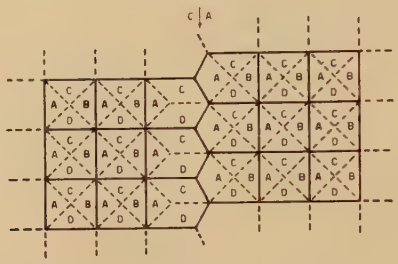

Formation of zig-zag line in a network of squares by the introduction of a singular dislocation line.

Fig. 7

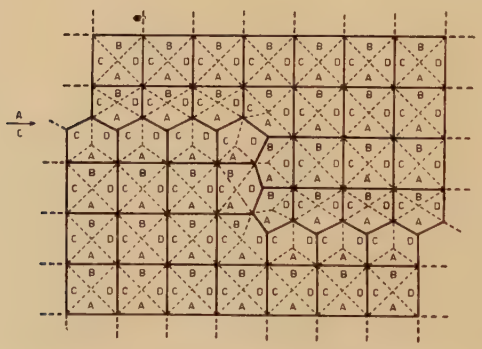

Pattern which is obtained when the singular dislocation line shifts from one row of squares to the following.

We will consider one example of each group ; for the combinations of the same group the results are very similar.

(i) XY=AC, UV=DB (fig. 8). The typical result is the formation of two zig-zag lines intersecting at a fourfold node.

(ii) XY=DB, UV=DB (fig. 9). At the point of intersection of the two singular dislocation lines a large hexagonal mesh is formed.

(iii) XY=DB, UV=DA. The pattern of fig. 10 results.

We have only considered the effect of one, or of two intersecting singular dislocations on the pattern. It will however be easy to deduce the resulting patterns when dislocations are added in a regular way; this will of course lead to a change in rotation axis. As pointed out by Frank such complicated regular pattern will be rare; the occurrence of singular dislocation lines is however very common and this is the reason why only this last eventually was considered.

Fig. 8

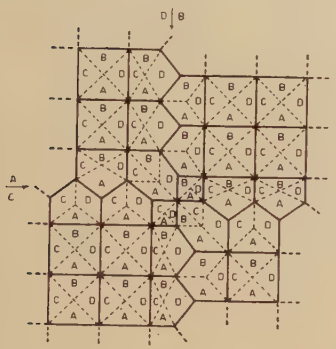

Fig. 9

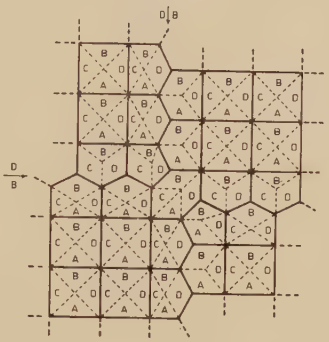

Fig. 10

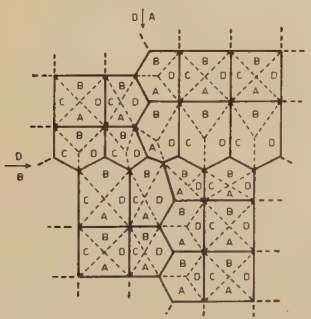

Complexities which arise from the introduction of two intersecting singular dislocation lines into a network of squares.

4.3. *Discussion of Observed Dislocation Nets*

The simplest patterns one observes are those consisting of parallel lines. This configuration is, according to theory, characteristic for pure tilt boundaries, i.e. boundaries for which the axis of rotation is contained in the contact plane. From Frank's formula (Frank 1950) follows that the axis of rotation should be parallel to the lines.

It has been possible to verify this directly in a simple case. We refer here to photograph 3 of the paper by Amelinckx, Gevers, Van der Vorst and Dekeyser (1955). This photograph was obtained from the c(001) face

of a crystal that had been bent about the [001] axis and annealed before being coloured. The dislocation walls, characteristic for polygonization are in the planes (110) and $(1\bar{1}0)$ i.e., normal to active glide planes. In some places the lines can be resolved into separate dots. The place of these dots only changes slightly when focussing deeper and deeper into the crystal. These dots represent consequently dislocation lines normal to the plane of observation : i.e., parallel to the rotation axis [001].

A good example of tilt boundaries lying approximately in the plane of observation is visible on photograph 10. The microscope was focussed on the points of intersection of the dislocations with the cleavage faces ; these points are preferentially attacked when the face is etched (see § 4.5).

The constancy of the spacings between dislocations is very striking ; the corresponding rotation angle is of the order of $\theta = 1{\cdot}2 \times 10^{-5}$ rad.

We will now discuss the network of photograph 1. It approaches quite well in aspect the ideal network one should expect, according to Frank, for a pure twist boundary having a rotation axis [111] and a contact plane (111). This network however lies approximately in a cube plane. The mean deviation does not exceed 7°, as measured from the ' in focus ' width.

Frank predicts hexagonal networks lying in a cube plane but they form only when dislocation lines having their Burgers vectors perpendicular should unite. This last condition seems however not to be fulfilled and it is thus thought that the observed network is characteristic for a rotation axis [111] but that its orientation is not yet stable. The rotation angle calculated on the basis of this assumption is of the order of $\theta = 6{\cdot}4 \times 10^{-5}$ rad.

Some details of the network can now be explained. It is visible on photographs 1 (*b*) and 1(*c*) which are taken at different depths, that a singular dislocation line (indicated by means of an arrow) is taken up into the net. In its inferior part, the line cuts at right angles a number of dislocation lines, forming fourfold nodes with them. At some places the line changes from one row of hexagonal meshes to the following (see 1 (*c*)) and this change is accompanied by a well visible interaction with the net. After having cut a certain number of meshes it seems to stop (see 1 (*b*)). Counting the number of hexagonal meshes on both sides of the singular line, one finds that there is one mesh more over the same distance in the right part. This proves that the singular dislocation is intimately tied into the net and forms now hexagonal meshes.

From this pattern we can conclude that in the circumstances where this net was formed fourfold nodes are stable. There is thus no reason to accept that the hexagons should originate in a square lattice of which some parts have united to form dislocations with a greater Burgers vector. Consequently it is justified to assume that the singular dislocation line and the dislocation lines that it cuts without visible interaction have mutually perpendicular Burgers vectors. Photograph 1 is thus in fact an example of fig. 3 (*a*). The complete analysis of this singularity leads

to the lettering of fig. 11 from which it is clear that for one row of letter fields the lettering has changed from B to D. We have here an example of the first complication described by Frank (his fig. 8), and which consists in formally changing the lettering of one row of lozenge shaped fields in an hexagonal network. Normally this operation would not lead to an observable difference in pattern, in this case however the conclusion was possible as a consequence of the change in orientation of the singular dislocation line.

The pattern represented on photograph 5 (*a*) and (*b*) (Plate 14) is probably another twist boundary about [111] the plane of contact has now an inclination of some 25° with the cube plane. It can directly be compared with Frank's fig. 11.

Fig. 11

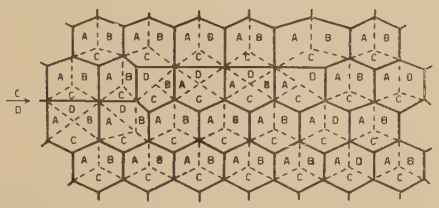

Lettering of the pattern corresponding to photograph 1.

We will now discuss the pattern of photographs 3 (*a*, *b*, *c* and *d*), which represent the same network at depths differing approximately by 5 microns. It is clear that the pattern contains predominantly fourfold nodes, and it should, as a consequence, be characteristic of a twist boundary having [001] as a rotation axis and (001) as a contact plane (Frank, *loc. cit.*). The lines are approximately parallel to [110] and [1$\bar{1}$0] i.e. in accordance with the predicted orientations. The plane of the net differs however considerably from this ideal orientation. The inclination with respect to the cube plane is of the order of 15°. This is in part due to the presence of foreign dislocations which are easily recognized in this case as they interact with the dislocations of the net and form zig-zag lines ; but it is, as in the case of the just described hexagonal net, mainly due to the non equilibrium orientation of the dislocation pattern.

The zig-zag lines of photograph 3 (*a*), visible in the region to which arrow 1 points, are readily interpreted by referring to fig. 6 where the lettering corresponding to this case is given. The zig-zag line is consequently due to a dislocation having a different Burgers vector. The zig-zag lines sometimes jump from one row of square meshes to the following ; this can e.g. be observed on photograph 3 (*d*), arrow 2, and also on photograph 3 (*b*), arrow 3. The lettering corresponding to this configuration has been given in fig. 7.

In some cases a row of hexagonal meshes is present in the square grid ; this is clearly visible on photograph 8 (*d*) (Plate 15, arrow 4) and other

examples can be found on photographs 3 (*d*) and 7 (*b*). This can be accounted for by assuming the introduction of two foreign dislocations, e.g. with Burgers vectors CA and DA as shown on fig. 12.

When the contact plane of a net with rotation axis [001] changes, the meshes may become rectangular ; such a net is visible on photographs 4 (*a*, *b*, *c*) (Plate 14). Some singular dislocation line, forming zig-zag lines of the kind considered here above is also present.

Fig. 12

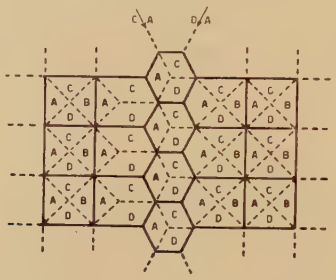

Lettering of the pattern visible on photograph 7.

Photographs 8 (*a*), (*b*), (*c*) and (*d*) represent another network seen at different levels. The inclination with respect to (001) is of the order of 8°. It consists of a complex mixture of fourfold and threefold nodes. On part (*d*) examples of the patterns of fig. 7 and fig. 12 are visible. On several places a dislocation line is cutting other dislocation lines of one set without visible interaction, whereas, unification takes place when cutting a dislocation line of another set. This confirms the stability of fourfold nodes in the circumstances of our experiments.

Photograph 7 (*a*) represents another complicated network containing at least three different sets of dislocations.

4.4. *Miscellaneous Features*

4.4.1. *Forces Between Dislocations*

Although we can only observe static patterns some conclusions concerning the forces between dislocations could be reached. It is foreseen by theory that crossing dislocation lines exert high local forces on one another ; in general they produce a torque that twists the dislocations into a curved configuration. According to Read (1954) configurations of the kind shown on fig. 13 (*b*) and (*c*) are to be expected. Many examples of this characteristic configuration have been observed ; one of them is reproduced on photograph 9 (*b*) (Plate 16). The photograph represents a set of parallel lines forming a tilt boundary ; another dislocation line crosses the same area : it is quite well visible that at every crossing point the characteristic deformation of fig. 13 (*c*) occurs. In this particular case the torque is visibly asymmetrical, i.e., the projected configuration has no line of symmetry. The largest torque is on the dislocations which

belong to the tilt boundary, i.e. on the dislocation which has certainly edge character when assuming the singular dislocation to have mainly screw character, this typical behaviour is completely in accordance with theory. In the case of photographs 9 (*a*) and 9 (*c*) the torque is much more symmetrical. Both patterns consist in fact of lozenges, which are very elongated in the case of fig. 9 (*a*). This last pattern is almost degenerated into a set of parallel lines, i.e. into the pattern characteristic for a tilt boundary.

Fig. 13

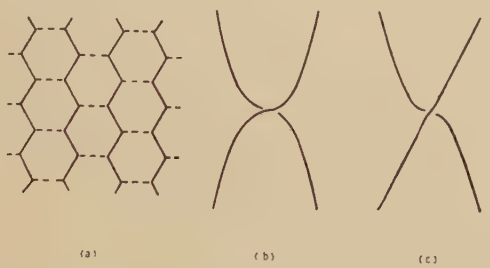

(*a*) Pattern observed on photograph 2 (*a*), dotted lines are not decorated. (*b*) and (*c*) Configuration of crossing dislocation lines. The torque which they exect one on the other can be symmetrical as in (*b*) or asymmetrical as in (*c*).

4.4.2. *Junctions of Sub-boundaries*

Special attention was paid to the way in which boundaries unite at the junction of three grains, and to their behaviour when the contact plane of the same boundary changes.

The case of two pure tilt boundaries is the most simple one ; it is found that they join in the way shown on fig. 14 (*a*). Junctions of this kind are

Fig. 14

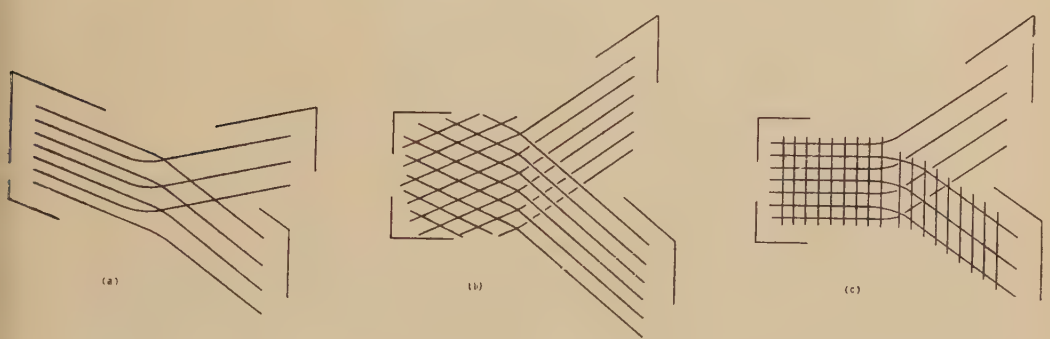

The junction of small angle boundaries :

(*a*) The junction of three tilt boundaries.

(*b*) The junction of two tilt boundaries with formation of a twist boundary.

(*c*) The junction of two twist and one tilt boundary.

of interest for the phenomenon of polygonization. The growth of domains consists in the unification of two tilt boundaries with tilt angles θ_1 and θ_2 into one having a tilt angle $\theta_1+\theta_2$. With the scheme of fig. 14 (*a*) it is clear that the growth process of the domains is reduced to the lateral movement of the junction line.

Photographs 11 (*a*), (*b*) and (*c*) (Plate 17) represent three sections of another junction of three boundaries. Two of them consist of parallel lines, and they are as a consequence tilt boundaries. The sets of parallel lines are best visible on photograph 11 (*c*) ; one set is in the plane of the photograph, the other is only seen as a row of dots as the lines are almost perpendicular to the plane. Photograph 11 (*a*) on the other hand shows the lozenge shaped network resulting from their unification, which is seen on 11 (*b*). Figure 14 (*b*) represents schematically this junction. Photograph 12 (Plate 17) represents the junction of two twist and one tilt boundary, whilst fig. 14 (*c*) is a schematic representation of this junction.

4.4.3. *Speck Formation Along Glide Planes*

In one case we observed the presence of specks along glide planes. Their concentration was however too small to give an image of individual dislocation lines. We think that this phenomenon is due to the deformation of the crystal under stress created by unhomogeneous cooling. The deformation probably took place during the period of coagulation of the colour centres, i.e. during cooling ; and the temperature was probably already too low to cause a marked displacement of the dislocations formed during the glide process. A controlled use of the phenomenon might be useful in revealing the configuration of dislocations immediately after deformation, with a minimum of anneal.

Some of the crystals were coloured immediately after deformation, i.e., without previous anneal. These crystals were characterized by the occurrence of concentric curved dislocation lines like those visible on photograph 6 (Plate 14). This is not in contradiction with the picture of Frank and Read for the gliding process (Frank and Read 1950).

4.4.4. *Mode of Deformation and Frequency of the Various Nets*

Frank (1955) has considered the probability of occurrence of the different kinds of nets in the case of a general deformation. It is to be expected that the frequency of the various types of nets will depend on the mode of deformation of the crystal.

Our crystals were deformed by compression under water and the active glide planes determined in polarized light. Deformation was found to take place on at least two sets of glide planes simultaneously. This is of course a consequence of the particular geometry of the glide elements with respect to the compression axis. When deformation was mainly on two families of glide planes (as e.g. in bending) the resulting patterns (after anneal) were nearly exclusively tilt boundaries, rarely square and lozenge shaped networks, and very rarely hexagonal networks. When on the contrary the mode of deformation was on two pairs of

mutually perpendicular glide planes, the patterns were with nearly equal frequency sets of parallel lines and hexagonal patterns, and less frequently square or lozenge shaped patterns. This can easily be understood from the way of formation of these nets, starting from their basic dislocation sets. It is clear that when in a region only one kind of dislocations is present, anneal will produce tilt boundaries.

When on the other hand two sets of dislocation lines with perpendicular Burgers vectors are present either parallel lines or square grids can result. If on the contrary the Burgers vectors enclose an angle of 60° (or 120°) hexagonal nets will result.

4.5. *Density of Decorating Particles*

It is quite well visible on all photographs of networks that the mean density of decorating particles is a function of the orientation of the lines. This is best seen on hexagonal networks ; the particle density is approximately the same for all parallel parts of the network but it may be different from that for another set of parallel lines. This is, e.g. clearly visible on photograph 2 (*a*) (Plate 12), where in some regions zig-zag shaped lines are seen, which are also represented in full line on fig. 13 (*a*). It is clear that this configuration of dislocation lines would not be stable ; the simplest explanation is that some parts of the pattern are not decorated ; these parts are shown as dotted lines on fig. 13 (*a*). From the orientation of these lines (parallel to [110]) with respect to the lattice follows that it is reasonable to suppose that these parts are pure screws. Moreover the proposed decoration mechanism accounts for the absence of particles along pure screws, so that there is no contradiction.

An implication of this conclusion is that networks consisting exclusively of screw dislocations would not show up with our method. Another example illustrating this point is visible on photograph 2 (*b*), which represents a part of the hexagonal net of photograph 1, degenerated into a set of parallel zig-zag lines as a consequence of the absence of decoration along one of the families of lines.

We think that the non-decorated parts of a network are in most cases those parts which were formed by the unification of lines of the two generating sets of dislocations. This opinion is justified by the following argument. It is known from theory that the elastic energy associated with a screw dislocation is smaller than the one associated with an edge dislocation of the same Burgers vector and in the same material. On annealing, a dislocation line will as a consequence tend to adopt the screw orientation ; this will in general only be possible locally as the ends of the lines are not free. We think that where new parts of dislocation line form they will preferentially do it in the pure screw orientation.

In relation with the foregoing it is interesting to note that in some cases only a plane lattice of dots is seen, as e.g. visible on photographs 13 (*a*) and (*b*) (Plate 17). This constellation of specks cannot be due to a coincidence. Even when assuming that the dots should lie on one set of parallel lines, it would be an incredible coincidence that they should form a two-dimensional

lattice. The only reasonable assumption is therefore that the observed dots are the nodes of a network containing at least two sets of parallel lines with lozenge shaped or square meshes. One hypothesis is now to accept that all dislocation lines are pure screws and that they are therefore not decorated except at their nodes. This is however not in accordance with the orientation of the lines ; they are *not* oriented parallel to [110] and [1$\bar{1}$0] ; the most reasonable assumption is therefore that the nodes are preferentially decorated. This is not in contradiction with the observation of other networks where the nodes are sometimes marked by larger dots.

Photograph 13 (*b*) presents a particularity (arrow) : one of the dots of the network is missing, leaving in this way *one* hexagonal mesh. It is possible that this is a coincidence, but it is also not excluded that we have to do here with a ' hole ' in the net, of the kind predicted by Franx (*loc. cit.*).

It will be seen on most of the photographs that a certain number of specks are distributed at random. It is however very striking that such spots are almost completely absent from the neighbourhood of the dislocation nets. It is probable that a good proportion of these specks are in fact on lines of the three dimensional network : it is however also possible that these specks have been formed from colour centres which have not been trapped by dislocations.

4.6. *Relation between the Etchstructure of Cleavage Faces and the Geometry of Dislocations*

It was shown earlier that the subboundaries in melt grown rocksalt single crystals can be revealed by means of a suitable etching technique (Amelinckx 1954). We now find that the patterns obtained in this way correspond exactly to the lines of intersection of the ' inner ' surfaces, obtained by decoration, and the face under examination ; the emergence point of each line being marked by an etch-pit.

This justifies our previous conclusion that there is a one to one correspondence between etch-pits and dislocations.

Assuming that at every moment in the course of the etching process the etch-pit is centred on the dislocation line, the final shape of the pit can give information concerning the orientation of the dislocation line, when this is assumed to be a straight line. The detailed structure of some etched boundaries can then be explained.

It is clear that when the dislocation line is normal to the cleavage face the etch-pit will have its normal shape, i.e., a perfectly square ' inverted ' pyramid, with its ' top ' in the centre of the base (fig. 15 (*a*)). The square character is a consequence of the fourfold symmetry of the face under examination. If on the other hand the line is oblique with respect to the cleavage face, the emergence point of the dislocation line will be out of the centre of the square (fig. 15 (*b*)) ; the angle ϕ of the dislocation line with the normal to the crystal plane is to be calculated from the depth d of the etch-pit and the distance a from the centre : $tg\phi = a/d$.

It is possible in some cases to draw conclusions from the etch pattern ; in particular one can decide whether a boundary consists of parallel lines or of a polygonal network. An example of a pattern which is to be expected in such a case is shown on fig. 15 (*c*).

Fig. 15

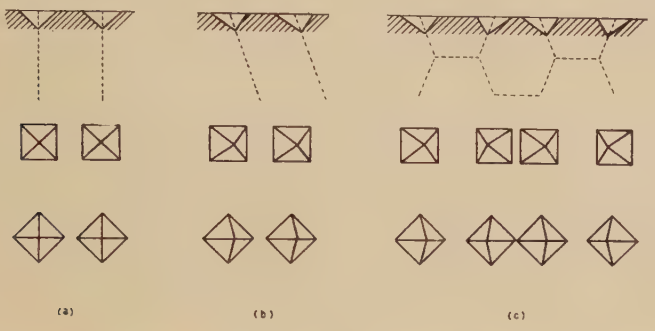

Relation between the shape of etch-pits and the direction of the dislocation lines responsible for their formation.
(*a*) The dislocations are parallel and perpendicular to the cleavage plane.
(*b*) The dislocations are parallel and oblique with respect to the cleavage plane.
(*c*) The dislocations form an hexagonal network.

Patterns of this kind have been observed in fact and photograph 14 (*d*) (Plate 18) is an example. The grainboundaries of photograph 14 (*b*) and 14 (*c*) contain parallel dislocations forming only a small angle with the normal to be cleavage plane whilst photograph 14 (*e*) shows a grainboundary containing dislocations of very different inclinations. One can conclude that photographs 14 (*b*) and 14 (*c*) represent probably tilt boundaries, whereas photograph 14 (*c*) is certainly a boundary having twist character.

It was found that some grainboundaries were marked by pits of different depths. In one case shown on photograph 14 (*a*) and (*a'*) there was a regular succession of etch-pits of different depths. This structure cannot be a coincidence as the same sequence is continued all along the boundary. This particular structure is clearly due to a difference in dissolution velocity between two successive centres of attack. Such a difference was assumed to result from the fact that one kind of etch-pits corresponds to the emergence point of a screw dislocation the other to the emergence point of an edge dislocation. It is indeed to be expected from theory that impurities will concentrate along edge dislocations, but much less along screw dislocations. The observed pattern is then a striking illustration of the existence of dislocations of different character. A possible model for the network which would give rise to the etch-pattern is obtained in the following way. Consider the square network of dislocations with Burgers vector AB and CD, as shown on fig. 13 of Frank's paper. Now replace the sequence AB by the sequence AB, CA,

AB, CA, AB. This gives rise to a pattern consisting in its equilibrium shape of a succession of straight lines having pure screw character and zig-zag lines having mainly edge character. We have in fact obtained a regular repetition of fig. 6.

When comparing the etch structure of the two halves of a cleavage more detailed information can be obtained, as the dislocation line is now explored over a greater length. Already earlier (Amelinckx 1954) we pointed out that the etch patterns on two halves of a cleavage are identical. Closer examination however reveals sometimes slight differences. Examples are visible on photograph 15 (Plate 18). With one pit on one half of the cleavage correspond three pits on the other half. The simplest interpretation is to accept that this is due to the branching of a dislocation line, the cleavage plane having passed very near to the branching point. On the same photograph other slight deviations between the two patterns are surrounded by lines of a different kind.

§ 5. Conclusion

From these observations it is concluded that a technique has been found to reveal individual dislocation lines. This constitutes clearly a powerful method for the study of the geometry of dislocations. The method has been applied to rocksalt, but it will be extended to other crystals.

The observations give further direct evidence for the interaction between colour centres and dislocations, and they prove the difference in character of dislocation lines ; it is even possible to establish directly the pure screw character of a dislocation.

I wish to thank Professor Dr. W. Dekeyser for his continuous interest, Professor Dr. Eeckhout for the spectrochemical analysis and Dr. Gevers for useful discussions. This work is part of a research scheme supported by I.R.S.I.A. (Centre d'étude de l'état solide), Brussels.

Bibliography

Amelinckx, S., 1954, *Acta Metallurgica*, **2,** 848.

Amelinckx, S., van der Vorst, W., Gevers, R., and Dekeyser, W., 1955, *Phil. Mag.*, **46,** 450.

Cottrell, A. H., 1949, *Bristol Conference on the Strength of Solids* (London : Phys.Soc.), p. 30 : 1953, *Dislocations and Plastic Flow of Crystals* (Oxford : University Press).

Françon, M., (1952), *Revue d'Optique*, **31,** 65.

Frank, F. C., 1950, *Pittsburgh Report Office Naval Research* (Navexos 834) ; 1955, *Proc. Phys. Soc.* (*Report of Bristol Conference*, 1954), p. 159.

Frank, F. C., and Read, T. W., 1950, *Phys. Rev.*, **79,** 722.

Hedges, J. N., and Mitchell, J. W., 1953, *Phil. Mag.*, **44,** 223.

Pratt, P. L., 1955, *Proc. Phys. Soc.* (*Report of Bristol Conference*, 1954), p. 402.

Read, T. W., 1954, *Dislocations in Crystals* (Mac-Graw Hill).

Rexer, E., 1932, *Z. Phys.*, **78,** 538.

Seeger, A., 1955, *Proc. Phys. Soc.* (*Report of Bristol Conference*, 1954), p. 391.

Seitz, F., 1951, *Rev. Mod. Phys.*, **23,** 328.

Sovastianova, M., 1930, *Z. Phys.*, **64,** 262.

XXVI. *Isotopic Spin Selection Rules—VI: The 6·88 MeV State of* ^{10}B

By D. H. Wilkinson and A. B. Clegg*
Cavendish Laboratory, Cambridge†

[Received October 31, 1955]

Abstract

The radiations emitted by the 6·88 MeV level of ^{10}B are described and analysed in detail. It is shown that in all probability this state is $1-$, $T=0$ but that it suffers some tens of per cent contamination by $T=1$. It is suggested that this state is formed of ^{9}Be in its ground state acting as the unique parent for an additional s-wave proton; this very strong contamination could then be due to the presumed near presence of the similarly constituted $T=1$ state.

§ 1. Introduction

The radiative capture of protons of less than 1 MeV in beryllium (A. B. Clegg, to be published) contains evidence for a large failure of the isotopic spin selection rules on electric dipole transitions in self-conjugate nuclei. This paper will describe this evidence in detail and suggest a possible reason for the failure.

The resonance observed at a proton energy of 330 kev in the reaction ^{9}Be (p, γ) ^{10}B corresponds to a state in ^{10}B at 6·88 MeV and emits 'resonant' gamma-rays to four states of ^{10}B:

To state of ^{10}B at (MeV):	0·72	1·74	2·15	5·11
Relative intensities:	40	100	20	25

This state has a total width of 160 kev and also emits alpha-particles to the ground state of ^{6}Li and deuterons to the ground state of ^{8}Be (see Ajzenberg and Lauritsen 1955).

§ 2. Particle Widths

From the results of Thomas *et al.* (1949) we can estimate the reduced widths for emission of protons, alpha-particles and deuterons from this 6·88 MeV state of ^{10}B. In doing this we have tried to separate out those parts of the cross sections of the ^{9}Be (p, α) ^{6}Li and ^{9}Be (p, d) ^{8}Be reactions that are due to the 330 kev resonance from those due to other overlapping resonances. The results of Thomas *et al.* are for one angle; we have assumed the yields to be isotopic (see discussion below). We get these

* Present address: California Institute of Technology, Pasadena, California.
† Communicated by the authors.

following values for the uncorrected partial widths which we shall use for discussion (reasonable variations in the values of the cross sections we take do not alter the argument significantly):

	Γ_p	Γ_d	Γ_α
Assuming smaller proton width	115 kev	13 kev	12 kev
Assuming larger proton width	25 kev	59 kev	57 kev

(All these widths are quoted in the centre-of-mass system.) It is shown in § 3 that we favour the smaller value of the two alternative proton widths as this leads to much better agreement between experiment and theory for the radiative width for the transition to the 1·74 Mev state. If we take the standard value for the interaction radius of

$$a=1{\cdot}45(A_1^{1/3}+A_2^{1/3})\times 10^{-13}\text{ cm},$$

and use full Coulomb wave-functions, we obtain values for the reduced widths, after applying the correction for the variation of Δ_λ across the resonance (Thomas 1951). These reduced widths are given below as ratios to the single-particle value $\hbar^2/Ma$ (M is in each case the appropriate reduced mass).

	Smaller proton width		Larger proton width
	s-wave protons forming state 1, 2−	p-wave protons forming state 1+	s-wave protons forming state 1, 2−
$Ma\gamma_p^2/\hbar^2$	0·22	∞	∞
$Ma\gamma_d^2/\hbar^2$	0·18	0·034	∞
$Ma\gamma^2/\hbar^2$	0·020	0·015	0·0065

The infinities in this table imply that a negative value was obtained for the reduced width, i.e. the Thomas correction is too large. Note that only a 1+ state is considered to be formed by p-wave protons because of the strength of the radiative transitions to the 0+ state at 1·74 Mev.

This seems to provide strong support for the conclusion that the 6·88 Mev state is formed by s-wave protons, with the smaller value of the proton width. However, we must consider the possibility that the ^{9}Be nucleus may have a larger radius than we have assumed above; such a larger radius might be expected since the last neutron in ^{9}Be is very loosely bound. Therefore an estimate was made of how much one has to increase the ^{9}Be radius to decrease the p-wave reduced width to $3\hbar^2/Ma$, making only a rough estimate of how Δ_λ changed. This gave a value for the interaction radius of about 6×10^{-13} cm which corresponds

to an increase of the ^{9}Be radius to about $2{\cdot}2A^{1/3}\times 10^{-13}$ cm. This seems an unreasonably large increase and it has not even decreased the reduced width to the Wigner limit. Lane (1954) has given reasons for believing that p-wave widths are usually small in p-shell nuclei. Therefore we could expect this reduced (p-wave) width to be small, which would need an even larger radius for the ^{9}Be nucleus. Thus there seems to be strong support for the conclusion that the 6·88 MeV state of ^{10}B is formed by s-wave protons. Further support is provided by the gamma-ray angular distributions, as described in § 4.

It seems quite probable from the large reduced deuteron width associated with s-wave proton formation that we should take the 6·88 MeV state as being chiefly $T=0$.

§ 3. Radiative Widths

The radiative width of the 6·88 MeV state has been measured: assuming small value of proton width $\Gamma_\gamma=4{\cdot}8$ ev, assuming large value of proton width $\Gamma_\gamma=1{\cdot}0$ ev. As is shown below we favour the smaller value of the proton width so we shall tentatively use $\Gamma_\gamma=4{\cdot}8$ ev. This leads to the following values of the partial radiative widths, expressed also as ratios ($|M|^2$) to the single particle radiative widths (Blatt and Weisskopf 1952, Chap. XII):

Transition to state of ^{10}B at (MeV)		0·72	1·74	2·15	5·11
Γ_γ (ev)		1·0	2·6	0·52	0·65
Values of $\lvert M\rvert^2$	if electric dipole	0·014	0·061	0·016	0·39
	if magnetic dipole	0·22	0·96	0·25	6·2

None of these values is large enough to disqualify either dipole assignment, particularly as the experimental value of the radiative width quoted is only accurate to a factor of two, but the radiative widths are large enough to disqualify quadrupoles and higher multipolarities. So if we assume formation of the 6·88 MeV state by s-wave protons, the strength of the transition to the 0+ state at 1·74 MeV implies that this must be electric dipole and so assigns 1− to the 6·88 MeV state. On the strength of this evidence we should say that the 6·88 MeV state was of $T=0$. This agrees with the remark at the end of § 2.

Following Inglis (1953) we can make rather unambiguous configuration assignments for the 1·74 MeV state of ^{10}B: in jj-coupling it is the $T=1$. $J=0$ level of $(p_{3/2})^6$; in LS-coupling it is the lowest ^{31}S state of p^6. Similarly, since the reduced proton width is so large, we can take the ^{9}Be ground-state to be the unique parent of the 6·88 MeV state of ^{10}B. i.e. we take the 6·88 MeV state to be $(p_{3/2})^5s$ in jj-coupling (where the

parent state is the $T=\frac{1}{2}$, $J=\frac{3}{2}$ state of $(p_{3/2})^5$), and as $^{11}P_1=(^{22}P_{3/2})s$ in LS-coupling. Then following Lane and Radicati (1954) we can calculate the values of $|M|^2$ in both extreme couplings

$$|M|^2_{jj}=0{\cdot}093, \qquad |M|^2_{LS}=0{\cdot}074.$$

It is striking that these values lie close to the observed value of 0·061. Although there is no guarantee that in intermediate coupling we would get values lying close to these extremes it very frequently happens that this is so, so that this agreement with experiment gives some support for our assuming the smaller value of the proton width.

We should also pause to consider the gamma-ray that seems with good probability to lead to the state of ^{10}Be at 5·11 MeV. On account of the 2+ state at 3·37 MeV in ^{10}Be we should expect to find a 2+, $T=1$ state in ^{10}Be at about 1·74+3·37=5·11 MeV. If our assignment of 1−, $T=0$ to the 6·88 MeV state is correct we expect an allowed E1 transition to this 2+, $T=1$ state; the fact that a strong transition to the 5·11 MeV state is observed may suggest that it be identified with the expected $T=1$ state. However, Jones and Wilkinson (1954) have given reasons for supposing that the expected 2+, $T=1$ state is in fact that at 5·16 MeV and that the 5·11 MeV state is rather 2−, $T=0$. We must now consider the expected strengths of the allowed E1 transitions to the 2+, $T=1$ state. This state is probably the $J=2$, $T=1$ member of $(p_{3/2})^6$ in jj-coupling and a $^{31}D_2$ member of p^6 in LS-coupling. We then get the following theoretical values for the transition strengths:

$$|M|^2_{jj}=0{\cdot}009, \qquad |M|^2_{LS}=0{\cdot}014 \text{ or } 0{\cdot}16.$$

The ambiguity in LS-coupling arises because there are two D states belonging to [42] in p^6 and they are expected to lie at about the same energy so we have little to guide us in choosing between them. We see that in the intermediate coupling in practice obtaining we should expect a fairly small value of $|M|^2$ for this transition, somewhat less than the (rather inaccurate) experimental value—which, we may remark, is not much changed if we measure it in terms of the single-particle unit calculated for realistic shell-model wave functions rather than for those of the Weisskopf unit. At all events it seems that if we are indeed dealing with an E1 transition we must be rather close to LS-coupling (as appears to be the case from the calculations on ^{9}Be and ^{10}B of French, Halbert and Pandya (1955)) and the 2+ state must be the D_{II} state of [42].

However this assignment would contradict the earlier conclusion and also be difficult to reconcile with the observation that the 5·11 MeV state is excited in ^{10}B(d, d′)^{10}B (C. K. Bockelman, private communication). It remains possible that we are seeing a strong M1 transition with perhaps the weaker E1 to the 5·16 MeV state lying beneath it. The 5·11 MeV state could be the $J=2$, $T=0$ linkage of an s-wave proton to the ^{9}Be ground state as unique parent just as we suppose the 6·88 MeV state to be the $J=1$, $T=0$ linkage of the same constituents. Two such closely related states would differ only be a spin-flip of the s-wave proton and

so combine very strongly (the vector-coupling situation is favourable in both extreme schemes). However it seems difficult to understand so strong a transition. Even allowing a 30% contribution for the competing E1 transition that we have just discussed and a factor of two experimental error in the widths we are still left with a value for the quantity Γ_γ (ev) divided by E_γ^3 (Mev) of 0·04. This is a very high value for an M1 transition; according to the latest survey (Wilkinson 1955) if the above quantity exceeds 0·02 the chances are about ten to one that we are dealing with an E1 transition; the largest well-established values are 0·042 and 0·032 in ^{7}Li–^{7}Be and ^{14}N respectively although poorly-established values as high as 0·08 are known (in ^{15}N).

If we are mistaken in our use of the smaller proton width the agreement between theory and experiment on the strength of the transition to the first $T=1$ state is spoiled but the present worry over a very strong M1 to a 2−, $T=0$ state at 5·11 Mev is removed. The situation is seen to be complicated and requires further study.

§ 4. Angular Distributions

The angular distributions of the gamma-rays to the 0·72 and 1·74 Mev states have been measured; they show no large departure from isotropy. This provides strong support for the conclusion that the 6·88 Mev state is formed by s-wave protons. However, it is possible to get isotropy with p-wave protons if we assume $a=5$ (a is the proportion of the compound nucleus formed by channel spin=2 relative to that formed by channel spin=1).

According to Christy (1953) LS-coupling is the more successful scheme for predicting channel spin ratios in the light elements; we then get theoretically $a=5$ and so isotropy if we assume the 6·88 Mev state to be $^{13}S_1$ or $^{13}D_1$. However, if we assume $^{13}S_1$ the transition to the 5·11 Mev state would be forbidden (a forbidden magnetic dipole transition if we assume the 5·11 Mev state to be 2+, $T=1$ or forbidden by the isotopic spin selection rules if we assume 2−, $T=0$), while if we assume $^{13}D_1$ the transition to the $^{31}S_0$ state at 1·74 Mev would be forbidden. As both these transitions are observed to be strong we see that if one invokes practically pure LS-coupling to explain the isotropic angular distributions one finds difficulty in explaining the observed radiative transitions.

This, taken with the evidence from the reduced widths presented in § 2, seems to indicate that the 6·88 Mev state is formed by s-wave protons. Further strong support for this is provided by observations on the elastic scattering of protons from ^{9}Be (W. A. Fowler, private communication). Then, as shown in § 3, it follows from the strength of the transition to the 0+ state at 1·74 Mev that the 6·88 Mev state must be assigned 1−.

§ 5. Isotopic Spin

We have assumed above throughout that the 6·88 Mev state has $T=0$. This is primarily based on the large deuteron width, though it is supported

by the fact that the alpha-particle width is not especially small. Further support is provided by the fact that the largest established electric dipole transition goes to the $T=1$ state at 1·74 MeV. However, the transitions to the $T=0$ states at 0·72, 2·15 MeV should then be forbidden by the isotopic spin selection rules on electric dipole transitions in self-conjugate nuclei. These $\Delta T=0$ transitions are certainly weaker than that to the $T=1$ state but they are not forbidden; they imply a $T=1$ impurity of order 20% in intensity in the 6·88 MeV state if we take the strength of the uninhibited transition as our reference. If we take the value $|M|^2=0{\cdot}032$ as our reference (this is the most likely value for an uninhibited E1 transition in the p-shell (Wilkinson 1955)) the impurity becomes about 50%. Even if we take the larger value of the proton width which we saw in § 3 to be most satisfactory for reconciling all observations concerning the 5·11 MeV state we should still find an impurity of about 10%.

This is distinctly the largest well-established isotopic spin impurity known in any light nucleus (see Wilkinson 1953 a). However, there is a possible reason for this impurity which we can explore. R. G. Thomas (quoted in Ajzenberg and Lauritsen 1952) points out that the near-zero spin-dependent cross section in the reaction ^{9}Be(n, n) for thermal neutrons implies that the neutron scattering is due to two bound states in ^{10}Be, respectively 1, 2−, with binding energies $\lesssim 1{\cdot}7$ MeV. This is supported by the remark of Wilkinson (1953 b) that the observations on thermal neutron capture in ^{9}Be are quite consistent with fairly strong electric dipole transitions from just such states. This suggests that these states are two of the three states reported in ^{10}Be at 5·96, 6·18, 6·26 MeV. One of these latter is probably the $T_z=+1$ analogue of the 2−, $T=1$ state of ^{10}B at 7·48 MeV, while another is probably 1−, so that we can expect to find a 1−, $T=1$ state in ^{10}B in the neighbourhood of the 7·48 MeV state. The 6·88 MeV state we believe to be the 1−, $T=0$ member of the group of broad s-wave states with the ^{9}Be ground state as unique parent (Lane 1954). It seems plausible that this 1−, $T=1$ state that we now seek is another member of this group. (There is some supporting evidence that it may have a large width since the corresponding state in ^{10}C seems to be 1 MeV lower than its partner in ^{10}Be; a large width would be necessary to produce such an Ehrman–Thomas displacement.) Thus these two states should have rather similar wave functions so that the $T=1$ state could produce a large $T=1$ impurity in the 6·88 MeV state.

An impurity of 20% in intensity corresponds roughly to 40% in amplitude. To get some idea of orders of magnitude let us take 1 MeV as the separation between these two 1− states. Then the Coulomb matrix element between them must be

$$H^c_{10} \sim 0{\cdot}4 \text{ MeV}.$$

Radicati (1953, 1954) and MacDonald (1954) calculate values of H^c_{10} for several cases in light nuclei and find them to be of the order of 0·1–0·3 MeV. In the present case, however, for reasons given above we think

the wave-functions may match rather well and can estimate an upper limit on H^c_{10} by considering them to match perfectly. Then H^c_{10} will be of the order of the Coulomb energy of either of the states and we can calculate this by considering the charge of the nucleus to be uniformly distributed over a sphere of radius $1{\cdot}45A^{1/3}\times10^{-13}$ cm; this gives a value of 5·5 MEV. So it seems quite probable that such a 1−, $T=1$ state in the neighbourhood of the 6·88 MEV state can quite easily contaminate the latter enough to explain the observed rather complete breakdown of the selection rules.

It is interesting to examine other states with large s- or d-wave widths discussed by Lane (1954) as probably having unique parents, to see if they have large isotopic spin impurities. Three such states are found:

Nucleus	State	Impurity
^{14}N	8·06 MEV*	$\alpha_1^2(0)\sim0{\cdot}02$
^{16}O	13·09 MEV†	$\alpha_1^2(0)>0{\cdot}06$
^{16}O	12·95 MEV†	$\alpha_1^2(0)>0{\cdot}05$

* See Clegg and Wilkinson (1953), Hird *et al.* (1954).
† See VII of this series.

This evidence is unfortunately meagre but the impurities do seem comparatively large. This seems to lend some slight support to the hypothesis offered to explain this large breakdown of the isotopic spin selection rules in the present case.

References

AJZENBERG, F., and LAURITSEN, T., 1952, *Rev. Mod. Phys.*, **24,** 321; 1955, *Ibid.*, **27,** 77.

BLATT, J. M., and WEISSKOPF, V. F., 1952, *Theoretical Nuclear Physics* (New York: John Wiley and Sons).

CHRISTY, R. F., 1953, *Phys. Rev.*, **89,** 839.

CLEGG, A. B., and WILKINSON, D. H., 1953, *Phil. Mag.*, **44,** 1269.

FRENCH, J. B., HALBERT, E. C., and PANDYA, S. P., 1955, *Phys. Rev.*, **99,** 1387.

HIRD, B., WHITEHEAD, C., BUTLER, J., and COLLIE, C. H., 1954, *Phys. Rev.*, **96,** 702.

INGLIS, D. R., 1953, *Rev. Mod. Phys.*, **25,** 390.

JONES, G. A., and WILKINSON, D. H., 1954, *Phil. Mag.*, **45,** 703.

LANE, A. M., 1954, *A.E.R.E. Report* T/R 1289.

LANE, A. M., and RADICATI, L. A., 1954, *Proc. Phys. Soc.* A, **67,** 167.

MACDONALD, W. M., 1954, *Thesis* (Princeton).

RADICATI, L. A., 1953, *Proc. Phys. Soc.* A, **66,** 139; 1954, *Ibid.*, **67,** 39.

THOMAS, R. G., 1951, *Phys. Rev.*, **81,** 148.

THOMAS, R. G., RUBIN, S., FOWLER, W. A., and LAURITSEN, C. C., 1949, *Phys. Rev.*, **75,** 1612.

WILKINSON, D. H., 1953 a, *Nature, Lond.*, **172,** 576; 1953 b, *Phil. Mag.*, **44,** 1019; 1955, *Ibid.* (in course of publication); A.E.C.L. document PD-260.

XXVII. CORRESPONDENCE

The Vibrations of a Perturbed Lattice

By R. J. Elliott
Physics Department, University of Reading

[Received October 21, 1955]

The introduction of defects into a lattice destroys the periodicity and in consequence the normal modes are, in the usual harmonic approximation, no longer waves. This behaviour is in many ways analogous to that of the electron energy states of a similar lattice on the band approximation. A general method of solution of the electron problem has recently been proposed by Slater and Koster (1954 a, b) and Koster (1954) and results calculated for a few simple cases. We wish to point out that this method is also applicable to the vibrational problem with qualitatively similar results. For the localized defects discussed, the normal modes continue to have frequencies in the same allowed bands as in the unperturbed lattice. But they are only wave like far from the defect and the amplitude of vibration is enhanced or diminished in a manner which falls off exponentially with distance from the defect. Details of this behaviour cannot be easily obtained by the above method, but the scattering of lattice waves by defects can be studied by Koster's (1954) method with obvious application to thermal conductivity. For certain perturbations, however, localized modes (in which the amplitude decays exponentially) can occur with isolated frequencies outside the bands.

Details of these localized modes can be obtained by an extension of Slater and Koster's (1954 a) method. The equations of motion for each atom (see Born and Huang 1954, §§ 18, 24) give a set of difference equations

$$\omega^2 M_\alpha(l)u_\alpha(l) = \sum_{\beta,l'} \Phi_{\alpha\beta}(l, l')u_\beta(l') \qquad . \quad . \quad . \quad . \quad . \quad (1)$$

in the displacements u. ω is the frequency and M the mass while Φ defines the interatomic forces. l labels the N unit cells centred at $\mathbf{R}(l)$ while α has $3n$ values labelling the x, y, z components of the n atoms in each cell. In the perfect lattice, because of the periodicity of Φ/M there are $3n$ normal modes for each of N wave vectors $\mathbf{k}$ ending in the first Brillouin Zone. These have frequency $\omega_i(\mathbf{k})$ say, and form

$$\sum_\alpha a_\alpha{}^i(\mathbf{k})q_\alpha(\mathbf{k}) \qquad . \quad . \quad . \quad . \quad . \quad . \quad . \quad . \quad (2)$$

where $q_\alpha(\mathbf{k})$ are the waves $\sum_l u_\alpha(l) \exp[i\mathbf{k} \cdot \mathbf{R}(l)]/N$ and the sets $a_\alpha{}^i(\mathbf{k})$ are normalized and orthogonal. In the perturbed lattice we transform the equations into these normal modes and then back transform to the u's. If Δ is the difference between Φ/M for the perturbed and unperturbed problems the equations become

$$u_\gamma(m) = \frac{1}{N} \sum_{k\ i} \sum_{\beta, l, l'} \exp[i\mathbf{k} \cdot (\mathbf{R}(l) - \mathbf{R}(m))] a_\alpha{}^i(\mathbf{k}) \alpha_\gamma{}^{i*}(K) \Delta_{\alpha\beta}(l, l') u_\beta(l')/\omega^2 - \omega_i(\mathbf{k})^2. \quad (3)$$

These $3nN$ equations are only compatible if the determinant of the coefficients is zero. This determinant has unity down the diagonal and zero elsewhere except for those columns β, l' where Δ is non-zero. The equation for ω is therefore a secular determinant of order $3n$ times the number of cells perturbed, while the amplitudes can be obtained from the minors of the large determinant. The calculations can be greatly simplified by taking account of the symmetry of the possible modes, which now have point symmetry about the defect.

The numerical solution of (3) is therefore complicated but not impossible. It involves the assumption of interatomic force constants for the perturbed and perfect lattices; a difficulty which is also present is calculating the frequency spectrum of a perfect lattice. We have solved analytically the problems of an impurity atom, vacancy and interstitial in a linear chain with nearest-neighbour interaction. Even in those cases, the solutions are complicated functions of the perturbation parameters. For the simplest case of a different isotope, mass M', in a chain of atoms mass M, there is only a localized mode if $M' < M$ when $\omega^2 = 4\Phi M/M'(2M - M')$ which lies above the allowed band where $\omega^2 = 2\Phi(1 - \cos kR)/M$. The amplitude of the nth atom away (the atoms need no longer have equal spacing R) falls off like $\exp(-\gamma n)$ where $\gamma = \log[(2M/M') - 1]$.

The qualitative results are of considerable interest. The perturbed modes, provided they produce a dipole moment will give infra-red absorption, forbidden in perfect crystals, in the band and at isolated frequencies outside. The localized modes and those in the band with increased amplitude near the defect will interact most strongly with electrons trapped at the defect and produce the vibrational fine structure on the optical absorption of luminescent centres. In fact these considerations grew out of an attempt to explain the infra-red and optical spectra of natural and irradiation damage centres in diamond (Clarke, Ditchburn and Dyer 1955) and they shed some light on these results. This and other applications are being considered and will be reported, with a more detailed treatment of the general problem, elsewhere.

Note added in proof:—It has been brought to the author's attention that this general method was first proposed by M. Lax, 1954, *Phys. Rev.*, **94**, 1391, who mentions its application to lattice vibrations.

References

Born, M., and Huang, K., 1954, *Dynamical Theory of Crystal Lattices* (Oxford : University Press).

Clark, C. D., Ditchburn, R. W., and Dyer, H. B., 1955, *Proc. Roy. Soc.* (to be published).

Koster, G. F., 1954, *Phys. Rev.*, **95**, 1436.

Slater, J. C., and Koster, G. F., 1954 a, *Phys. Rev.*, **95**, 1167 ; 1954 b, *Ibid.*, **96**, 1208.

[*The Editors do not hold themselves responsible for the views expressed by their correspondents.*]

Photograph 1

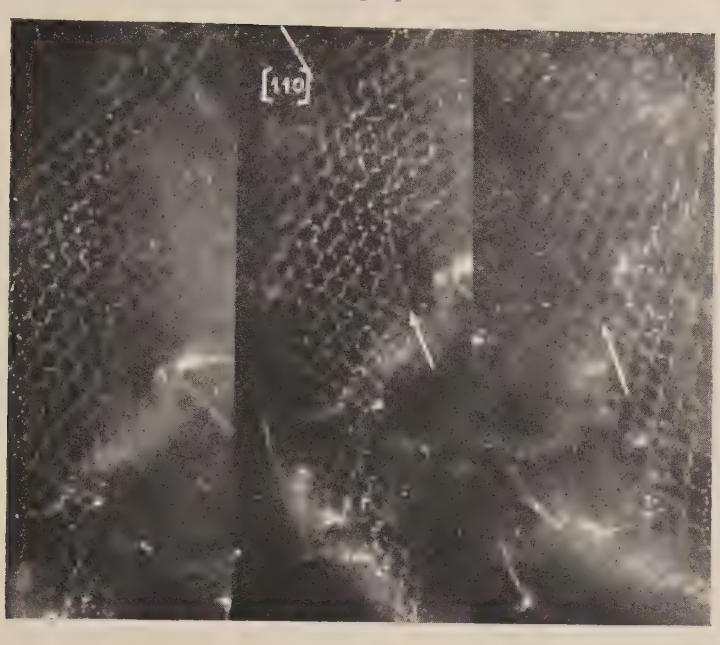

(*a*) (*b*) (*c*) (760×)

20 μ

Hexagonal pattern photographed at three different levels. Note the singular line indicated by an arrow. Numerical magnification factors (e.g. 760×) refer to the original print; after reduction during reproduction the magnification is given by the 20 μ rod.

Photograph 2

(710×) (*a*) 20 μ (*b*) (650×)

Hexagonal network. One family of lines is not decorated; it is supposed that these are pure screw dislocations. Phot. (*b*) is a part of the network of phot. 1 at a fourth level.

Photograph 3

(*a*) (*b*) (*c*) (*d*)

(850×)

20 μ

Network consisting mainly of square meshes. Singularities are indicated by means of arrows.

Photograph 4

20 μ (*a*) (*b*) (*c*) (650×)

Network containing mainly rectangular meshes. Singular dislocation lines form zig-zag lines.

Photograph 5

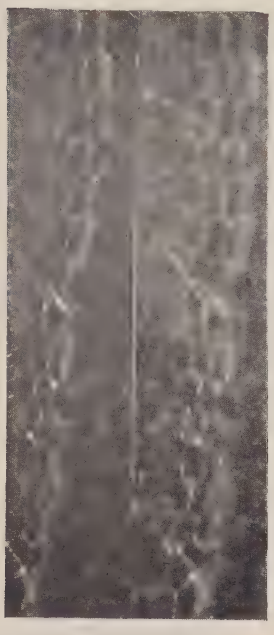

(*a*) (*b*)

20 μ (700×)

Hexagonal network in a plane enclosing an angle of 25° with the cube plane.

Photograph 6

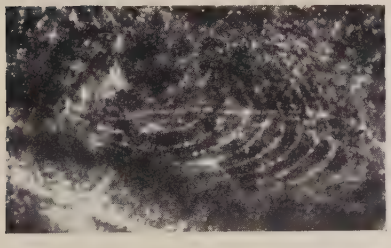

20 μ (650×)

Curved dislocation lines which are typical for specimens which have not been annealed before coloration.

Photograph 7

20 μ (*a*)

20 μ

(*b*)

(650×) (760×)

(*a*) Complicated network containing at least three kinds of dislocations;
(*b*) Hexagonal meshes in a network of squares.

Photograph 8

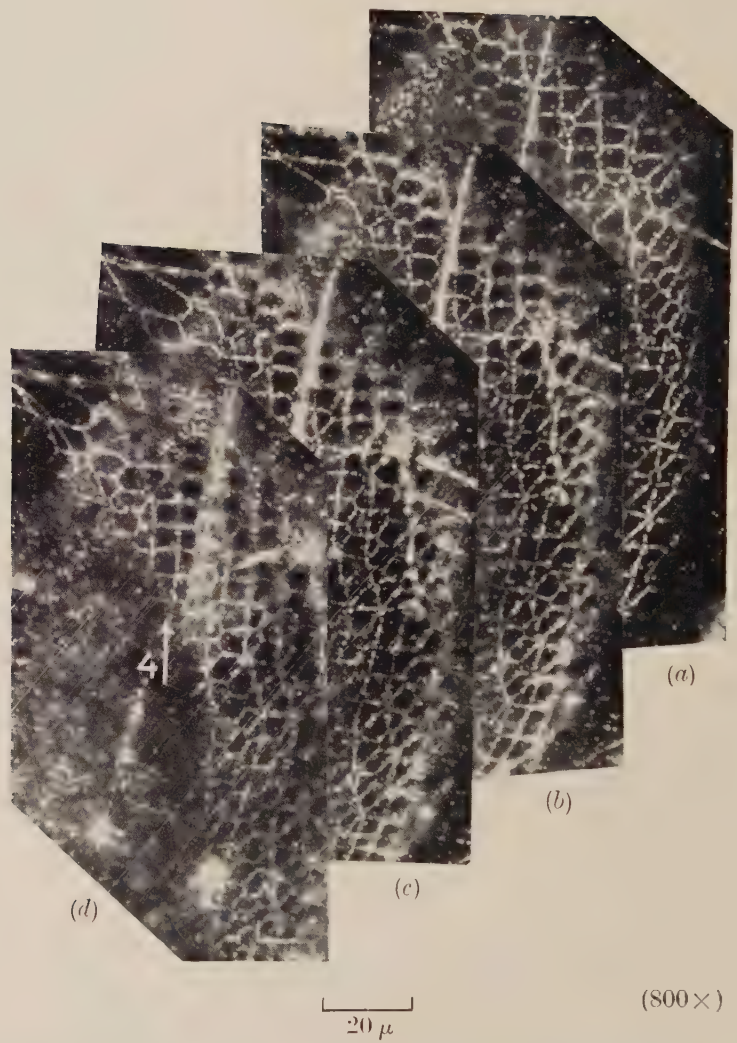

Complicated network containing as well fourfold as threefold nodes. Singularities to which is referred in the text are indicated by means of arrows.

Photograph 9

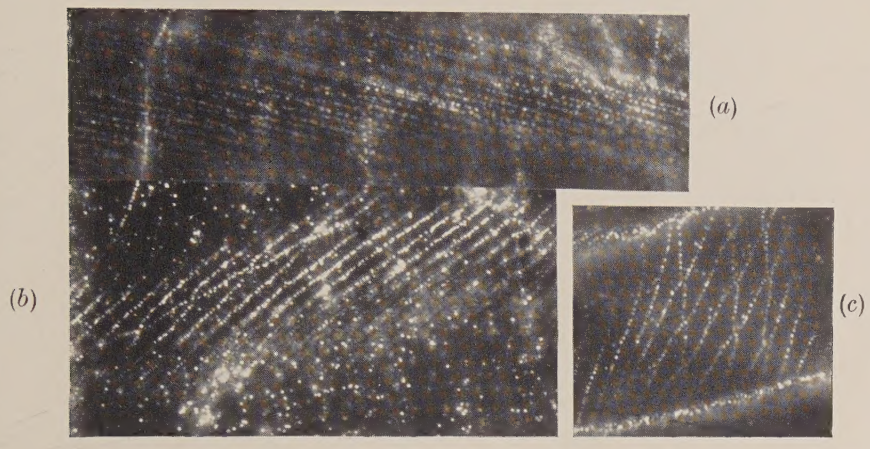

To illustrate the torque that crossing dislocation lines exert one on the other. The resulting figuration can be either symmetrical (*a*) and (*c*) or asymmetrical (*b*).

Photograph 10

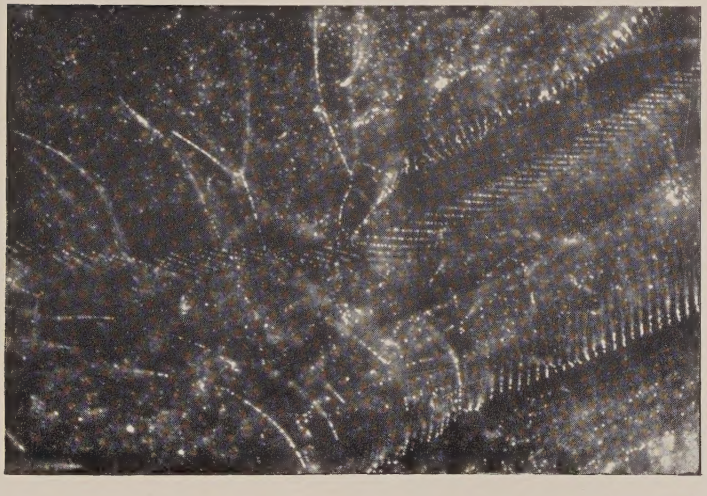

The emergence points of the dislocation lines of two tilt boundaries.

Photograph 11

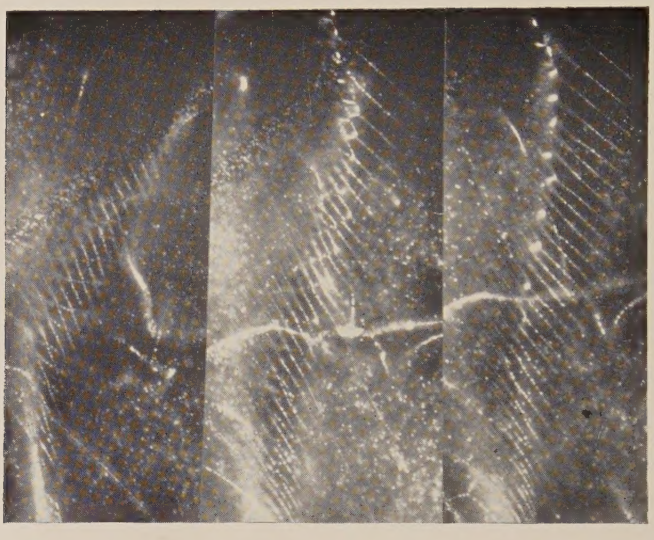

(*a*) (*b*) (*c*)

20 μ (500×)

Junction of two tilt boundaries and one twist boundary seen at three different levels. (*a*) The twist boundary consisting of lozenge-shaped meshes. (*b*) The junction line (cf. scheme of fig. 14 (*b*)). (*c*) The two tilt boundaries.

Photograph 12

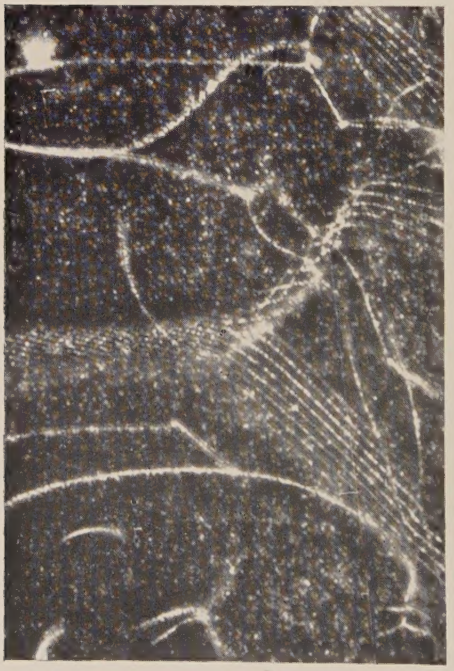

20 μ (350×)

Junction of two twist boundaries and one tilt boundary.

Photograph 13

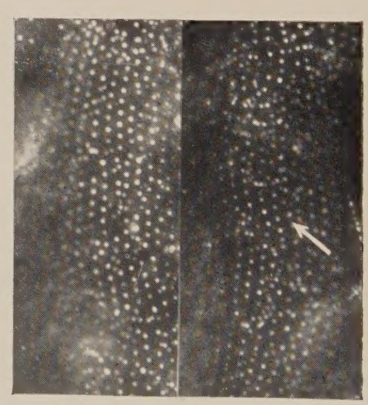

(*a*) (*b*)

(1050×)

20 μ

Two-dimensional lattice of dots, showing that the nodes of a network are decorated preferentially.

Photograph 14

(250×)
(250×)
(250×)
(250×)
(250×)

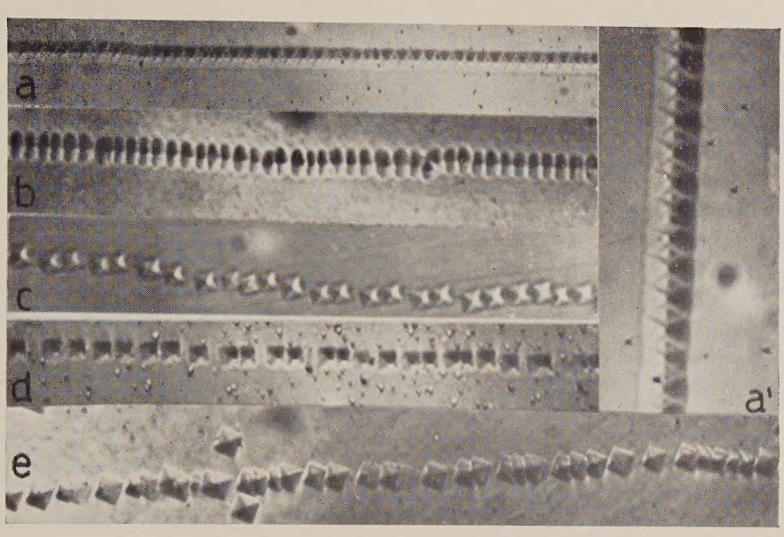

(630×)

Details of the etch structure of small angle grain boundaries.

Photograph 15

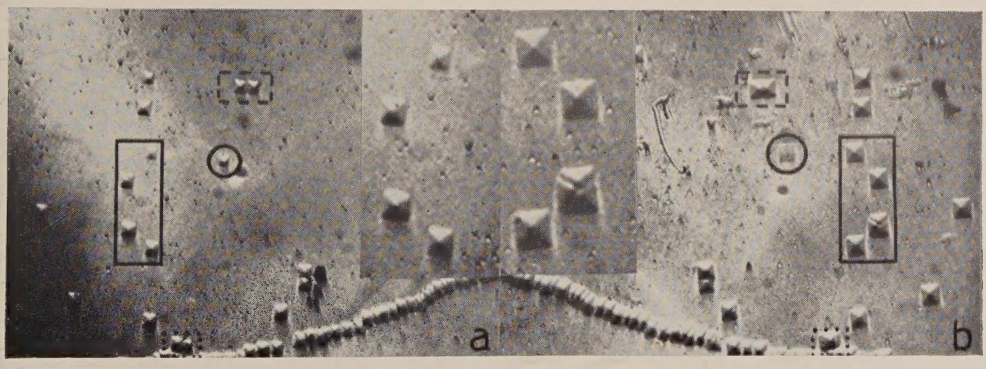

(590×) (590×)

Comparing the etch structure of two halves of a cleavage. The small differences give evidence for the branching of dislocation lines.